

**FUNCTIONAL CHARACTERISATION OF Asn¹⁸³ IN
THE TRANSMEMBRANE $\alpha 5$ CRITICAL FOR TOXICITY OF
THE *Bacillus thuringiensis* Cry4Ba TOXIN**



SUPAPORN LIKITVIVATANAVONG

**A THESIS SUBMITTED IN PARTIAL FULFILLMENT OF
THE REQUIREMENTS FOR
THE DEGREE OF DOCTOR OF PHILOSOPHY
(MOLECULAR GENETICS AND GENETIC ENGINEERING)
FACULTY OF GRADUATE STUDIES
MAHIDOL UNIVERSITY**

2006

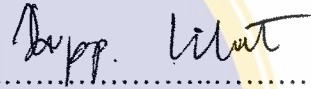
ISBN 974-04-6807-1

COPYRIGHT OF MAHIDOL UNIVERSITY

Thesis

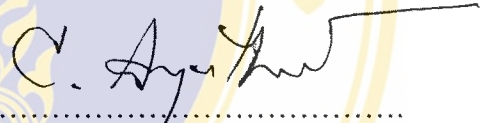
Entitled

**FUNCTIONAL CHARACTERISATION OF Asn¹⁸³ IN
THE TRANSMEMBRANE α 5 CRITICAL FOR TOXICITY OF
THE *Bacillus thuringiensis* Cry4Ba TOXIN**



.....

Miss Supaporn Likitvivatanavong
Candidate




.....

Assoc. Prof. Chanan Angsuthanasombat, Ph.D.
Major-Advisor



.....

Dr. Panapat Uawithya, MD., Ph.D.
Co-Advisor



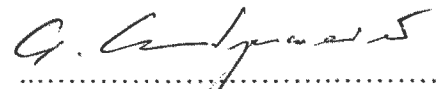
.....

Asst. Prof. Kusol Pootanakit, Ph.D.
Co-Advisor



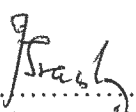
.....

Asst. Prof. Panadda Boonserm, Ph.D.
Co-Advisor



.....

Asst. Prof. Gerd Katzenmeier, Ph.D.
Co-Advisor



.....

Prof. M.R. Jisnuson Svasti, Ph.D.
Dean
Faculty of Graduate Studies



.....

Asst. Prof. Varaporn Akkarapatumwong, Ph.D.
Chair
Doctor of Philosophy Programme in
Molecular Genetics and Genetic Engineering
Institute of Molecular Biology and Genetics

Thesis

Entitled

**FUNCTIONAL CHARACTERISATION OF Asn¹⁸³ IN
THE TRANSMEMBRANE $\alpha 5$ CRITICAL FOR TOXICITY OF
THE *Bacillus thuringiensis* Cry4Ba TOXIN**

was submitted to the Faculty of Graduate Studies, Mahidol University for the degree of
Doctor of Philosophy (Molecular Genetics and Genetic Engineering)

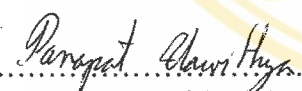
on
10 January, 2006






Miss Supaporn Likitvivatanavong
Candidate

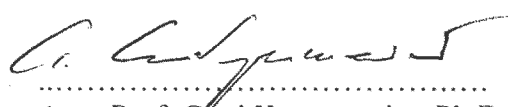
.....
Assoc. Prof. Jaume Torres, Ph.D.
Member

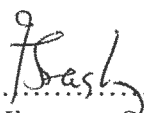

.....
Assoc. Prof. Chanan Angsuthanasombat, Ph.D.
Chair



.....
Dr. Panapat Uawithya, MD., Ph.D.
Member


.....
Asst. Prof. Kusol Pootanakit, Ph.D.
Member


.....
Asst. Prof. Panadda Boonserm, Ph.D.
Member


.....
Asst. Prof. Gerd Katzenmeier, Ph.D.
Member


.....
Prof. M.R. Jisnuson Svasti, Ph.D.
Dean
Faculty of Graduate Studies
Mahidol University


.....
Asst. Prof. Chartchai Krittanai, Ph.D.
Acting Director
Institute of Molecular Biology and Genetics
Mahidol University

ACKNOWLEDGMENT

I wish to express my sincere thanks to my advisor, Dr. Chanan Angsuthanasombat, for his comments, suggestions and constructive criticisms. He always ready to help, lead, and advice me in every way that would bring me success and great development. I am also grateful to my co-advisors, Dr. Gerd Katzenmeier, Dr. Panadda Boonserm, Dr. Kusol Pootanakit and Dr. Panapat Uawithya for their constructive comments and supervision.

I would like to thank all members in the Institute of Molecular Biology and Genetics for their kindly advice and sharing a valuable experience. I am greatly indebted to staffs in the Central Equipment Laboratory, especially for their kindly technical supports and helpful secretary works. I am also indebted to my friends and all previous/present members of *Bt* group who all share any success of this work.

Finally, I am grateful to express my deepest appreciation to my family for their entirely care, love and encouragement. The usefulness of this thesis, I dedicate to my father, my mother and all teachers who have taught me since my childhood.

Supaporn Likitvivatanavong

FUNCTIONAL CHARACTERISATION OF Asn¹⁸³ IN THE TRANSMEMBRANE α 5
CRITICAL FOR TOXICITY OF THE *Bacillus thuringiensis* Cry4Ba TOXIN

SUPAPORN LIKITVIVATANAVONG 4638488 MBMG/D

Ph.D. (MOLECULAR GENETICS AND GENETIC ENGINEERING)

THESIS ADVISORS: CHANAN ANGSUTHANASOMBAT, Ph.D.,
PANADDA BOONSERM, Ph.D., PANAPAT UAWITHYA, MD., Ph.D.,
KUSOL POOTANAKIT, Ph.D., GERD KATZENMEIER, Ph.D.

ABSTRACT

The proposed toxicity mechanism of the *Bacillus thuringiensis* Cry insecticidal proteins involves the penetration of α -helices 4 and 5 to form a lytic pore in the target epithelial cell membrane. In this study, alanine substitutions of selected polar residues (Tyr¹⁷⁸, Gln¹⁸⁰, Asn¹⁸³, Asn¹⁸⁵ and Asn¹⁹⁵) in the hydrophobic helix α 5 of the Cry4Ba mosquito-larvicidal protein were initially conducted *via* PCR-based directed mutagenesis. Upon IPTG induction, all mutant proteins were highly expressed in *Escherichia coli* as cytoplasmic inclusions, with yields similar to the wild-type protoxin. When *E. coli* cells expressing each mutant toxin were tested against *Stegomyia aegypti* mosquito larvae, the larvicidal activity was almost completely abolished for the N183A mutation, whereas the four other mutant toxins showed only a small reduction in toxicity. Additionally, replacements of this critical residue with various amino acids revealed that the uncharged polar residue at position 183 in α 5 is crucial for larvicidal activity. The N183K bio-inactive mutant, which was relatively stable upon inclusion solubilisation and trypsin activation, was purified by size exclusion chromatography and further examined for secondary and tertiary structural elements using far-UV CD and fluorescence spectroscopy in comparison with the wild-type protein. It was found that both of the purified toxins exhibited similar spectra. A membrane perturbation assay on calcein entrapped liposomes revealed that the activity of N183K was significantly lower than that of the wild type. In addition, SDS-PAGE analysis revealed that the N183K mutant was unable to form oligomers in lipid vesicles, unlike the wild-type toxin or the α 4 bio-inactive mutant (R158A). These results suggest that the highly conserved Asn¹⁸³ located in the middle of the transmembrane α 5 plays a crucial role in toxicity as well as in the oligomerisation of the Cry4Ba toxin.

KEY WORDS: *Bacillus thuringiensis*/ / DIRECTED- MUTAGENESIS/
LARVICIDAL ACTIVITY/ MEMBRANE PERTURBATION/
OLIGOMERISATION / POLARITY

126 P. ISBN 974-04-6807-1

การศึกษายาบทบาทหน้าที่ของกรดอะมิโน Asn¹⁸³ ในส่วนเกลียวอัลฟาที่ 5 ที่มีต่อความเป็นพิษ
ของโปรตีน Cry4Ba จากแบคทีเรีย *Bacillus thuringiensis*

(FUNCTIONAL CHARACTERISATION OF Asn¹⁸³ IN THE TRANSMEMBRANE α 5
CRITICAL FOR TOXICITY OF THE *Bacillus thuringiensis* Cry4Ba TOXIN)

สุภาภรณ์ ลิขิตวิวัฒนวงษ์ 4638488 MBMG/D

ปร.ด. (อณูพันธุศาสตร์และพันธุวิศวกรรมศาสตร์)

คณะกรรมการควบคุมวิทยานิพนธ์ : ชนันท อังศุชนสมบัติ, Ph.D., ปนัดดา บุญเสริม, Ph.D.,
ปณัฏฐ เอื้อวิทยา, MD., Ph.D., กุศล ภูชนกิจ, Ph.D., GERD KATZENMEIER, Ph.D.

บทคัดย่อ

แบบจำลองกลไกการออกฤทธิ์ของโปรตีนสารพิษจาก *Bacillus thuringiensis* นั้นเกี่ยวข้องกับเกลียวอัลฟาที่ 4 และ 5 ของโปรตีนที่สามารถทำให้เกิดรูรั่วนบนผนังหุ้มเซลล์บุกระเพาะแมลงตัวอ่อน งานวิจัยนี้ได้ศึกษาหาความสำคัญของกรดอะมิโนแบบมีขั้ว (Tyr¹⁷⁸, Gln¹⁸⁰, Asn¹⁸³, Asn¹⁸⁵ and Asn¹⁹⁵) ภายในเกลียวอัลฟาที่ 5 ที่ยังผลสำคัญต่อฤทธิ์ฆ่าลูกน้ำยุงลาย (*Stegomyia aegypti*) ของโปรตีน Cry4Ba โดยอาศัยวิธีการเปลี่ยนแปลงอินเฉพาะที่ด้วยเทคนิคปฏิกิริยาลูกโซ่โพลีเมอเรส (PCR) จากการศึกษาพบว่าโปรตีนกลายพันธุ์ซึ่งถูกสร้างในเชื้อ *E. coli* มีขนาด 130 กิโลดาลตัน เท่ากับของโปรตีนต้นแบบ (wild-type) และเมื่อนำไปทดสอบความสามารถในการฆ่าลูกน้ำยุงลาย พบว่า การแทนที่กรดอะมิโน ณ ตำแหน่ง Asn¹⁸³ เป็น alanine (N183A) นั้นทำให้โปรตีนสูญเสียความเป็นพิษต่อลูกน้ำยุงลาย เมื่อศึกษาเพิ่มเติมด้วยการแทนที่กรดอะมิโนต่างๆ ณ ตำแหน่ง Asn¹⁸³ สามารถสรุปได้ว่ากรดอะมิโนแบบมีขั้วที่ตำแหน่ง 183 ในเกลียวอัลฟาที่ 5 นั้นมีความสำคัญต่อความสามารถในการฆ่าลูกน้ำยุง ส่วนโปรตีนกลายพันธุ์ N183K ที่สูญเสียความเป็นพิษต่อลูกน้ำยุงลายนั้นยังมีความเสถียรเช่นเดียวกับโปรตีนต้นแบบเมื่อถูกละลายและตัดย่อยด้วยเอนไซม์ trypsin ซึ่งถูกนำไปแยกให้บริสุทธิ์ด้วยวิธีการ size exclusion chromatography เพื่อนำไปศึกษาในด้านโครงสร้างทุติยภูมิ และตติยภูมิ เปรียบเทียบกับโปรตีนต้นแบบ จากการทดลองพบว่าโปรตีนทั้งสองชนิดแสดงออกในด้านโครงสร้างคล้ายคลึงกันทุกประการ และเมื่อทดสอบความสามารถในการทำให้ liposomes แตก พบว่าโปรตีนกลายพันธุ์นั้นไม่มีความสามารถดังเช่น โปรตีนต้นแบบ และเมื่อวิเคราะห์โดยวิธีการ SDS-PAGE พบว่าโปรตีนกลายพันธุ์ N183K ไม่สามารถรวมตัวกันเป็น oligomeric complex บน lipid vesicle ได้ ซึ่งต่างจากของโปรตีนต้นแบบ หรือของโปรตีนกลายพันธุ์ R158A ที่มีการเปลี่ยนแปลงกรดอะมิโนที่เกลียวอัลฟาที่ 4 ทั้งนี้จากการศึกษาทั้งหมดสามารถเสนอได้ว่ากรดอะมิโน asparagine ณ ตำแหน่ง 183 มีบทบาทสำคัญต่อการออกฤทธิ์ฆ่าลูกน้ำยุง ซึ่งน่าจะเกี่ยวข้องกับขบวนการเกิด oligomerisation ของโปรตีนสารพิษ Cry4Ba

CONTENTS

	Page
ACKNOWLEDGEMENT	iii
ABSTRACT	iv
LIST OF TABLES	x
LIST OF FIGURES	xi
LIST OF ABBREVIATIONS	xv
CHAPTER	
I. INTRODUCTION	1
OBJECTIVES	2
II. LITERATURE REVIEW	3
1.1 <i>Bacillus thuringiensis</i> δ -endotoxins	3
1.2 The <i>Bt</i> Cry gene family	4
1.3 Structure-function relationships of the Cry proteins	7
1.4 Mechanism of action of the <i>Bt</i> Cry toxins	9
1.4.1 Inclusion solubilisation and proteolytic activation	9
1.4.2 Receptor recognition and the removal of α helix-1 region	13
1.4.3 Toxin oligomerisation	16
1.4.3.1 Pre-pore oligomerisation	16
1.4.3.2 Intermolecular interactions	17
1.4.4 Toxin-induced pore formation	20
1.5 Alkalisiation of larval mosquito midgut and the role of midgut proteases	23
III. MATERIALS AND METHOD	25

CONTENTS (continued)

	Page
3.1 Materials	
3.1.1 Chemicals	25
3.1.2 Enzymes	25
3.1.3 Bacterial strain	26
3.1.4 Recombinant plasmid	26
3.1.5 Synthetic oligonucleotide primers	28
3.1.6 Culture media	29
3.1.7 Miscellaneous	29
3.2 Methods	30
3.2.1 Plasmid DNA extraction	30
3.2.2 Agarose gel electrophoresis of DNA	30
3.2.3 Site-directed mutagenesis	31
3.2.4 Digestion the PCR products	35
3.2.5 Preparation of competent cells	35
3.2.6 Transformation of plasmid DNA into competent cells	35
3.2.7 Screening for mutant plasmids	36
3.2.8 DNA sequencing analysis	36
3.2.9 Expression of toxins	36
3.2.10 Sample preparations	37
3.2.11 SDS-polyacrylamide gel electrophoresis analysis	37
3.2.12 Partial purification of protein inclusions	37

CONTENTS (continued)

	Page
3.2.13 Protein concentration assays	38
3.2.14 Solubilisation of toxin inclusions and proteolytic processing of protoxins	38
3.2.15 Gut juice extraction	38
3.2.16 Mosquito larvicidal activity assays	38
3.2.17 Purification of Cry4Ba toxins and its mutants	39
3.2.18 Circular dichroism measurement	39
3.2.19 Intrinsic fluorescence measurement	40
3.2.20 Membrane perturbation assays	40
3.2.20.1 Preparation of entrapped-calcein liposomes	40
3.2.20.2 Calcein release assays	41
3.2.21 Oligomerisation study	41
3.2.21.1 Liposome preparation	41
3.2.21.2 Liposome concentration assays	42
3.2.21.3 Incorporation of toxin to liposome	42
3.2.21.4 Western blotting	42
IV RESULT I: Mutagenesis of Cry4Ba	44
4.1 Constructions of the alanine-substituted Cry4Ba mutant plasmids	44
4.2 Expression of the alanine-substituted Cry4Ba mutant toxins	45
4.3 Solubilisation and proteolytic processing of the alanine-substituted Cry4Ba mutant toxins	45

CONTENTS (continued)

	Page
4.4 Mosquito-larvicidal activity of the alanine-substituted Cry4Ba mutant toxins	45
4.5 Constructions of Cry4Ba mutant plasmids substituted at Asn ¹⁸³	58
4.6 Expression of Cry4Ba mutant toxins substituted at Asn ¹⁸³	58
4.7 Solubilisation of the Cry4Ba mutant inclusions substituted at the positions 183	59
4.8 Larvicidal activity of Cry4Ba-N183 mutant toxins	59
4.9 Mutagenesis of the hydrophobic residues in $\alpha 5$ of Cry4Ba toxin	77
V RESULT II: Characterisation of Cry4Ba-N183 mutant toxins	82
5.1 Purification of Cry4Ba and Asn ¹⁸³ mutant toxins	82
5.2 Structural determination of Cry4Ba and Asn ¹⁸³ mutant toxins	82
5.2.1 Secondary structure of Cry4Ba and Asn ¹⁸³ mutant toxins	82
5.2.2 Tertiary structure of Cry4Ba and Asn ¹⁸³ mutant toxins	82
5.3 Membrane perturbing activity of Cry4Ba and Asn ¹⁸³ mutant toxins	86
5.4 Oligomerisation study of Cry4Ba and Asn ¹⁸³ mutant toxins	86
VII DISCUSSIONS	94
VIII CONCLUSION	106
REFERENCES	108
APPENDIX	121
BIOGRAPHY	126

LIST OF TABLES

Table		Page
1	Temperature cycling parameters for site-directed mutagenesis	33
2	Annealing temperature (T_a) for each mutants	34



LIST OF FIGURES

Figure		Page
1	Positions of conserved blocks among Cry proteins	6
2	The ribbon illustrations of crystallographic resolved Cry toxins	8
3	Ribbon representation of the Cry4Ba structure	10
4	The proposed mechanism of Cry toxins	11
5	The proposed mechanism of Cry1A toxins	15
6	AFM images of lipid bilayers containing the activated Cry4Ba toxin prepared from Langmuir-Blodgett transfer	19
7	An umbrella model for Cry toxins	22
8	Larval midgut of <i>Stegomyia aegypti</i>	24
9	Physical map of the plasmid pMU388	27
10	Overview of QuickChange Site-Directed Mutagenesis method	32
11	Sequence alignment and ribbon representation of Cry4Ba- α 5	46
12	PCR amplification of Cry4Ba mutant plasmids: pY178A, pQ180A, pN183A, pN185A, and pN195A	47
13	Digested PCR amplification products of Cry4Ba wild-type and its mutant plasmids: pY178A, pQ180A, pN183A, pN185A, and pN195A with <i>DpnI</i>	48
14	Restriction digestion and DNA sequence analysis of pY178A	49
15	Restriction digestion and DNA sequence analysis of pQ180A	50
16	Restriction digestion and DNA sequence analysis of pN183A	51

LIST OF FIGURES (continued)

Figure	Page
17 Restriction digestion and DNA sequence analysis of pN185A	52
18 Restriction digestion and DNA sequence analysis of pN195A	53
19 Expression of the Cry4Ba wild-type toxin and Y178A, Q180A, N183A, N185A, N195A mutant toxins	54
20 Solubility of Cry4Ba wild-type and its mutant inclusions	55
21 Trypsinised products of the Cry4Ba wild-type toxin and Y178A, Q180A, N185A, N195A mutant toxins	56
22 Larvicidal activity of the wild-type Cry4Ba and its alanine-substituted mutant toxins	57
23 PCR amplification of Cry4Ba mutant plasmids: pN183Q, pN183R, pN183T, pN183H, pN183D, pN183K, pN183F, and Y267A	61
24 Restriction digestion and DNA sequence analysis of pN183Q	62
25 Restriction digestion and DNA sequence analysis of pN183R	63
26 Restriction digestion and DNA sequence analysis of pN183T	64
27 Restriction digestion and DNA sequence analysis of pN183H	65
28 Restriction digestion and DNA sequence analysis of pN183D	66
29 Restriction digestion and DNA sequence analysis of pN183K	67
30 Restriction digestion and DNA sequence analysis of pN183F	68
31 Restriction digestion and DNA sequence analysis of pY267A	69
32 Expression of the Cry4Ba wild-type toxin and N183Q, N183R, N183T, N183F, N183K, Y267A mutant toxins	70

LIST OF FIGURES (continued)

Figure	Page
33 Expression of the Cry4Ba wild-type toxin and N183H, N183D mutant toxins	71
34 Solubility of Cry4Ba wild-type and its N183 mutant inclusions <i>in vitro</i>	72
35 Trypsinised products of the Cry4Ba toxin and N183K, N183Q mutant toxins	73
36 Solubility of Cry4Ba and its mutant inclusion using gut juice extraction	74
37 Larvicidal activity of the wild-type Cry4Ba and its mutants substituted at the position 183	75
38 Larvicidal activity using toxin inclusions of Asn ¹⁸³ mutants	76
39 PCR amplification of Cry4Ba mutant plasmids: pV181S and pA182S	77
40 DNA sequence analysis of pV181S and pA182S	78
41 DNA sequence analysis of pV181S/A182S	79
42 Expression of the Cry4Ba toxin and V181S, A182S and V181S/A182S mutant toxins	80
43 Larvicidal activity of the wild-type Cry4Ba and its mutants substituted at the position 181 and 182	81
44 Chromatogram and SDS-PAGE analysis of purified Cry4Ba toxin and N183K mutants	83
45 CD spectra of wild-type Cry4Ba and N183K mutant	84
46 Intrinsic spectra of the wild-type Cry4Ba toxin and the N183K mutant toxin	85
47 Effects of the Cry4Ba toxin on calcein release from liposomes	87
48 The relative release activities of the wild-type Cry4Ba and the Asn ¹⁸³ mutant, with varying concentrations	88
49 Oligomerisation state of the Cry4Ba wild-type in the varying of time incubation and temperature	89

LIST OF FIGURES (continued)

Figure	Page
50 Western blot analysis of the oligomeric of the Cry4Ba toxin	90
51 Oligomerisation state of the Cry4Ba wild-type in the presence of liposome and glutaraldehyde cross-linking agent	91
52 Oligomerisation state of the N183K and R158A mutant toxins	92
53 Oligomerisation state of the N183K mutant in the presence of liposome and DTT with the varying of glutaraldehyde concentrations	93
54 Hydrogen bonding between Asn ¹⁸³ and Tyr ²⁶⁷ in Cry4Ba	96
55 The topological maps of interhelical H-bonds (top view) of the TM region of several transmembrane proteins	103
56 Schematic views of trimeric association of Cry4Ba	104
57 Helical wheel projections of helix 5 of Cry4Ba with three different pitches	105

LIST OF ABBREVIATIONS

%(V/V)	Percent volume by volume
%(W/V)	Percent weight by volume
%(W/W)	Percent weight by weight
Amp.	Ampicillin
BASED	Bis-[β -(4-azidosalicylamido)ethyl]disulfide
BBMV	Brush border membrane vesicle
bp	Base pair
BSA	Bovine serum albumin
<i>Bt</i>	<i>Bacillus thuringiensis</i>
<i>Bti</i>	<i>Bacillus thuringiensis</i> subsp <i>israelensis</i>
°C	Degree Celsius
ca	Approximately
Ch	Cholesterol
Cry	Crystal protein
Cyt	Cytolytic protein
DTT	Dithiothreitol
<i>E. coli</i>	<i>Escherichia coli</i>
EDTA	Ethylenediaminetetraacetic acid
et al.	and others
hr(s)	Hour(s)
IPTG	Isopropyl- β -D-thiogalactopyranoside

LIST OF ABBREVIATIONS (continued)

kDa	Kilodalton(s)
LB	Luria-Bertani medium
μg	microgram
μl	Microlitre(s)
μM	Micromolar
μm	Micrometre
M	Molar
mg	Milligram(s)
ml	Millilitre(s)
mM	Millimolar
ng	Nanogram
nM	Nanomolar
nm	Nanometre
OD	Optical density
PC	Phosphatidylcholine
PE	Phosphatidylethanolamine
PLBs	Planar Lipid Bilayers
Rpm	round per minutes
SDS-PAGE	Sodium dodecyl sulphate polyacrylamide gel electrophoresis
TEMED	N,N,N',N' - tetramethylenediamine
Tris	Tri(hydroxymethyl)- aminoethane

CHAPTER 1

INTRODUCTION

As a member of α -helical channel forming toxins, *Bacillus thuringiensis* Cry δ -endotoxins are present in the form of inactive protoxins as crystalline inclusion bodies (1). Upon ingestion by susceptible larvae, these insecticidal inclusions are solubilised and subsequent proteolytic activation to transform the initially soluble protoxins into a structure that is able to insert into the membrane. By analogy with proposals for the pore-forming domain of colicins (2), the conformational change of the Cry toxins was envisaged to expose a relatively non-polar helix hairpin from pore-forming domain to initiate membrane penetration (3). Currently, the umbrella model best explains the Cry mechanism of toxicity. It was proposed that $\alpha 4$ and $\alpha 5$ of the pore-forming domain (*see* more details in Chapter II) would insert into the membrane as a helical hairpin in an antiparallel manner, while the other helices would lie on the membrane surface like the ribs of an umbrella (4). Concrete with evidence of the 130-kDa Cry4Ba toxin that substitutions with proline in the middle of five helices (i.e., $\alpha 3$, $\alpha 4$, $\alpha 5$, $\alpha 6$, $\alpha 7$) revealed only $\alpha 4$ and $\alpha 5$ being important for toxicity and likely to be involved in membrane pore formation (5, 6). A number of studies suggested that $\alpha 4$ which lines the pore lumen is essential for toxicity and passage of ions through the channel (7, 8). Compared to the co-inserting $\alpha 5$ which is relatively hydrophobic and having more conserved amino acid sequence. It has been shown that $\alpha 5$ of Cry1Ab and Cry1Ac seems to be very important for membrane insertion as well as oligomerisation (9, 10). Although, it has been postulated that all Cry toxins should adopt a similar folding pattern and they are likely to share the same pore-forming mechanism (11, 12), there is limited information for the pore-forming process, especially the identity of an oligomeric complex in the membrane.

In the study of helix-helix interactions contributing to protein oligomerisation, the force within lipid membranes which is considered to be one of the major contributors is an interhelical polar interaction (13). A number of evidence suggested

that polar residues in a transmembrane helix could provide a strong driving force for oligomer formation (14, 15). Moreover, the mutation of these polar residues essentially eliminated oligomerisation of the membrane-soluble peptide (16).

In this thesis, these attempts were made to study a possible role of polar residues in the transmembrane $\alpha 5$ of Cry4Ba. This would provide detailed information leading to molecular understanding of the interactions between transmembrane helices *via* certain polar side chains which are critical for toxicity. Therefore, the objectives of this study were:

- (1) To identify a critical residue in $\alpha 5$ of the Cry4Ba toxin for larvicidal activity by replacing polar amino acids with alanine *via* site-directed mutagenesis.
- (2) To investigate the structural significance of the identified critical residues by functional group substitutions.
- (3) To structurally and functionally characterise the 65-kDa activated Cry4Ba toxin and its inactive mutant by using far-UV circular dichroism (CD) and fluorescence spectroscopy, membrane perturbation assays and SDS-PAGE analysis.

CHAPTER 2

LITERATURE REVIEW

1.1 *Bacillus thuringiensis* δ -endotoxins

Bacillus thuringiensis (*Bt*) is a rod shaped, aerobic, spore-forming bacterium. It is related to other *Bacillus* species such as *B. cereus*, the causative agent of some types of food poisoning, and *B. anthracis*, the causative agent of anthrax. During sporulation, *Bt* produces protein crystals known as δ -endotoxins which are toxic to insect larvae. The *Bt* species comprises of diverse strains with different toxin profiles, and the range of toxins can affect several different types of insect larvae.

Bt was first isolated in 1901 by a Japanese biologist, S. Ishiwata. He identified the bacterium as the causal agent of a disease of silkworms. Subsequently in 1915 a German scientist, named Ernst Berliner, isolated this toxin from a dead Moth in Thuringen region of Germany. And thus the name *Bacillus thuringiensis*. (17). In 1938, commercial production of *Bt* as a spray for insect control began in France, and the first commercial *Bt* formulations were made available for field testing in the USA in 1958 (18). Until the 1970s, it was generally accepted that lepidopteran insects (moths and butterflies) were the only targets of *Bt*. New *Bt* markets were opened by the discovery in 1976 of *israelensis* subspecies, which is toxic to larvae of mosquitoes and black flies (known as sand flies in New Zealand), and the *tenebrionis* subspecies which is toxic to several beetle species. In the 1980s, commercial interest in *Bt* grew as alternatives to synthetic pesticides were sought. The use of *Bt* toxin genes in genetically modified plants for pest control became an established field of research in the mid-1980s. From the mid-1990s, a number of plants that were genetically modified to express the *Bt* toxin have become increasingly common, and are now grown widely in the USA and other countries, though their use remains controversial (19).

1.2 The *Bt* Cry gene family

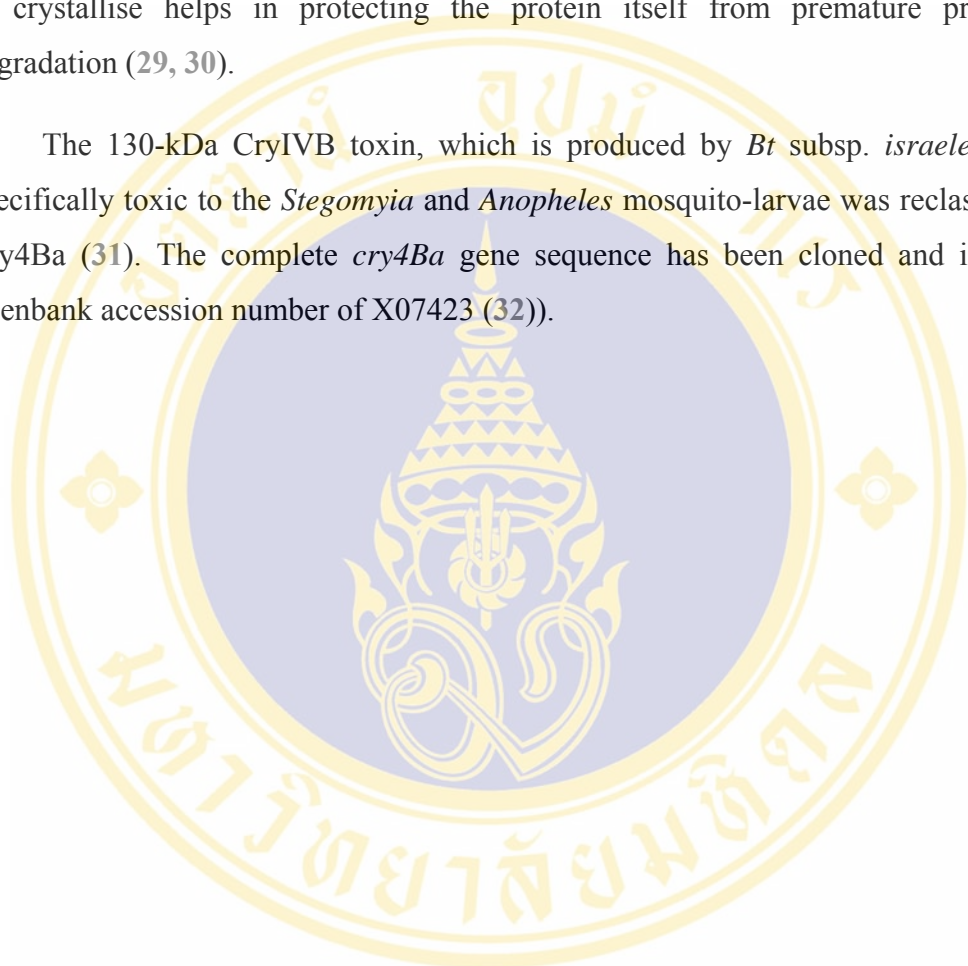
Strains of *Bt* producing different larvicidal proteins are variously toxic to insect larvae in the orders Diptera (mosquitoes and flies), Lepidoptera (moths and butterflies), Coleoptera (beetles and weevils) and Hymenoptera (wasps and bees) (20-22). For example, the δ -endotoxins produced by *Bt* subsp. *israelensis* are highly active against the larvae of mosquito and blackfly which are vectors of several tropical diseases (22).

Bt δ -endotoxins belong to two distinct gene families named Cry (crystal) and Cyt (cytolytic) toxins. Cry proteins were originally classified on the basis of the insect order to which the species they affect belong (1). However, as the number and variety of Cry proteins grew, this classification was abandoned for the current system based on amino acid sequence similarity. Proteins with less than 45% sequence homology are separated in the primary rank, while further separation at the secondary and tertiary ranks is based on 78% and 95% homology respectively. Recently, De Maadje *et al.* provided a useful summary of the putative evolutionary relationships between the different Cry genes and their phylogenetic interactions (36). Additionally, Roman numerals have been exchanged for Arabic numerals in the primary rank (e.g., CryIAa to Cry1Aa) to better accommodate the large number of expected new sequences. In this new nomenclature, 133 crystal proteins comprising 24 primary ranks are systematically arranged.

The common characteristic of the *cry* genes is their expression during the sporulation stage. Their gene products generally accumulate in the mother cell compartment to form a crystal inclusion that can account for 20-30% of the dry weight of the sporulated cells. The high level of synthesis and coordination with the stationary phase are controlled by a variety of mechanisms occurring at the transcriptional, posttranscriptional and posttranslational levels (22, 29). At the transcriptional level, the development of sporulation is controlled by successive activation of sigma factors. At the posttranscriptional level, the stability of the mRNA is enhanced by the formation of a stemloop structure during termination of transcription. This protects the mRNA from the activity of exonucleases present in the cell from degrading the mRNA. The 5' end of the mRNA is protected due to the presence of the perfect Shine-

Dalgarno sequence designated as STAB-SD. The interaction with the 16s rRNA of the 30s subunit of the ribosome confers stability to the mRNA. At the posttranslational level, these proteins form crystalline inclusions in the mother cell compartment. Depending on the protoxin composition, the crystals have various forms. This ability to crystallise helps in protecting the protein itself from premature proteolytic degradation (29, 30).

The 130-kDa CryIVB toxin, which is produced by *Bt* subsp. *israelensis* and specifically toxic to the *Stegomyia* and *Anopheles* mosquito-larvae was reclassified as Cry4Ba (31). The complete *cry4Ba* gene sequence has been cloned and identified (Genbank accession number of X07423 (32)).



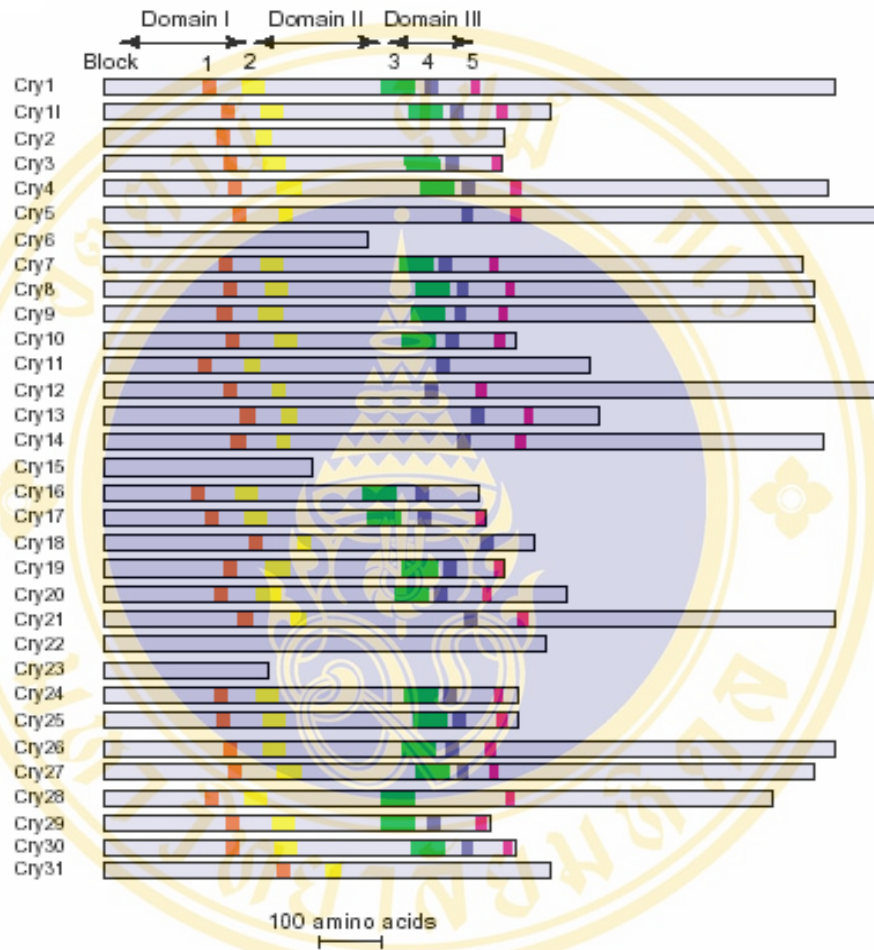


Figure 1: Positions of conserved blocks among Cry proteins.

The schematic shows the five conserved blocks of Cry toxins (22).

1.3 Structure-function relationships of the Cry proteins

To date, tertiary structures of five different Cry toxins, Cry1Aa, Cry2Aa, Cry3Aa, Cry3Bb and, recently, Cry4Ba, have been determined by X-ray crystallography (26, 32, 3, 34, 35). Despite the differences in their insect specificity and the comparatively low amino-acid sequence identity between these proteins, alignment of the Cry toxins reveals the five conserved sequence blocks which are common to a large majority of the Cry proteins. The presence of these conserved blocks indicates that the topology of all Cry toxins would be similar (36, 37) (**Fig. 1-3**). The Cry toxin structures consist of three distinct domains.

The N-terminal domain (domain I) is a bundle of seven α -helices in which the central helix ($\alpha 5$) is relatively hydrophobic and is encircled by six other amphipathic helices. This domain is likely to be transmembrane pore-forming apparatus in which five of the helices ($\alpha 3$ - $\alpha 7$) are more than 30Å long and could span the hydrophobic region of lipid bilayers. Atomic Force Microscopy (AFM) imaging suggests that the pores are composed of four subunits surrounding a 1.5 nm diameter central depression (38). Domain II appears as a triangular column of three anti-parallel β -sheets. Domain III contains anti-parallel β -strands in the form of a beta sandwich. Though the structure of domain III has been elucidated, its function remains obscure.

From amino acid sequence alignments (**Fig. 1**), five conserved blocks can be described as; block 1 corresponds to $\alpha 5$ of domain I and block 2 consists of $\alpha 7$ of domain I and the first β -strand of domain II. The middle part of the toxin does not contain any conserved regions and shows hypervariable sequences. Block 3 contains the last β -strand of domain II. A conserved alternative arginine sequence tract in domain III lies in block 4. Block 5 is located at the end of domain III. The presence of five conserved blocks in all Cry toxins indicates that the topology of all these toxins could be based upon the resolved Cry1Aa, Cry2Aa, Cry3Aa, Cry3Bb and Cry4Ba consensus fold. Consequently, aligning this sequence with those of known 3D structures would make a plausible prediction of the secondary structure for the other Cry toxins.

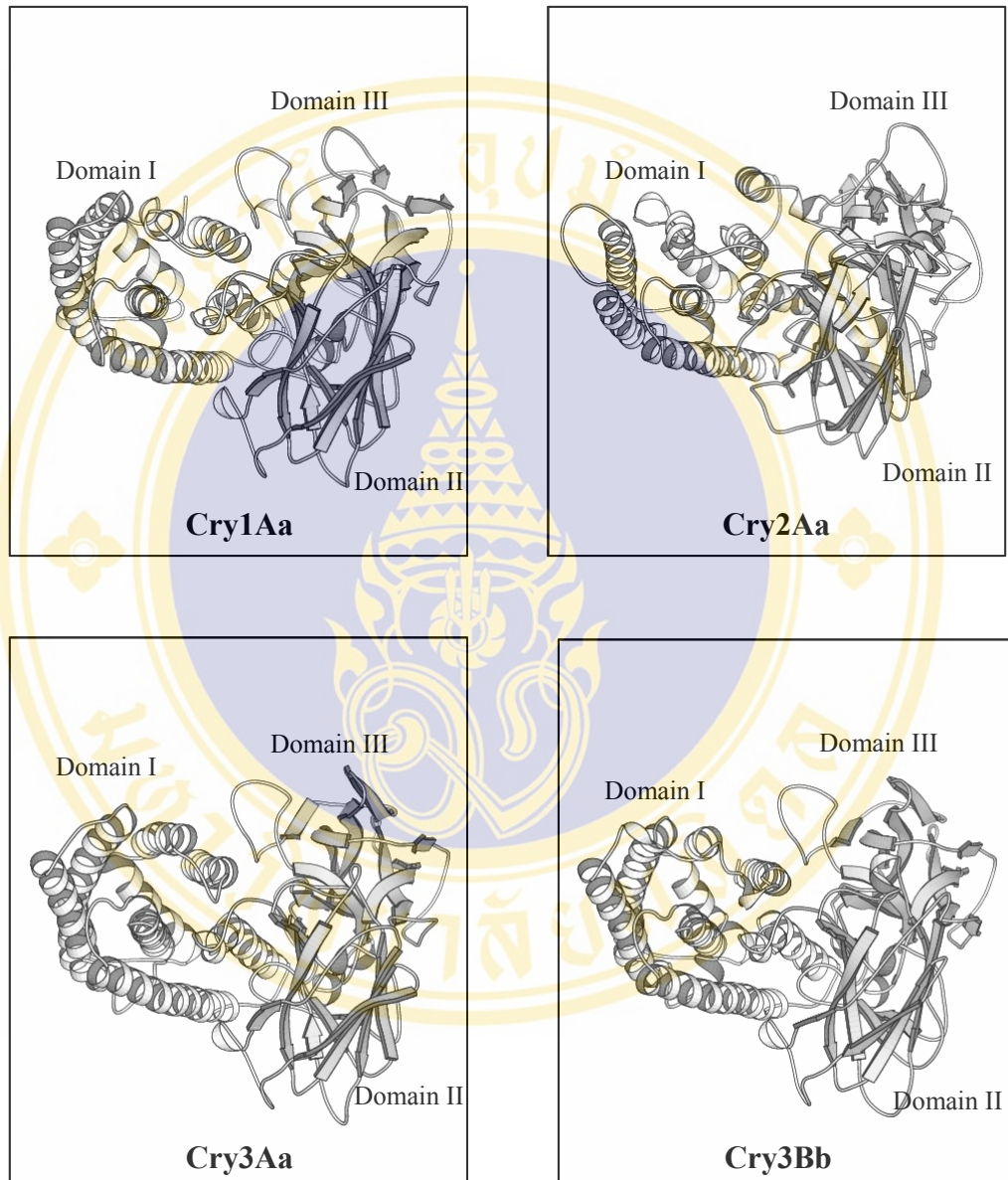


Figure 2: The ribbon illustrations of crystallographic resolved Cry toxins.

The figure illustrates top view of 3D structures which were resolved by X-ray crystallography. All four structures, Cry1Aa (26), Cry2Aa (33), Cry3Aa (3) and Cry3Bb (34), show high similarity of their overall structures with the three-domain organizations.

1.4 Mechanism of action of the *Bt* Cry toxins

Although several *Bt*-Cry crystal structures have been known for more than 10 years, the mode of action which involves insertion into the membrane and pore formation is still unclear. Generally, *Bt* toxins are present in the form of inactive protoxins as inclusion bodies (1). Upon ingestion by susceptible larvae, the inclusions are solubilised in the alkaline pH of larval midgut. The solubilised protoxins are cleaved *in vivo* by gut proteases to release active toxins. The activated toxin then binds to a specific receptor on the epithelial cells lining in the midgut before insertion into the membrane and creating pores (39). The resulting lytic pores allows ions, such as K^+ , and small molecules (40) to pass through the membrane, thus disrupting the insect ability to regulate osmotic balance (Fig. 4). Histologically, the toxin-induced pores cause swelling and disruption of the epithelial cells (41). Due to massive water uptake, the epithelial cells eventually lyse and/or slough off into the midgut lumen. The midgut becomes paralysed and the insect larvae ultimately stop feeding and subsequently starve to death with concomitant septicemia (42, 43).

1.4.1 Inclusion solubilisation and proteolytic activation

Unlike the mammalian gastrointestinal tract, dipteran and lepidopteran insect larvae have an alkaline midgut with an approximate pH of 9.5 or above. This pH range fosters the solubilisation of the protoxin crystals. The solubilised protoxins are subsequently cleaved *in vivo* by gut proteases to release active toxins. The toxin activation can be simulated *in vitro* by incubating the protoxins with larval gut extracts or trypsin (44). Upon ingestion by a susceptible insect larvae, the protoxin is activated through the proteolytic removal of some residues at N-terminal and approximately half of the remaining protein from the C-terminus. The role of the C-terminal extension to the active toxin is believed to be in the formation of crystalline inclusion bodies within the bacterium and is dispensable for toxicity (45).

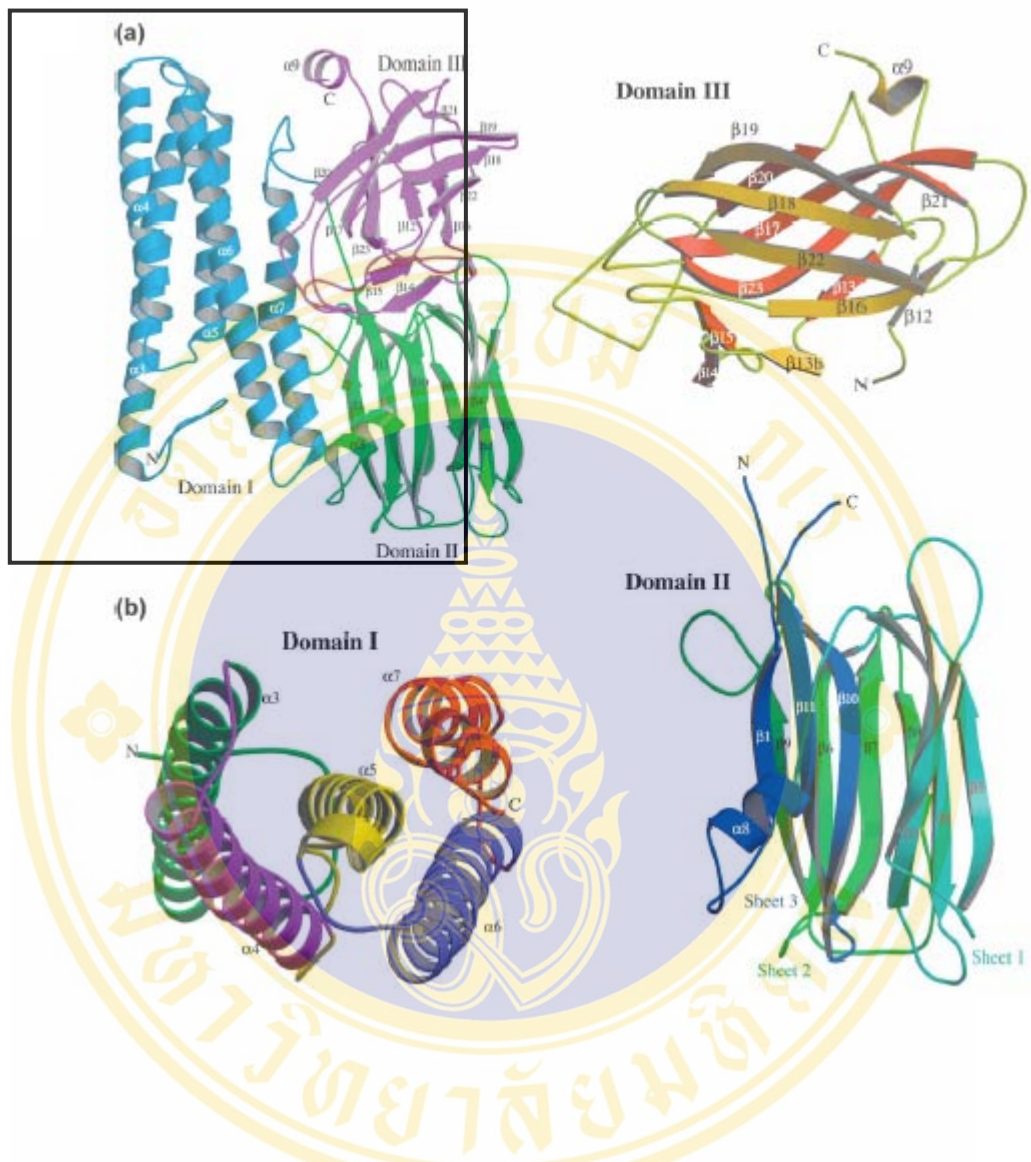


Figure 3: Ribbon representation of the Cry4Ba structure.

The figure illustrates side view of 3D structure of Cry4Ba toxin with three domain organisation. In domain I the helix bundle contains only the helices $\alpha 3$ - $\alpha 7$. The N-terminal helices $\alpha 1$ - $\alpha 2$ b, absent due to protolysis during crystallization, appear non-essential to toxicity (35).

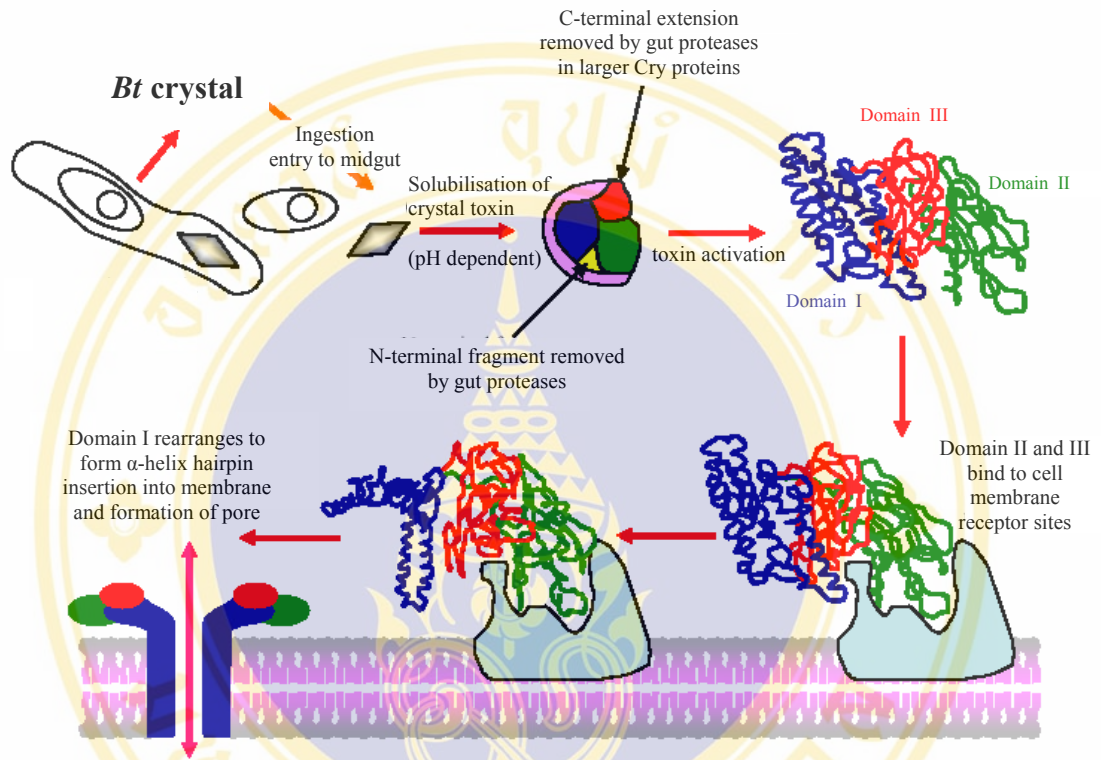


Figure 4: The proposed mechanism of Cry toxins.

The figure shows the process of solubilisation, proteolysis and receptor binding of Domain II and III, followed by insertion and pore formation of Domain I of *Bt* toxin. Adapted from de Maagd et al (36).

The Cry toxins can be divided into 2 groups based on the size of protoxins and their proteolysis processing. In the large Cry protoxins of ca. 130 kDa, e.g. Cry1Aa, Cry4Aa or Cry4Ba, approximately half of the molecule is removed from C-terminus during proteolytic activation (ca. 600 amino acids). Activation of these large toxins is also accompanied by removing about 30 residues from the N-terminus (46). However, the interhelical cleavage site is also required for toxin activation of the dipteran-specific Cry4 toxins. *In vitro* proteolytic activation of the 130-kDa Cry4 toxin with mosquito larval gut extracts or trypsin showed that the protoxins were processed to two major stable fragments of 46-48 kDa and 18-20 kDa, in addition to the removal of the C-terminal half of the protoxins. These two fragments were produced by the cleavage at Arg203 of Cry4Ba and Arg235 of Cry4Aa locating in the solvent exposed loop linking helices 5 and 6 within the pore forming domain I (48).

For the small Cry toxins (ca. 70 kDa) e.g. Cry2Aa, Cry3Aa or Cry11Aa, activation occurs by cleaving mostly at the N-terminus where approximately 50 residues are removed. The activation occurs with little or no proteolysis at their C-terminal. The resistance in cleavage is thought to be due to the location of the C-terminus in the middle strand (β 23) of a buried β -sheet in Domain III. Some studies showed that the *in vitro* activation of the 70-kDa Cry3Aa toxin from *Bt* subsp. *tenebrionis* 1911 yielded a ca. 65-kDa trypsin-resistant protein (44, 49).

Little is known about the role of the N-terminal peptide and whether its removal is important in the mechanism of action of the toxin. However, indirect evidence for a possible role of the N-terminal fragment in modulating binding of the toxin has come from the solution of the structure of the Cry2Aa toxin (34). The structure revealed that the N-terminal region masks a region of the toxin believed to be involved in the interaction between the toxin and the brush border membrane of the target insects. Bravo *et al.* showed that the mutant toxin Cry1Ac, which is not cleaved at the N terminus during proteolytic activation with trypsin, was found to be incapable of forming pores in *Manduca sexta* brush border membrane vesicles *in vitro* and had reduced insecticidal activity *in vivo* (50). These results suggest that proteolytic removal of the N-terminal peptide of Cry1Ac is an important step in toxin activation.

1.4.2 Receptor recognitions and the removal of α -helix 1 region

It is believed that the activated toxins would diffuse through the peritrophic membrane and then bind to specific receptors located on the apical membrane of the midgut epithelial cells of the target insect larvae (51-54). It has been reported that midgut brush-border membranes (BBMVs) of Cry-resistant insect larvae were shown to have reduced binding affinity to their specific Cry proteins. So far, loss or mutational changes of Cry receptors in midgut epithelial cells were thought to be involved in Cry-resistance development (55-57).

Nowadays, at least two proteins have been identified as specific receptors *i.e.* aminopeptidase-N (APN) and cadherin-like proteins, which both are glycoproteins. In *Manduca sexta*, Cry1Aa, Cry1Ab and Cry1Ac proteins have been shown to bind to a 120-kDa APN (58, 59) and to a 210-kDa cadherin-like protein (Bt-R₁) (60, 61). In *Bombyx mori*, Cry1Aa binds to a 175-kDa cadherin-like protein (Bt-R₁₇₅) (62, 63) and to a 120-kDa APN (64). In *Heliothis virescens*, Cry1Ac binds to two proteins of 120 and 170 kDa, both identified as APN (65, 66). In *Plutella xylostella* and *Lymantria dispar* APNs were identified as Cry1Ac receptors (67, 68). It seemed that the interaction between toxin and its receptor can be complex. There is evidence indicated that binding affinities between APN (100 nM) and Bt-R₁ (1 nM) to the Cry1Ab toxin are different, suggesting that binding to Bt-R₁ might be the first event in toxin recognition (58, 59). Recently, it has been confirmed that both receptor proteins were sequentially involved in Cry1A toxicity. Binding to cadherin-like proteins probably be the initial line in the interaction with the microvilli membrane. Then, APNs might be another target of the toxin before insertion into the membrane (69).

In mosquitoes, the nature and identity of the Cry toxin-receptor protein is unknown. Using RT-PCR, the result showed that two isoforms of the APN transcripts in the *S. aegypti* mosquito larval midgut were identified (70). Krieger et al. (71) isolated proteins with molecular mass of 65 and 62 kDa from brush border membranes of *S. aegypti* larvae. Using a ligand blotting technique, they showed that the binding of these proteins to the biotinylated toxins is reversible and that the two toxins (Cry4Ba and Cry11Aa) compete with each other for binding to the two binding proteins. These proteins are likely to be Cry4Ba and Cry11Aa toxin receptors in gut epithelial cells of *S. aegypti* larvae. However the function of these proteins is not clear.

Following binding, the evidence of further proteolytical cleavages of the N-terminal region were observed. For instances, Aronson et al. (9) showed that about 60 amino acids were removed from the Cry1Ac amino terminus including primarily helix 1 after binding to vesicles from the midguts of *M. sexta* larvae. Similar results were obtained for Cry1Ac protoxins activated with midgut juice from *Pieris brassica* (72) and for Cry1Ab protoxins (73, 74) and the highest *in vitro* pore formation activity was observed after α -helix 1 was removed, suggesting that this helix 1 is dispensable for Cry1A activity (73). In addition, the N-terminal region of the oligomeric form of the Cry1Ab was found to correspond to the removing of helix 1, whereas of the monomeric form corresponds to the beginning of helix 1 (74), suggesting that further proteolytic processing may serve to remove regions that sterically hinder assembly process of the Cry1A toxins. As in Cry4Ba toxin, the N-terminal helices α 1- α 2b, which is absented due to proteolysis during crystallisation, appear non-essential to toxicity (35). Recently, it has been shown that cleavage of helix 1 of Cry1Ab might occurred after first binding to cadherin-like proteins. The result of removal of this helix could promote the formation of an oligomeric structure before providing insertion through the membrane (69) (Fig. 5).

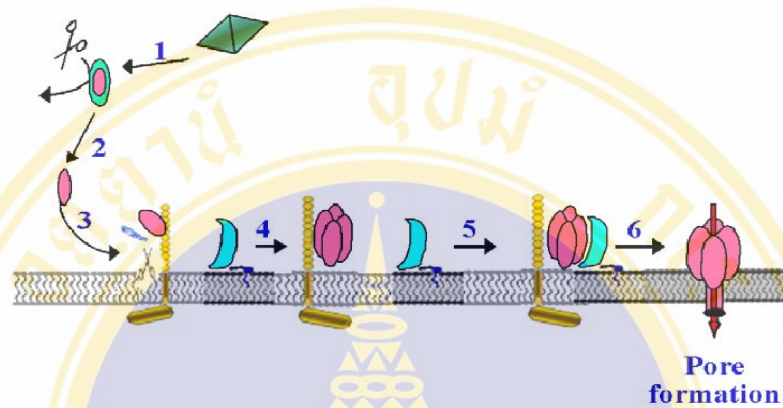


Figure 5 The proposed mechanism of Cry1A toxins (69).

The figure shows toxicity mechanism of Cry1A proteins. (1) Crystal solubilisation; (2) protoxin proteolytic activation; (3) monomer binding to cadherin-like protein and cleavage of helix1; (4) pre-pore oligomeric structure formation; (5) oligomer binding to aminopeptidase N and mobilisation to lipid raft domain; (6) pore formation.

1.4.3 Toxin oligomerisation

Following binding, it is proposed that at least part of the Cry toxins inserts into the membrane resulting in pore formation. So far, the intermolecular interaction of toxin monomers is a necessary step for toxicity. However, it is controversial and less well understood whether how and when the oligomeric complex might be occurred. Recently, it has been performed a structural study of the Cry4Ba toxin within lipid membranes *via* electron microscopy, and found that the monomer toxins were mixed together with the oligomeric forms (Puey Ounjai: personal communication). This could suggest that toxin oligomerisation and pore formation might occur after or simultaneously with membrane insertion.

1.4.3.1 Pre-pore oligomerisation

However, to date, there are some evidence to support the toxin oligomerisation formed after receptor binding and prior to membrane insertion. Gomez et al. (74) showed that the Cry1Ab toxin, which was activated to a 250-kDa oligomer, had the capability of membrane insertion as judged by 8-anilino-1-naphthalenesulfonate binding (ANS) comparing with the Cry1Ab monomers. The ANS specifically reacts with solvent-accessible clusters of nonpolar residues, suggesting that Cry1Ab is accompanied by the exposure of hydrophobic surfaces, forming a pre-pore structure that is insertion competent. They also provided the supported evidence that K⁺ permeability in BBMV isolated from *M. sexta* was rather high for the oligomeric structure of the Cry1Ab toxin, suggesting that there was a better interaction of oligomeric structures with the membrane.

Rausell et al. (75) had analysed the structural changes presented by the Cry1Ab toxin upon membrane insertion at which the location and environment of tryptophans (Trp) in the solution and membrane-bound forms of pure monomeric and oligomeric structures were monitored using intrinsic Trp fluorescence. Fluorescence quenching of the toxin monomer in solution revealed the varying degrees of Trp burial within the protein interior, whereas the membrane-bound form resulted in a conformational change leading to further concealing of the Trp residues at which principally located close to the membrane-water interface. In addition, studies of ionic currents in planar lipid bilayers revealed that the oligomeric structure could form channels with kinetics

different from those of the monomer. The oligomers could produce stable channels with a high probability of being open in contrast to the monomer that exhibited unstable opening patterns. These data show that the oligomer, in contrast to the monomer, is the membrane-insertion intermediate, which has the capability to interact efficiently with phospholipids membranes forming stable pores. The supported evidence *via* Atomic Force Microscopy (AFM) showed that the 65-kDa Cry4Ba toxin, which spontaneously inserts into receptor-free lipid bilayers, preferentially in an aggregated form, rather than as a single monomeric toxin, suggesting that aggregated might be a possible form of insertion molecules (76). Moreover, the pore-like structures of these toxin molecules were provided, which are likely to be tetrameric association in high magnification AFM images (**Fig. 6**). Similarly, the Cry1Aa toxin was also shown to spontaneously insert into lipid monolayer and bilayer membranes forming pores that are composed of four subunits surrounding a 1.5 nm diameter central depression (38). Non-electrolyte exclusion technique using polyethylene glycols of various molecular weights were employed to estimate the size of the channels formed by Cry1Ca. The result shows that Cry1Ca forms clusters composed of a variable number of channels having a similar pore radius of between 1.0 and 1.3 nm (77).

Recently, it has been shown as a model that monomeric toxins of Cry1Ab could be formed into oligomeric structure before membrane insertion (69). After binding to the Bt-R1 protein, the changed conformation of monomeric toxins would expose regions consequently to oligomerisation. The pre-pore oligomeric structure of Cry1Ab would then bind to another receptor before insertion into lipid membranes.

1.4.3.2 Intermolecular interactions

Due to an importance of intermolecular interaction, evidence of toxin oligomerisation has been reported. Recently, it has been shown that only domain I of the Cry1Ab toxin is involved in monomer-monomer interactions of the pre-pore oligomer (78). Partial unfolding and limited proteolysis studies demonstrated that domain II and III could be excised from the pre-pore complex without provoking complete disassembly of the complex, suggesting that these domains are not involved in the oligomerisation. Wu and Aronson (9) had analysed the wild-type Cry1Ab and

Cry1Ac toxins by using immunoblotting, it was found that most of the toxins formed a large aggregate of ca. 200 kDa after incubation with vesicles, suggesting possible oligomerisation occurring to form channel. Soberon *et al.* (79) revealed that the pore could be formed by an oligomer containing four to six Cry toxin monomers. They also provided that two kinds of monomers mutated in different steps of their mode of action (F371A in receptor binding and H168F in pore formation) can form functional hetero-oligomers indicating that intermolecular interaction between toxin monomers is a necessary step for pore formation and toxicity. It has been suggested *via* mutagenesis studies of conserved residues in $\alpha 5$ of Cry1Ab that His¹⁶⁸ is important for pore formation, possibly involved in toxin oligomerisation since the H168F mutant was found to have a severe loss in K⁺ permeability across the brush border membrane vesicles (10). However, there is still no experimental evidence to support a function for this residue in $\alpha 5$ in oligomerisation of the Cry1Ab toxin. Aronson *et al.*, (9) and Tigue *et al.* (80) had performed mutagenesis experiments in Cry1Ab and Cry1Ac, and found that mutations in $\alpha 4$, $\alpha 5$ and in the loop connecting $\alpha 2$ and $\alpha 3$ adversely affected the irreversible binding, toxicity, and toxin oligomerisation. They also showed that after binding to membrane about 90% of the toxin molecule of Cry1Ab is protected from proteases.

Gazit *et al.* (81) have studied the binding of synthetic peptides and showed that only $\alpha 4$ and $\alpha 5$ insert into the membrane, while the kinetics of binding for $\alpha 5$ indicated a cooperative interaction, suggesting oligomerisation.

Feng and Becktel (82) have studied Cry3Aa, Cry1Aa and Cry1Ac by means of size exclusion and found that the relative amounts of oligomer depended upon pH; specifically Cry3Aa exist as a monomer at neutral pH, suggesting that alkaline pH promoted toxin oligomerisation. Besides, they found that temperature and buffer composition also affect the amounts of monomers to oligomers. Guereca and Bravo (83) have reported that Cry1Aa, Cry1Ac, Cry1Ca, Cry1Da and Cry3Aa toxins formed an oligomer consisting of more than ten units in both neutral and alkaline solutions. It was also suggested that oligomer formation might be a time-dependent process that would possibly occur after the toxin binds to the receptor and inserts into the membrane.

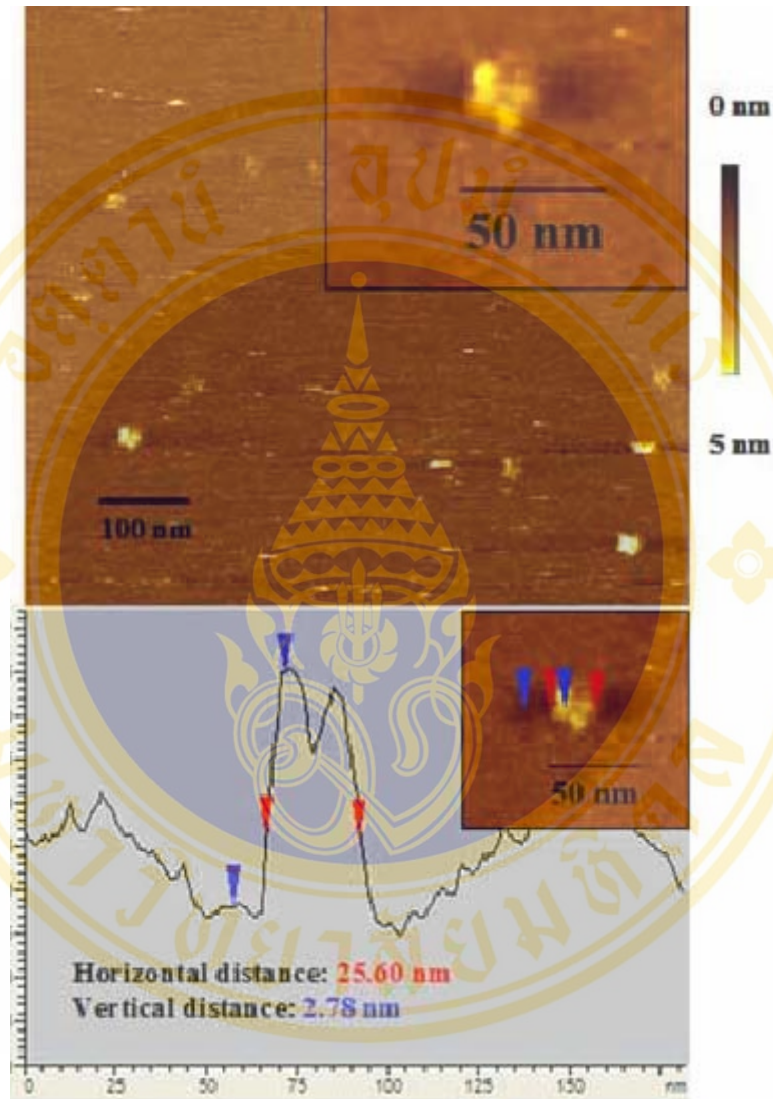


Figure 6: AFM images of lipid bilayers containing the activated Cry4Ba toxin prepared from Langmuir-Blodgett transfer.

The small-scale image exhibits a structure of about 25 nm in diameter, protruding about 3 nm from the lipid membrane. The inset displays the four subunits and the central depression visible in the cross-section indicates the cavity of a Cry4Ba toxin-induced pore.

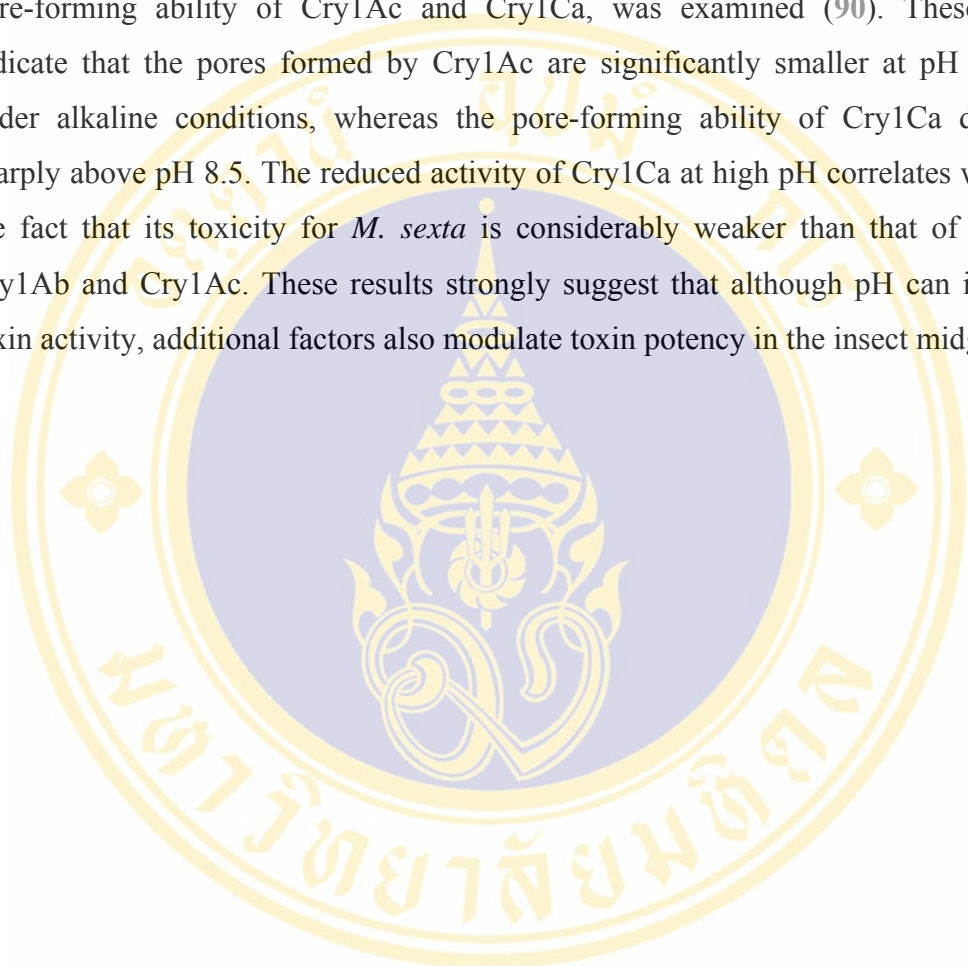
1.4.4 Toxin-induced pore formation

Currently, the umbrella model (**Fig. 7**) would best explain the Cry mechanism of toxicity. Gazit et al. (81) have used resonance energy transfer measurements of all possible combinatorial pairs of membrane-bound helices of Cry3Aa to map the network of interactions between helices in their membrane-bound state. It was proposed that $\alpha 4$ and $\alpha 5$ would insert into the membrane as a helical hairpin in an antiparallel manner, while the other helices would lie on the membrane surface like the ribs of an umbrella. Recently, Rausell et al. (75) have shown that domain I in the Cry1Ab pre-pore complex is more resistant to urea and heat denaturation than domain II and III. Furthermore, in the presence of lipids, domain I of the membrane-inserted pore complex would be prevented from heat unfolding. These results supported the umbrella model that only domain I is lipid-protected by its insertion into the membrane whereas domain II and III are very sensitive to heat or urea denaturation as lipids do not protect these domains. In addition, Gerber et al. (84) showed that the Cry1Ac $\alpha 4$ -loop- $\alpha 5$ segment is much more active in membrane permeation than either of the two helices ($\alpha 4$ or $\alpha 5$). This provides strong evidence that both helices and the loop connecting them are needed for insertion into the membrane.

The channel formation was first proposed by Knowles and Ellar (54) who reported the effect of the Cry toxin on CF-1 cells. They proposed the colloidal osmotic lysis model that involves influx of water and ion resulting in cell swelling and lysis. BBMV permeability assay was also used for examining membrane insertion and pore formation via an osmotic swelling/shrinkage in hyperosmotic solute (85). It has been shown that Cry1C and Cry1D could induce an increase in cation-membrane permeability involving ion channel formation in *S. frugiperda* BBMV-containing functional receptors (86).

Slatin et al. (87) showed that Cry1Ac and Cry3Aa could interact with receptor-free planar lipid bilayers and form ion-conducting channels. They suggested that channels formed by both toxins were cation-selective and exhibited several conductance states, ranging from 200 pS to about 4,000 pS. Recently, Puntheeranurak et al. (88) have also demonstrated that the Cry4Ba toxin could penetrate into planar lipid bilayers and form cation-selective channels. Schwartz et al. (89) have also demonstrated that the Cry1Ca toxin could penetrate into planar lipid bilayers and form

ion-selective channels with a large range of conductances. These channels displayed complex activity patterns with subconducting states and were selective to either anions or cations. These properties appeared to be pH dependent. The effect of pH on the pore-forming ability of Cry1Ac and Cry1Ca, was examined (90). These results indicate that the pores formed by Cry1Ac are significantly smaller at pH 6.5 than under alkaline conditions, whereas the pore-forming ability of Cry1Ca decreases sharply above pH 8.5. The reduced activity of Cry1Ca at high pH correlates well with the fact that its toxicity for *M. sexta* is considerably weaker than that of Cry1Aa, Cry1Ab and Cry1Ac. These results strongly suggest that although pH can influence toxin activity, additional factors also modulate toxin potency in the insect midgut.



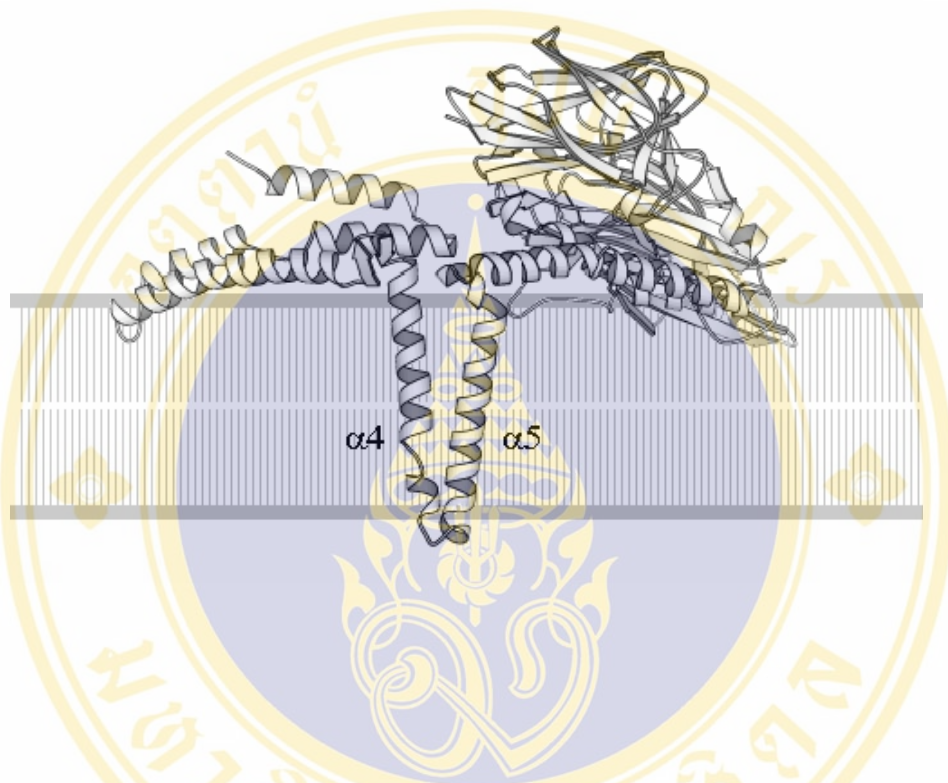


Figure 7: An umbrella model for Cry toxins.

This figure shows an umbrella model proposed for organisation of the pore-forming domain. A pair of $\alpha 4$ - $\alpha 5$ helices on the side of domain I drop down into the membrane while the remaining helices are rearranged on the membrane surface like the ribs of an umbrella. The phospholipid membrane is simplified as gray lines.

1.5 Alkalisiation of larval midgut and the role of midgut proteases

The mosquito larval midgut (**Fig. 8**) is divided into three main regions: gastric caeca, anterior, and posterior stomach. Recently, the pH in the gastric caeca and posterior midgut of all mosquito species has been reported to be close to 7.4. The pH would increase towards the anterior portion of the midgut where the pH would be close to 9.0 or higher (91). Similar observations have been reported; the increased pH in the anterior midgut, depending on species but being maintained within the 10.5-11.0 range (92). This high pH in the anterior midgut has been shown to associate with a high concentration of bicarbonate/carbonate ions and hence a presence of carbonic anhydrase (93). This carbonic anhydrase plays an important role in the alkalisiation mechanism in the midgut of *S. aegypti*.

As mentioned earlier, the alkaline pH range would foster the solubilisation of the protoxin crystals and the solubilised protoxins are cleaved by gut proteases to release active toxins. In fact, trypsin-like protein found in the midgut is not stored in the epithelial cells as an inactive enzyme, but is synthesised, activated and released into the gut lumen after the blood meal (94). The full-length Cry1Ab protoxin has been reported to be solubilised in gut juice of *Lepidoptera Crambidae* within 30 minutes (95). Further incubation up to 24 hrs would complete the proteolytic activation of protoxin to yield a band corresponding to that of the bovine trypsin activated toxin. However, there is still no evidence of solubilisation of the Cry toxins using gut extraction juice from mosquito larvae. Only proteolytic processing was determined using the solubilised Cry4 protoxins as substrates (96, 97).

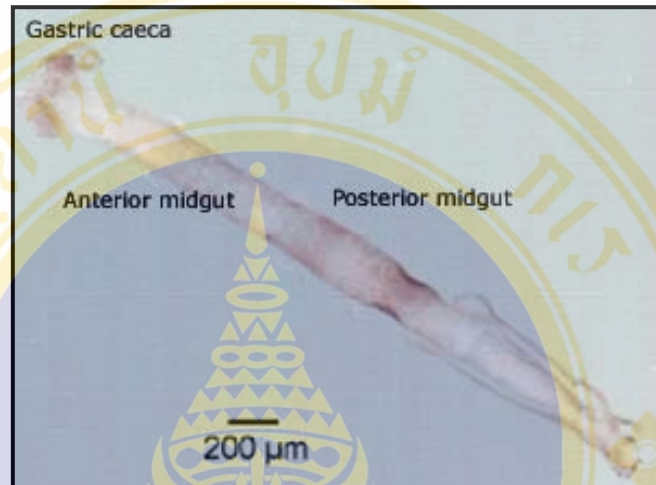


Figure 8: Larval midgut of *Stegomyia aegypti*.

Larval midgut of *S. aegypti* which is divided into three parts, gastric caeca, anterior midgut, and posterior midgut.

CHAPTER 3

MATERIALS AND METHODS

3.1 Materials

3.1.1 Chemicals

Ampicillin	Sigma
Cetyl trimethyl ammonium bromide (CTAB)	Sigma
RNaseA	Sigma
Isopropyl- β -D-thiogalactopyranoside (IPTG)	Sigma
1,4-Dithiothreitol (DTT)	Sigma
Coomassie brilliant blue R-250	Sigma
Protease K	Sigma
Mannitol	Sigma
Chloroform	Merck
Calcein	Molecular Probes
L- α -Phosphatidylcholine (egg)	Avanti Polar Lipids, Inc
L- α -Phosphatidylethanolamine (egg)	Avanti Polar Lipids, Inc
Cholesterol (purity>98%, wool grease)	Avanti Polar Lipids, Inc
Hepes	Gibco

Other chemicals and reagents used were analytical grade purchased from various suppliers.

3.1.2 Enzymes

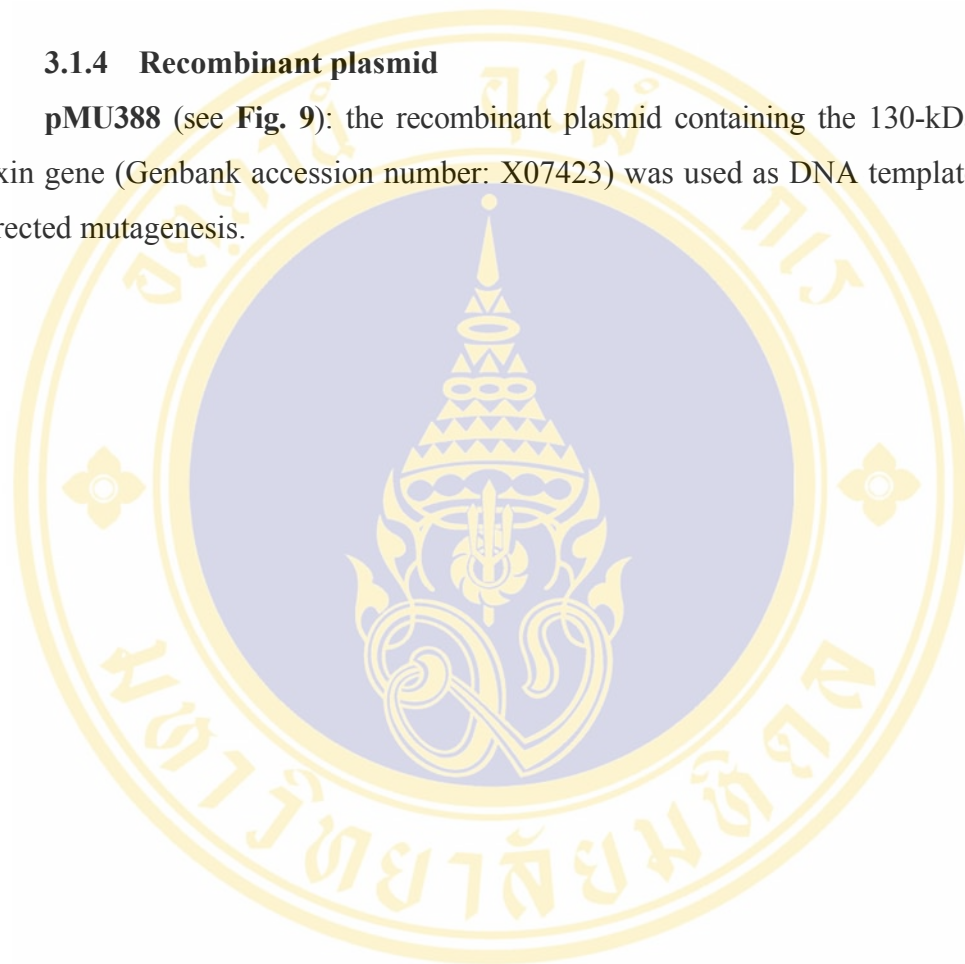
<i>Pfu</i> DNA polymerase (cloned)	Promega
Trypsin (Bovine pancreas, TPCK treated)	Sigma
Restriction endonucleases	Biolabs / Promega

3.1.3 Bacterial strain

E. coli strain **JM109** [*endA1*, *recA1*, *gyrA96*, *thi*, *hsdR17*, (r_K^- , m_K^+), *relA1*, *supE44*, λ^- , $\Delta(lac-proAB)$, (F', *traD36*, *proAB*⁺, *lacI*^q, *lacZ* Δ M15)] was purchased from Promega.

3.1.4 Recombinant plasmid

pMU388 (see **Fig. 9**): the recombinant plasmid containing the 130-kDa Cry4Ba toxin gene (Genbank accession number: X07423) was used as DNA template for site-directed mutagenesis.



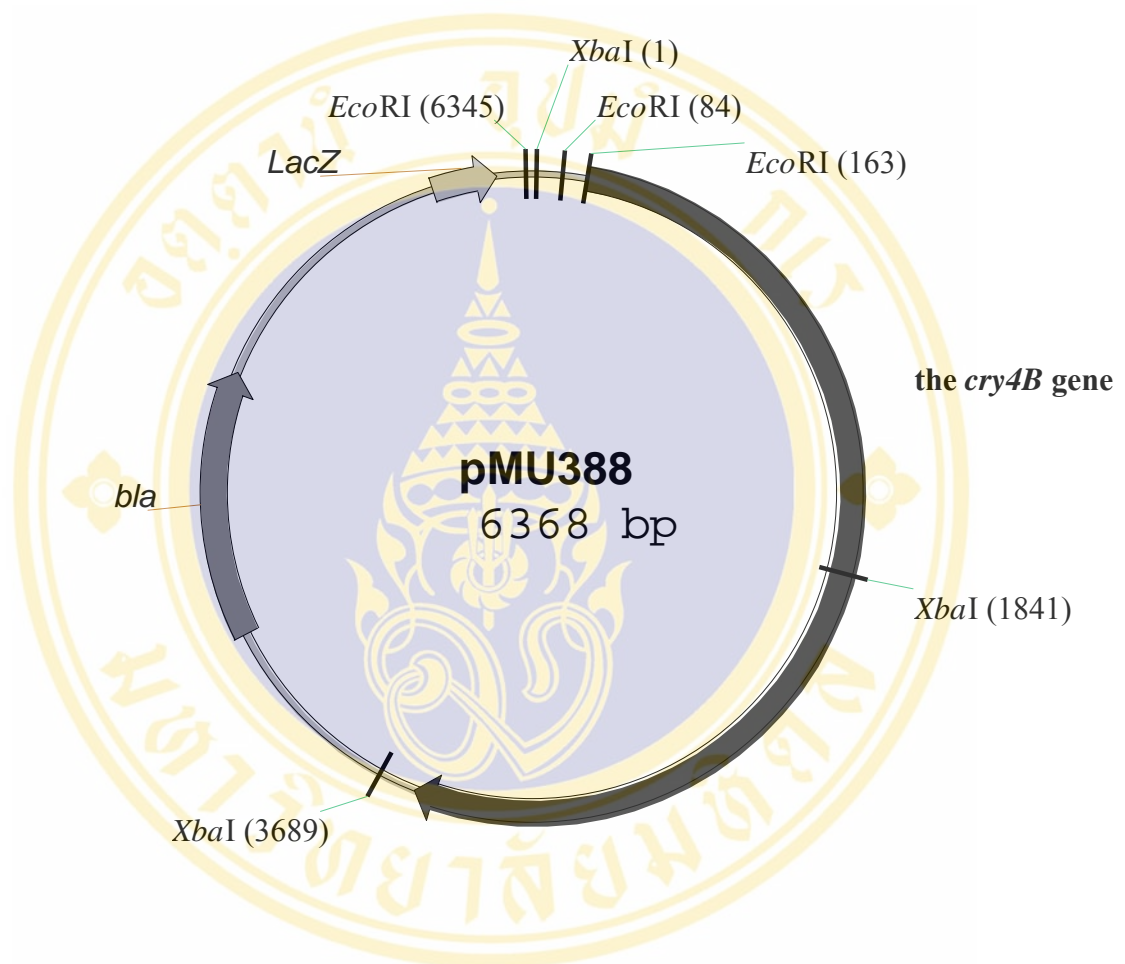


Figure 9: Physical map of the plasmid pMU388.

This figure shows the diagram of plasmid-pMU388, containing the gene for the 130-kDa Cry4B toxin, multiple cloning sites, *LacZ* gene and *bla* gene encoding β-lactamase (Amp^r). For clarity, not all of the restriction endonucleases sites are shown.

3.1.5 Synthetic oligonucleotide primers

All synthetic oligonucleotides served as primers were purchased from PROLIGO, Singapore. The sequences of all oligonucleotides are shown below. Mutated nucleotides or amino acid residues are indicated with bold letters. Introduced restriction enzyme recognition sites are underlined. Single code amino acid letters are placed above their corresponding nucleotide sequences.

Y178A-f:	5'-TACCAATAGCCGCCCAAGTGGCAAATTTCAATT-3'	<i>Bgl</i> I
Y178A-r:	5'-AAATTTGCCACTTGGGCGGCTATTGGTAATAAC-3'	
Q180A-f:	5'-ATACGCAGCTGTAGCAAATTTTC-3'	<i>Pvu</i> II
Q180A-r:	5'-TGCTACAGCTGCGTATATTGG-3'	
N183A-f:	5'-ATATACGCCCAAGTGGCAGCTTTCAATTTACTT-3'	<i>Bgl</i> I
N183A-r:	5'-AAATTGAAAGCTGCCACTTGGGCGTATATTG -3'	
N185A-f:	5'-CAAATTTCCGCGCTACTTTTAATAAGA-3'	<i>Hha</i> I
N185A-r:	5'-ATTAAAAGTAGCGCGAAATTTGCTAC -3'	
N195A-f:	5'-CCTCATAGCTGCGCAAGAATGGTC-3'	<i>Hha</i> I
N195A-r:	5'-ATTCTTGCGCAGCTATGAGGCCAT-3'	
N183Q-f:	5'-CAAGTAGCGCAGTTCAATTTACTTT-3'	<i>Hha</i> I
N183Q-r:	5'-GTAAATTGAACTGCGCTACTTGTG-3'	
N183T-f:	5'-ATATACGCCCAAGTGGCAACCTTCAATTTACTTT-3'	<i>Bgl</i> I
N183T-r:	5'-TAAATTGAAGGTTGCCACTTGGGCGTATATTGG-3'	
N183R-f:	5'-CAAGTAGCGCGATTCAATTTACTTT-3'	<i>Hha</i> I
N183R-r:	5'-TAAATTGAATCGCGCTACTTGTG-3'	
N183H-f:	5'-ATATACGCCCAAGTGGCAACCTTCAATTTACTTT-3'	<i>Bgl</i> I
N183H-r:	5'-TAAATTGAAGGTTGCCACTTGGGCGTATATTGG-3'	
N183D-f:	5'-CAAGTAGCGCGATTCAATTTACTTT-3'	<i>Hha</i> I
N183D-r:	5'-TAAATTGAATCGCGCTACTTGTG-3'	

	Q V A K F N	
N183K-f:	5'-TATAC <u>GCCCAAGTGGC</u> AAAGTTCAATTTACTTT-3'	<i>Bgl</i> I
N183K-r:	5'-TAAATTGAACTTT <u>GCCACTTGGGC</u> GTATATTGG-3'	
	Q V A F F N	
N183F-f:	5'-TATAC <u>GCCCAAGTGGC</u> ATTTTTCAATTTACTTT-3'	<i>Bgl</i> I
N183F-r:	5'-TAAATTGAAAAAT <u>GCCACTTGGGC</u> GTATATTGG-3'	
	F A S A D P R	
Y267A-f:	5'-TTTTGCCT <u>TCTGC</u> AGATCCACGTC-3'	<i>Pst</i> I
Y267A-r:	5'-GTGGAT <u>TGCAGA</u> GGCAAAAAGAG-3'	
	A Q S A N F	
V181S-f:	5'-CGCACAA <u>AGCGC</u> AAATTTCAATT-3'	<i>Hha</i> I
V181S-r:	5'-GAAATTT <u>GCGCT</u> TTTGTGCGTATAT-3'	
	Y A Q V S N F	
A182S-f:	5'-AATATACGCT <u>TCAGGTAT</u> CAAATTTCAATTTA-3'	<i>Dde</i> I
A182S-r:	5'-TGAAATTTG <u>ATACCTGAG</u> CGTATATTGGT-3'	
	A Q S S N F	
V181S/A182S-f:	5'-ATATAC <u>GCGCAGAGCT</u> CAAATTTCAATTTAC-3'	<i>Hha</i> I
V181S/A182S-r:	5'-TGAAATTTGAGCT <u>TGCGC</u> GTATATTGG-3'	

3.1.6 Culture media

3.1.6.1 Luria-Bertani (LB) medium (98)

One litre of LB broth contains 10 g of casein hydrolysate, 5 g of yeast extract and 5 g of NaCl. LB agar was prepared by adding 15 g of bacto-agar in one liter of LB broth. The medium was sterilised by autoclaving at 15 p.s.i. for 30 min. For selective medium, ampicillin was added to 100 µg/ml final concentration.

3.1.6.2 SOC medium

One liter of SOC medium contains 20 g of tryptone, 5 g of yeast extract, 0.58 g of NaCl and 0.19 g of KCl. The pH of medium was adjusted with NaOH to 7.0 and then autoclaved. After being autoclaved, 1 ml of 2 M MgSO₄ stock and 1 ml of 2 M glucose were added in 98 ml of medium.

3.1.7 Miscellaneous

Deoxyribonucleotide triphosphates (dNTPs)

Promega

Standard DNA markers

Gibco BRL, Biolabs

SDS-PAGE molecular mass standards (broad range)	BIO-RAD
Bradford protein assay reagent	BIO-RAD
Centrifugal filter tube (MWCO 30 kDa)	Eppendorf
Capillary pasteur pipette (9")	Corning

3.2 Methods

3.2.1 Plasmid DNA extraction

Plasmid extraction was performed using cetyl ammonium bromide (CTAB) method (98). A single colony was inoculated in 3 ml LB broth [1% (w/v) casein hydrolysate, 0.5% (w/v) bacto-yeast extract, 0.5% (w/v) NaCl] containing 100 µg/ml ampicillin and incubated at 37°C with 200 rpm shaking for 16-20 hr. The pellet was collected in a microcentrifuge tube by centrifugation at 12,000 rcf for 10 sec, and resuspended in 200 µl of STET buffer (8% sucrose, 0.1% Triton X-100, 50 mM EDTA, 50 mM Tris-HCL, pH 8.0). A 10-µl freshly prepared lysozyme solution (10 mg/ml) was added and incubated for 10 min at room temperature. The mixture was boiled for exactly 45 sec and centrifuged at 12,000 rcf for 15 min at room temperature. The pellet (cell debris and chromosomal DNA) was removed by using toothpick. Plasmid was recovered by adding 20 µl of 5% CTAB into supernatant. The contents were mixed by inversion and centrifuged at 12,000 rcf for 10 min at room temperature. The pellet was resuspended in 300 µl of 1.2 M NaCl by vortex. In order to remove RNA, 5 µl of RNaseA (10 mg/ml) was added and incubated at 37°C for 30 min. Protein was removed by adding 300 µl of chloroform, vigorous inversion and centrifugation at 12,000 rcf for 5 min at room temperature. The aqueous phase was transferred to new microcentrifuge tube. The plasmid DNAs were precipitated with 500 µl of isopropanol at room temperature or absolute ethanol at -20°C for 10 min and centrifuged at 12,000 rcf for 15 min at room temperature. The final DNA pellets were washed in 70% ethanol. After removal of the supernatant following with air dry, the DNA pellet was resuspended in 20 µl of distilled water.

3.2.2 Agarose gel electrophoresis of DNA (98)

An appropriate amount of agarose powder was dissolved in 1X TBE buffer (89 mM Tris-HCl, 89 mM boric acid, 2.5 mM EDTA, pH 8.0) or TAE buffer (40 mM

Tris-HCl, 40 mM acetic acid, 2.5 mM EDTA, pH 8.0) under boiling temperature to ensure the homogeneity of the gel solution. When the gel mixture cooled down to about 60°C, the mixture was poured into the mold and allowed to cool and to solidify at room temperature. DNA sample was mixed with gel-loading dye (15% (w/v) Ficoll 400, 0.1% Bromophenol blue, 5 mM EDTA) at ratio 1:5 and loaded in to a well of the gel submerged in TBE buffer. After electrophoresis was completed, the gel was stained in ethidium bromide solution for 5 min and destained in water for 10 min. The DNA patterns were visualised under UV light.

The amount of DNA were estimated by comparing the stained DNA bands with the standard DNA markers (λ DNA digested with *Hind*III) of known concentrations under UV light. The total DNA in solution was performed using 260 nm-absorbance (A260). One optical density of DNA at 260 nm is about 50 μ g/ml of double stranded DNA.

3.2.3 Site-directed mutagenesis

The method used in this project was based on Stratagene's QuickChange™ Site-Directed Mutagenesis Kit (**Fig. 10**). The recombinant plasmid-pMU388 containing the full length of *cry4Ba* gene which has been cloned from *Bt* subsp. *israelensis* into pUC12 vector, was used as a template. The method would make use of *Pfu* DNA polymerase which replicates both strands of DNA plasmid with high fidelity without displacing the mutant oligonucleotide primers.

A GeneAmp®PCR System 2400 (Perkin Elmer Cetus) was used to perform polymerase chain reactions (PCR) for all samples. The PCR reaction mixture (50 μ l) is composed of

DNA template	100 ng
dNTPs	50 μ M each
Forward primer	20 pmole
Reverse primer	20 pmole
10x <i>Pfu</i> buffer	5 μ l
<i>Pfu</i> DNA polymerase	2.5 U
Sterile distilled water making total volume to	50 μ l

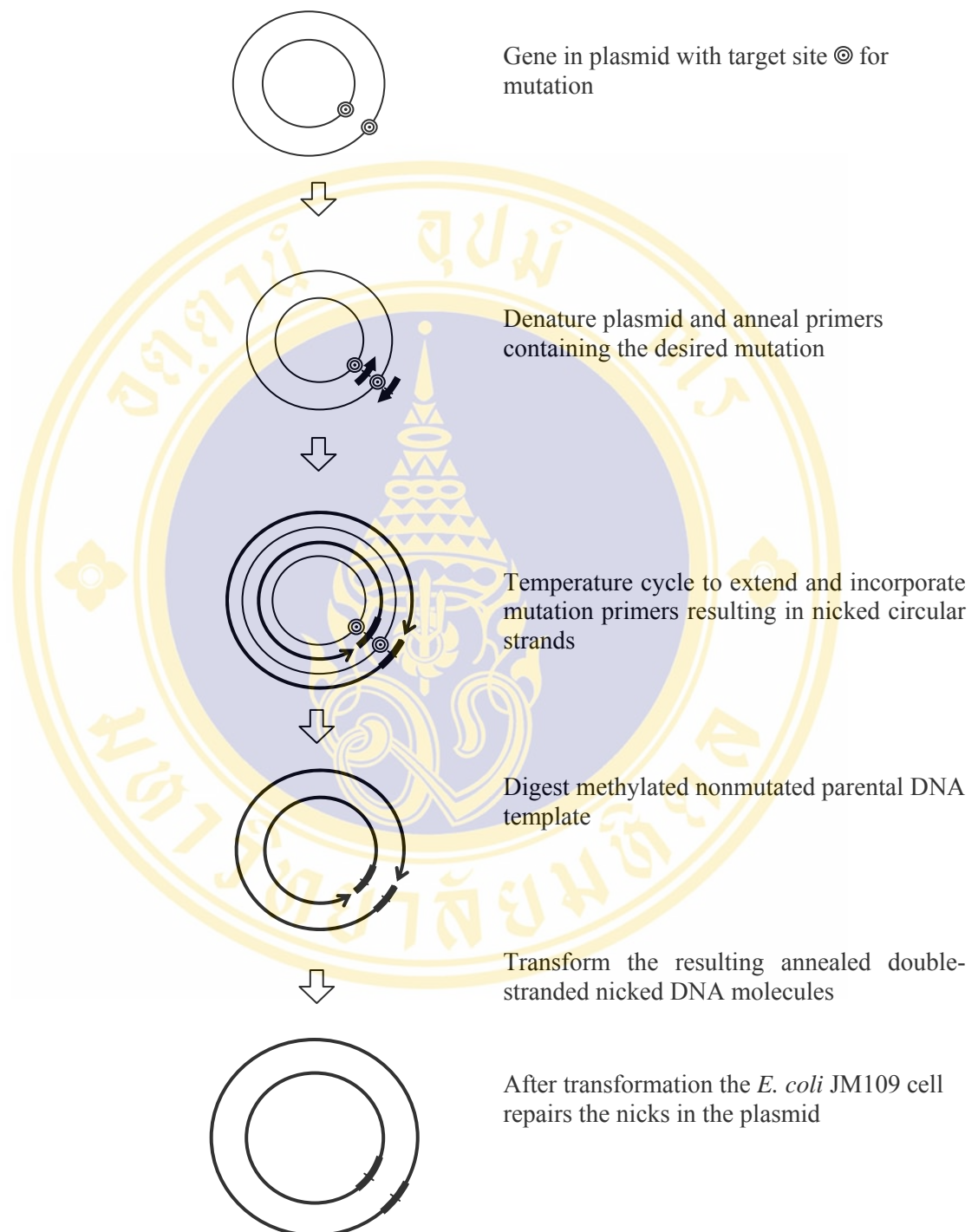


Figure 10: Overview of QuickChange Site-Directed Mutagenesis method.

The figure shows site-directed mutagenesis method redrawn from Stratagene's QuickChange instruction manual.

The reaction mixture was carried out with the following conditions as shown in

Table 1 and 2:

Table 1: Temperature cycling parameters for site-directed mutagenesis

Temperature (celsius)	Time (min:sec)	Cycles
95	0:30	1
95	0:30	18
*T _a	1:00	
68	13:00	
68	7:00	1

*The annealing temperature (T_a) are shown in Table 2

Table 2: Annealing temperature (T_a) for each mutants

Mutants	Annealing Temperature (°C)
Y178A	50
Q180A	50
N183A	50
N185A	45
N195A	50
N183R	50
N183T	50
N183K	50
N183F	50
N183Q	50
N183H	50
N183D	50
Y267A	52
V181S	48
A182S	48
V181SA182S	50

The amino acid change was performed. After the amplification reaction was finished, the PCR products were examined on 0.8% agarose gel electrophoresis.

3.2.4 Digestion of PCR products

Each amplified reaction was added with 1 μ l of *DpnI* restriction endonuclease and incubated at 37°C for 1 hr. The *DpnI* will digest the parental DNA template and leave only mutated nicked plasmid. *DpnI* restriction endonuclease is specific for methylated and hemimethylated DNA (5'-G^{me}A↓TC-3'). DNA isolated from almost all *E. coli* strains is *dam* methylated and it would be therefore susceptible to *DpnI* digestion. The *DpnI*-digested PCR products were analysed on 0.8% agarose gel electrophoresis before being subsequently transformed into *E. coli* competent cells.

3.2.5 Preparation of competent cells (98)

A single colony of *E. coli* was picked from a plate freshly grown for 16-20 hr at 37°C and transferred into 100 ml of LB broth in a 1-liter flask. The culture was incubated at 37°C with 250 rpm shaking until OD₆₀₀ reached 0.3-0.5. The culture was cooled down by storing the tube on ice for 15 min. Cells were packed by centrifugation at 2,000 rcf, 4°C for 15 min. The supernatant was discarded and the pellet resuspended in one-third of the origin volume with ice-cold TFB I solution (30 mM potassium acetate, 100 mM RbCl, 10 mM CaCl₂, 50 mM MnCl₂, 15% V/V glycerol) and stored on ice for 30 min. Cells were recovered by centrifugation at 2,000 rcf for 15 min at 4°C and the pellet was resuspended in 2 ml of ice-cold TFB II (10 mM MOPS, 75 mM CaCl₂, 10 mM RbCl, 15% V/V glycerol) for each 50 ml of origin culture. A 200 μ l of each suspension of competent cells was transferred using a sterile pipette tip into a sterile microcentrifuge tube and stored at -80°C until required. The efficiency of the competent cell was determined by transforming 10 ng of pUC12 into 200 μ l of the competent cell suspension.

3.2.6 Transformation of plasmid DNA into competent cells (137)

The *DpnI*-digested PCR product was mixed with 200 μ l of competent cells. The mixture was immediately chilled on ice for 30 min, following by incubation at 42°C for 90 sec, and then immediately placed on ice for 5 min. A 800 μ l of LB broth was added into the transformed cells, gently mixed and incubated at 37°C for 1 hr. Transformed cells were collected by centrifugation at 3,000 rcf for 2 min. Medium was decanted and the cell pellets were gently resuspended in 200 μ l of LB broth. The transformed cell was spread gently over the surface of the LB agar plate containing

100 µg/µl ampicillin by a sterile glass rod. The agar plate was incubated at 37°C for 16-20 hr until *E. coli* colonies were clearly seen on agar plate.

3.2.7 Screening for mutant plasmids (98)

Restriction endonuclease analysis was used to screen for each mutant plasmid based on a recognition site which is silently introduced into each pair of mutagenic oligonucleotide primers. The 20 µl digestion reaction was composed of 0.5-1 µg of DNA sample, 1x restriction enzyme digestion buffer, and approximately 5 U of restriction endonuclease and sterilised distilled water to make up to the 20 µl total volume. The digestion reaction was incubated at 37°C for 2 hr with appropriate enzymes. The recommended restriction enzyme digestion buffers were supplied by enzyme manufacturers. To visualise the restriction patterns, electrophoresis of the digested DNA was carried out in the horizontal 0.8% agarose gel in TBE buffer at 100 V for 1 hr.

3.2.8 DNA sequencing analysis

To confirm the resulting mutation, a BigDye™ Terminator Cycle Sequencing Kit (Perkin-Elmer, Norwalk, USA) was used to prepare samples for sequence analysis based on fluorescent-labeled terminator cycle sequencing.

3.2.9 Expression of toxins (98)

Each clone of *E. coli* expressing either wild-type Cry4Ba or each mutant toxin was inoculated into 3 ml of LB broth containing 100 µg/ml ampicillin and grown at 37°C with 250 rpm shaking for 16-20 hr. The overnight culture was transferred into fresh LB broth containing ampicillin to make up 1% of the final concentration and incubated further until OD₆₀₀ reached 0.3-0.5. Then, the expression was induced with IPTG at a final concentration of 0.1 mM at 37°C for 4 hr. The cell cultures were collected by centrifugation at 10,000 rpm for 10 min. The 0.1 OD of *E. coli* cells were subjected to analyse the protein profiles on 10% SDS-polyacrylamide gel electrophoresis (SDS-PAGE).

3.2.10 Sample preparations

Protein sample was prepared by mixing the sample with 4X loading buffer (60 mM Tris-HCl pH 7.5, 2% of SDS, 10% glycerol, 0.025% bromophenol blue, 100 mM DTT) in the ratio of 3:1 and boiled at 100°C for 5 min. The heated samples were vigorously mixed using vortex and centrifuged at 12,000 rcf for 10 min. Supernatant equivalent to 0.15 OD. of cell culture was loaded into each well of SDS-PAGE.

3.2.11 SDS-polyacrylamide gel electrophoresis

SDS-PAGE was performed using the Bio-Rad Mini-Protein II system. The separating gel is consisted of 3% crosslinker, 10% or 13% gel, 0.375 M Tris-HCl (pH 8.8) and 0.1% SDS. The stacking gel contains 3% crosslinker, 5% gel, 0.125 M Tris-HCl (pH 6.8) and 0.1% SDS. Tris-glycine buffer (25mM Tris, 192 mM glycine, 0.1% SDS) was used as buffer. Electrophoresis was performed with constant voltage 100 V at room temperature. After electrophoresis, the protein band on the gel was visualised by 1 hr-soaking in staining solution containing 50% methanol, 10% glacial acetic acid and 0.1% Coomassie Brilliant Blue R-250 in water. The gels were then soaked in destaining solution (10% methanol and 10% glacial acetic acid) overnight or until the background was clear.

3.2.12 Partial purification of protein inclusions (99)

After expression of the target protein, *E. coli* cell pellet was resuspended in a 30 ml of distilled water. French Press machine was employed to disrupt the cells at 900 psi. The inclusion bodies were collected by centrifugation at 12,000 rcf for 20 min at 4°C. The supernatant was removed. The pellet was resuspended in distilled water and washed three times by sonication. The suspension was sedimented by centrifugation at 12,000 rcf for 10 min at 4°C. The cell debris on the top of inclusion bodies was removed with a micropipette. The cleaned inclusion bodies were resuspended in distilled water and collected about 15 µl for analysis the protein profile. The inclusion bodies were then solubilised with an appropriate buffer or transferred to a small aliquot and kept at – 20°C.

3.2.13 Protein concentration assays

Protein concentrations were determined by using BIO-RAD protein assay reagent based on the method described by Bradford (100). The calibration curve was constructed using bovine serum albumin (BSA) as a protein standard. BSA standards were prepared by making dilution ranging from 1, 2, 3, 4 and 5 $\mu\text{g}/50\ \mu\text{l}$ of BSA in distilled water. Each standard protein and sample solution were mixed with 200 μl of dye reagent (Bradford reagent) in a 96-well flat bottom Sero-Wel microtitre plate (Bibby Sterilin, England). The solution was mixed and incubated at room temperature for 10 min. The absorbance of samples and standards were measured at 595 nm using the SpectraMAX 250 ELISA plate reader (Molecular Device). The protein concentrations of samples were calculated from the standard curve.

3.2.14 Solubilisation of toxin inclusions and proteolytic processing of protoxins

1 mg of protoxin inclusions was solubilised in 1 ml of 50 mM Na_2CO_3 , pH 9.0 at 37°C for 1 hr. For solubility test, the incubated toxins were subjected to centrifugation at 12,000 rcf for 10 min. Pre- and post-centrifugation toxin samples were quantitated. The samples were then analysed on SDS-PAGE.

The soluble protoxin was digested with trypsin (N-Tosyl-L-phenylalanine chloromethyl ketone treated, Sigma) at a 1:20 (w/w) ratio of enzyme: protoxin. The protoxin-trypsin mixture was incubated at 37°C for 16 hr. The trypsin digested products were analysed on SDS-PAGE (12% gel).

3.2.15 Gut juice extraction

The gut juice extracts were obtained from the fourth instar *Stegomyia aegypti* larvae. The guts were excised and collected in buffer (Mannitol 300 mM, Tris pH 8.0). Sample was spinned at 15,000 rcf for 3 min, and the supernatants containing alkaline condition of soluble gut proteinases were determined in protein content by Bradford microassay. The samples were incubate at 37°C for 16 hr.

3.2.16 Mosquito-larvicidal activity assays (101)

The 2-day old of *S. aegypti* mosquito larvae were used for toxicity test of toxins. The larvae were obtained from the mosquito-rearing facility, the Institute of Molecular

Biology and Genetics, Mahidol University. *E. coli* cells expressing Cry4Ba or mutant toxins were grown in LB broth with 100 µg/ml ampicillin at 37°C. Protein expression was induced with 0.1 mM IPTG at 37°C for 4 hr. Cell pellet (10 OD₆₀₀ ~ 10⁹ cells) was harvested by centrifugation at 12,000 rcf for 10 min at room temperature and resuspended in 2 ml of distilled water (10⁸ cells/200 µl). Each assay was carried out in a 48-well microtitre plate (11.3-mm well diameter, Costar, USA), with 10 larvae per well in 800 µl of distilled water. Then, 200 µl of induced *E. coli* cells (10⁸ cells) or 3 µg inclusion proteins were added into each well. 100 larvae were used for each sample in one experiment. Three independent experiments were performed. *E. coli* cells containing the pMEx8 vector were used as a negative control. Mortality was recorded after 24-hr incubation period.

3.2.17 Purification of Cry4Ba and its mutant

The 65-kDa activated Cry4Ba toxin and its mutants were first passed through a 0.45 µm filter and injected into AKTApurifier liquid chromatography system equipped with a Superose 12 HR 10/30 column (Amersham Pharmacia Biotech Inc., NJ, USA). The column was equilibrated with eluent at flow rate 0.4 ml/min before operation. Protein fractions were monitored by UV absorption at 280 nm and the 400 µl fractions were collected and then analysed by SDS-PAGE (15% gel). The fractions containing a 65-kDa activated toxin were pooled together and concentrated with a 30-kDa cutoff centrifugal filter tube (Eppendorf, Germany). Protein concentration was determined by Bradford assays.

3.2.18 Circular dichroism (CD) measurement

CD spectroscopy was used to gain information about the secondary structure of Cry4Ba toxin and its mutants. CD spectra were measured in 50 mM carbonate buffer with a Jasco J-715 spectropolarimeter (Jasco Inc., Japan) and were scanned between 190 and 280 nm at room temperature in a rectangular quartz cuvette with a 0.2 mm optical path length. Spectra were recorded using a 2 nm spectral bandwidth at 50 nm/min scan speed and 2 ms response time. Spectra were corrected for the solvent baseline obtained under the same condition. The molar circular dichroism $\Delta\epsilon$ at a given wavelength was calculated by the following formula:

$$\Delta\varepsilon = (\theta) \times 10^6 / (c \times d \times \text{mdeg}_{\text{CSA290}})$$

where

θ is the measured ellipticity (millidegrees)

c is the sample concentration (M)

$\text{mdeg}_{\text{CSA290}}$ is milidegrees of standard camphorsulfonic acid (CSA) at 290 nm ($\cong 42.34$)

d is the optical path length of the sample cell (cm)

The helical contents of the protein and its fragment were derived from their $\Delta\varepsilon$ determined at 222 nm.

3.2.19 Intrinsic fluorescence measurement

The fluorescence spectra were obtained by emission scanning of protein using RF-5301PC spectrofluorophotometer at the excitation wavelength 280 nm. The emission wavelengths were observed from 300 to 500 nm. The scanning rate was 50 nm/min, excitation and emission slit 5.0 nm. One spectrum was averaged from 2 scans and all spectrum were subtracted with baseline.

3.2.20 Membrane perturbation assays

3.2.20.1 Preparation of entrapped-calcein liposomes (102)

A lipid mixture (2 mg) composed of L- α -phosphatidylethanolamine (PE), L- α -phosphatidylcholine (PC) and cholesterol (Ch) at a ratio of 10:10:1 (w/w). 95.2 μl of PE (10 mg/ml), 47.6 μl of PC (20 mg/ml) and 9.52 μl of Ch (10 mg/ml) were placed in a bottle and were dried under a gentle stream of oxygen-free nitrogen gas. The resulting lipid film was resuspended with 60 mM calcein solution, pH 10.0. Large unilamellar vesicles (LUVs) were prepared by squeezing the suspension through the extruder membrane (0.1 mm in diameter, Avanti Polar Lipid, USA) for 13-20 passes. Unentrapped calcein was removed from the LUV by using three serial connected Hitrap columns (Pharmacia, Uppsala, Sweden) equilibrated with 150 mM NaCl and 10 mM Tris, pH 10.0). The collected fractions were tested for their liposome concentrations by measuring absorbance at 600 nm. The entrapped-calcein liposomes

were then diluted to a lipid concentration of 2.5 μM with 10 mM Tris, pH 10.0 for the membrane perturbation assays.

3.2.20.2 Calcein release assays

Membrane-damaging activity was evaluated by the release of the liposome-entrapped self-quenching fluorescent dye (2', 7'-bis (carboxymethyl) aminomethylfluorescein, Calcein, Molecular Probe C-481, Molecular weight 622.54). The loss of liposome membrane-integrity results in dilution of the fluorophore with a consequent increase in the fluorescence signal. Thus, membrane perturbation can be detected by an increase in fluorescence as toxins are added and immediately assayed for calcein fluorescence (λ_{ex} , 485 nm, λ_{em} , 520 nm) with a LS50 luminescence spectrofluorometer (Perkin-Elmer). Each experiment was conducted by measuring a fluorescence intensity of 400 μl of entrapped-calcein liposome until the fluorescence intensity was stable. Then 3 μg of purified toxin was added and fluorescence from the leaked calcein was monitored until fluorescence intensity was stable. Finally, 10 μl of 0.1% Triton X-100 was added to determine 100% calcein leakage from the vesicles. The percentage of fluorescence recovery, F_t , was defined as

$$F_t = (I_f - I_0)/(I_{\text{max}} - I_0) \times 100$$

where

I_0 = initial fluorescence

I_f = fluorescence observed after adding the toxin at time t

I_{max} = the total fluorescence observed after the adding triton-X

3.2.21 Oligomerisation study

3.2.21.1 Liposome preparation

PE, PC, Ch dissolved in chloroform (ratio 10:10:1) was dried under N_2 gas. Lipid mixtures were resuspended in 10 mM Tris pH 8.0. Large unilamellar vesicles were prepared by extrusion through 100-nm polycarbonate filter as previously describe in section Method **3.2.20.1**.

3.2.21.2 Liposome concentration assays

Liposome concentration was estimated by measuring the phospholipid contents (103). The calibration curve was plotted from a standard phosphate solution. Phosphate standards were prepared by making dilution ranging from 0, 30, 50, 70, and 90 μl of 1 mM Na_2HPO_4 . Each standard solution was dried on heating box and 150 μl of 70% perchloric acid were added and allowed to heat at 180°C for 1 hr. After the mixtures were cooled down, 2.7 ml of phosphate assay solution (0.33 g of ascorbic acid, 2 ml of ammonium molybdate solution, and 21 ml of distilled water) was added then incubated at 80°C for 10 minutes before measuring an absorbance at 820 nm. 50 μl of liposome solution were used and the phospholipid concentrations were calculated from the standard curve.

3.2.21.3 Incorporation of toxin to liposome and protease treatment

5 to 10 μg of purified toxin was incubated with liposome suspension (200 $\mu\text{g}/\text{ml}$ of total lipids) in 20 μl of 50 mM HEPES-100 mM NaCl, pH 8.0, at 37 °C for 30-90 min. For protease digestion, liposome plus toxin was incubated as described and protease K (Sigma) at 0.2-0.5 $\mu\text{g}/\text{ml}$ was added and the suspension were incubated at 37°C for 45 min. Controls were 5 to 10 μg of toxin plus protease K with no liposome and the liposome-toxin mixture incubated without protease K. These samples were heated in loading buffer (with and without DTT) at 60°C for 10 min and fractionated by SDS-8% PAGE.

3.2.21.3 Western blotting

For western blot analysis, transfer of proteins from gel onto a PVDF membrane can be achieved by semi-dry blotting. Briefly, the protein gel was equilibrated in transfer buffer (39 mM glycine, 48 mM Tris-HCl pH 9.2, 0.0375% SDS, 10% methanol), four sheets of absorbent paper and one of PVDF membrane were also prepared by wetting in the transfer buffer. Finally all of sheets and protein gel were transferred onto electrophoresis transfer cell in appropriate layering. The electroblotting was carried out at constant current of 3 x mA per cm^2 of the gel for 1 hr.

After the electrotransfer process was completed, the PVDF membrane was soaked in distilled water for 5 min and soaked in Ponceau S staining solution (2% Ponceau S,

30% Trichloroacetic acid) at room temperature for 5 min and then washed several times with distilled water. Then the membrane was rinsed twice with TBS (10 mM Tris-HCl pH 7.5, 150 mM NaCl) following by soaking in blocking solution (5% BSA in TBS buffer) for 1 hr at room temperature or overnight at 4°C. The membrane was washed 3 times with TBS-Tween buffer (20 mM Tris-HCl pH 7.5, 500 mM NaCl, 0.05% Tween 20). The antibody against Cry4Ba domain III, diluted to 1:50 in the blocking solution, was incubated with the membrane. Then the membrane was washed with TBS-Tween buffer 5 min for 3 times before adding 1:20,000 diluted alkaline phosphatase conjugated with goat anti-mouse Ig. The blotted membrane was washed with TBS-Tween buffer. The membrane was soaked in 10 ml of developing buffer (100 mM Tris-HCl pH 9.5, 100 mM NaCl, 5 mM MgCl₂) containing 66 µl of 5% NBT (nitroblue tetrazolium) and 33 µl of 5% BCIP (5-bromo-4-chloro-3-indolyl phosphate) until reactive bands were visible. To stop the reaction, the membrane was rinsed twice with distilled water and then soaked in 3% trichloroacetic acid (TCA) for 5 minutes to fix the colour. The membrane was washed with distilled water again to remove TCA and kept dried in dark.

CHAPTER 4

RESULT I: MUTAGENESIS OF Cry4Ba

Several studies have demonstrated that $\alpha 5$ in domain I of Cry toxins is an essential determinant of toxicity, likely to be involved in structural integrity and oligomerisation (9, 10). As determined from the crystal structure of Cry4Ba (35), $\alpha 5$ is composed of 22 amino acids with the majority being nonpolar residues (Fig. 11A). In this study, site-directed mutagenesis was employed to identify a critical residue in $\alpha 5$ for larvicidal activity of the Cry4Ba toxin.

4.1 Constructions of the alanine-substituted Cry4Ba mutant plasmids

Substitutions of the polar amino acids (Tyr¹⁷⁸, Gln¹⁸⁰, Asn¹⁸³, Asn¹⁸⁵, and Asn¹⁹⁵) in $\alpha 5$ with alanine (gray circled in Fig. 11B) were performed *via* PCR-based directed mutagenesis. The pMU388 plasmid (Fig. 9) containing the gene sequence encoding the 130-kDa Cry4Ba toxin was used as a template together with oligonucleotide primers containing mutated nucleotides and an introduced restriction enzyme recognition site for screening the mutant plasmids. Following the thermal cycle, the amplified products were digested with *DpnI* endonuclease and analysed on agarose gel electrophoresis as shown in Fig. 12. It was found that all PCR products showed a 6.3-kb major DNA band, corresponding to the size of pMU388.

The *DpnI*-treated digested PCR products (Fig. 13) were transformed into *E. coli* JM109 competent cells. 10 transformants from each mutation were screened for the presence of the mutant plasmids by restriction endonuclease analysis. After being treated with an appropriate restriction endonuclease, the digested DNA fragments of the mutant plasmids could be distinguished from that of the wild-type plasmid as shown in Fig. 14A-18A. Each mutant plasmid was verified in the mutated region by DNA sequencing as shown in the sequencing chromatograms (Fig. 14B-18B). The results showed that all mutant plasmids contain nucleotide changes at the desired positions.

4.2 Expression of the alanine-substituted Cry4Ba mutant toxins

E. coli cells harboring the wild-type and its mutant plasmids (Y178A, Q180A, N183A, N185A and N195A) were expressed upon IPTG induction as described in **Methods: 3.2.9**. The crude extracts were analysed by SDS-PAGE in which the expression levels among the wild-type and the mutants were found to be comparable to that of the wild-type Cry4Ba protoxin (**Fig. 19**).

4.3 Solubilisation and proteolytic processing of the alanine-substituted mutants

When the partially purified inclusions of each mutant toxin were solubilised in carbonate buffer (pH 9.0) at 37°C for 1 hr, the amounts of 130-kDa soluble proteins in the supernatant were compared with that of total proteins initially used in order to determine the percentages of solubility. It was found that the solubility of all the alanine-substituted Cry4Ba mutants, Y178A, Q180A, N185A and N195A, except for N183A is relatively similar to that of the wild-type Cry4Ba toxin (**Fig. 20**).

The solubilised mutant protoxins were also assessed for their proteolytic stability by digestion with TPCK-treated trypsin at 37°C for 16 hr and the proteolytic patterns were analysed on SDS-PAGE. Similar to the wild-type protoxin, all trypsin digestions of the solubilised mutant protoxins yielded proteolytic resistant products of ca. 47 kDa and ca. 20 kDa (**Fig. 21**).

4.4 Mosquito-larvicidal activity of the alanine-substituted Cry4Ba mutant toxins

Mosquito bioassays were performed to determine the effect of alanine substitutions on toxicity. *E. coli* whole cells expressing either wild-type Cry4Ba or each mutant toxin were tested for their biological activity towards *S. aegypti* larvae. Percentage mortality of the larvae after 24-hour incubation is shown in **Fig. 22**. Almost complete loss of larvicidal activity was observed for only the substitution at Asn¹⁸³, while replacements at the other positions (Y178A, Q180A, N185A and N195A) did not affect the toxicity. The results suggested that Asn¹⁸³ is important for larvicidal activity of the Cry4Ba toxin.

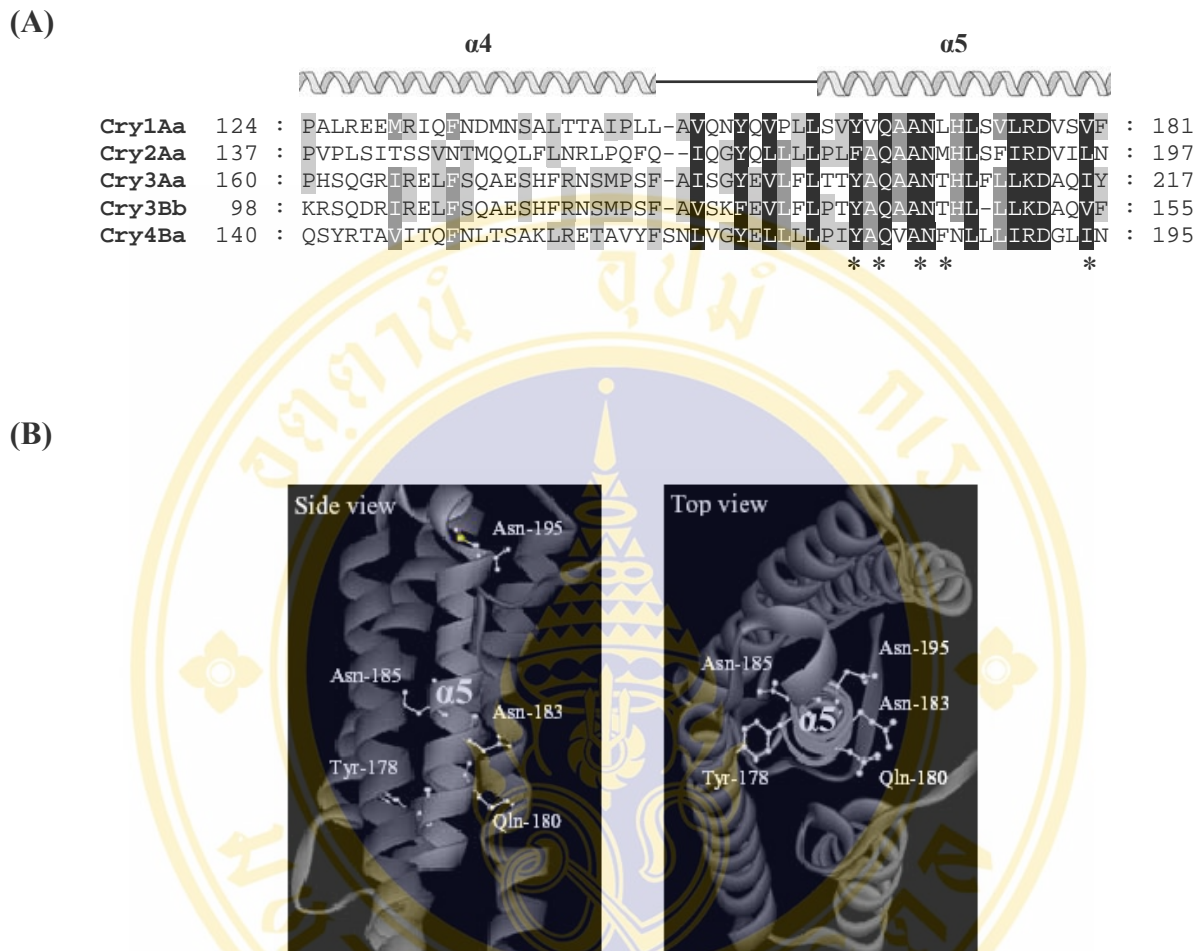


Figure 11: Sequence alignment and ribbon representation of Cry4Ba- $\alpha 5$.

- (A) Multiple sequence alignment of the transmembrane helices 4 and 5 of Cry4Ba with those of four different crystal structures, Cry1Aa, Cry2Aa, Cry3Aa and Cry3Bb. The degree of conservation among the five sequences is represented by background shading of the residues with black, dark gray and gray shading for 100%, 80% and 60% sequence homology, respectively. Mutated residues in this study are indicated by *. The sequences were aligned using the program Clustal X *v.1.83*.
- (B) Side and top views of the N-terminal helical domain of the Cry4Ba toxin in which $\alpha 5$ is encircled by other helices. The structures were generated by WebLab ViewerPro (Accelrys Inc.). The five mutated residues as indicated by * in A are shown in ball-and-stick model.

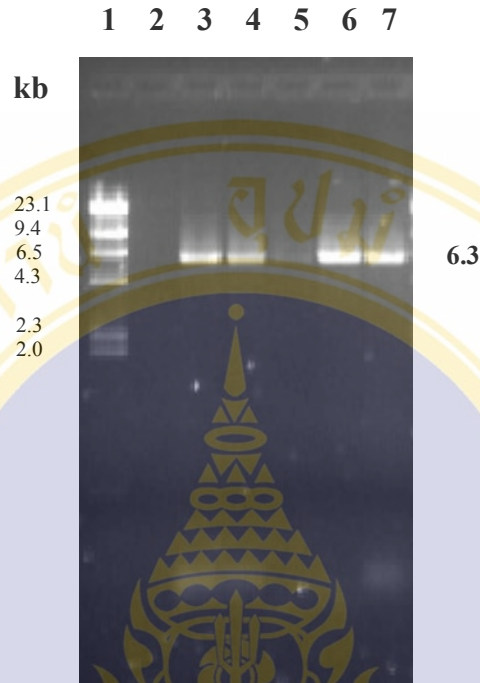


Figure 12: PCR amplification of Cry4Ba mutant plasmids: pY178A, pQ180A, pN183A, pN185A and pN195A.

The figure shows 1.0 % agarose gel electrophoresis (ethidium bromide-stained) of PCR products of Cry4Ba mutant plasmids, amplified at 50°C. The expected 6.3-kb DNA band is indicated with the bold label.

Lane 1: λ /*Hind*III digested DNA markers

Lane 2: A negative control

Lane 3: The PCR product of the pY178A plasmid

Lane 4: The PCR product of the pQ180A plasmid

Lane 5: The PCR product of the pN183A plasmid

Lane 6: The PCR product of the pN185A plasmid

Lane 7: The PCR product of the pN195A plasmid

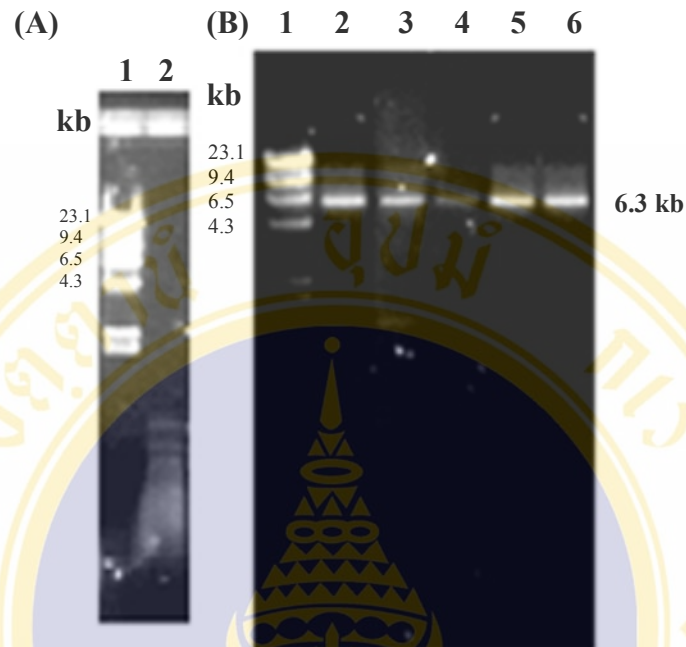


Figure 13: *DpnI* digested PCR amplification products of Cry4Ba wild-type and its mutant plasmids: pY178A, pQ180A, pN183A, pN185A and pN195A.

The figure shows 1.0 % agarose gel electrophoresis (ethidium bromide-stained) of PCR products of Cry4Ba wild-type and its mutant plasmids digested with *DpnI*. The expected 6.3-kb DNA band is indicated with the bold label.

(A) Lane 1: λ /*HindIII* digested DNA markers

Lane 2: The PCR product of the Cry4Ba wild-type plasmid digested with *DpnI*

(B) Lane 1: λ /*HindIII* digested DNA markers

Lane 2: The PCR product of the pY178A plasmid digested with *DpnI*

Lane 3: The PCR product of the pQ180A plasmid digested with *DpnI*

Lane 4: The PCR product of the pN183A plasmid digested with *DpnI*

Lane 5: The PCR product of the pN185A plasmid digested with *DpnI*

Lane 6: The PCR product of the pN195A plasmid digested with *DpnI*

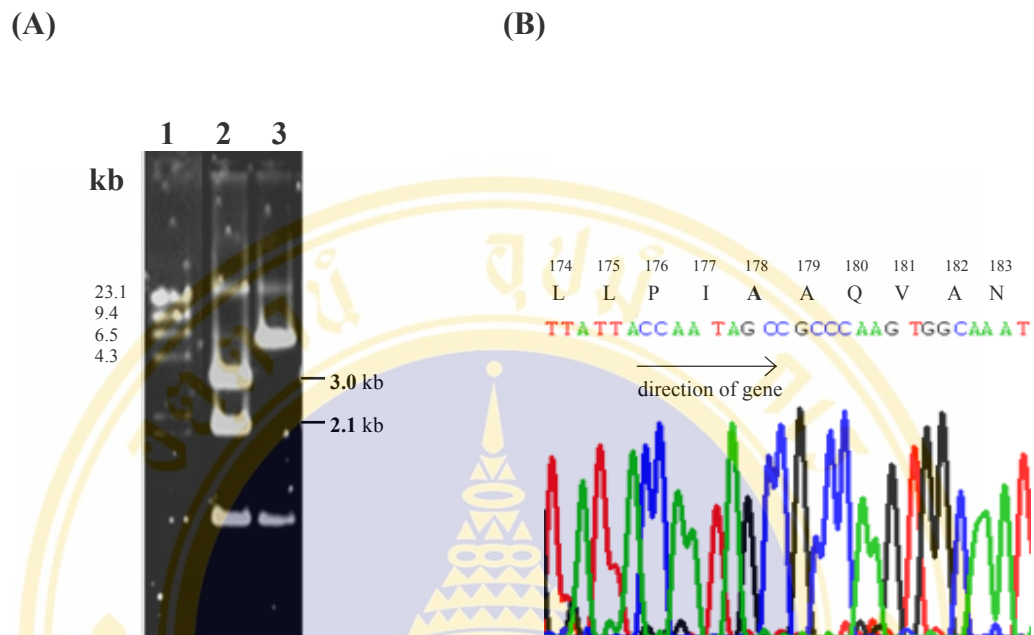


Figure 14: Restriction digestion and DNA sequence analysis of pY178A.

(A) 1% agarose gel electrophoresis (ethidium bromide-stained) of *Bgl*II digestion patterns of the wild-type and mutant plasmids. The 3.0- and 2.1-kb mutant specific bands are indicated.

- Lane 1: λ /*Hind*III digested DNA markers
- Lane 2: The *Bgl*II digested mutant plasmid, pY178A
- Lane 3: The *Bgl*II digested wild-type plasmid, pMU388

(B) The DNA sequencing chromatogram of pY178A, using N155A-f as a sequencing primer. Part of the sense strand sequence is shown. The bold letter represents the substituted amino acid residue.

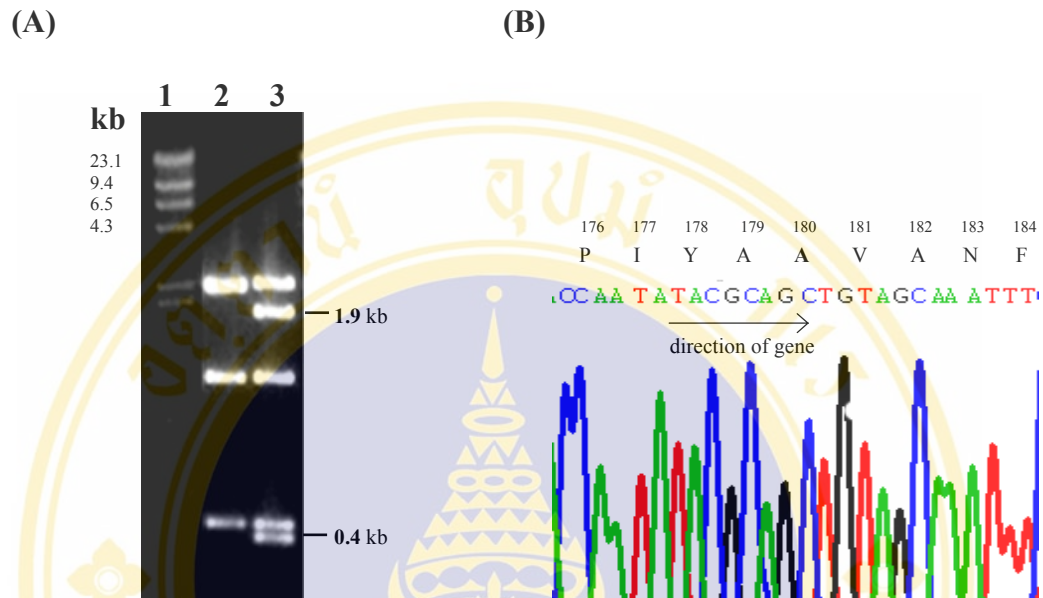


Figure 15: Restriction digestion and DNA sequence analysis of pQ180A.

(A) 1% agarose gel electrophoresis (ethidium bromide-stained) of *Pvu*II digestion patterns of the wild-type and mutant plasmids. The 1.9- and 0.4-kb mutant specific bands are indicated.

- Lane 1: λ /*Hind*III digested DNA markers
- Lane 2: The *Pvu*II digested wild-type plasmid, pMU388
- Lane 3: The *Pvu*II digested mutant plasmid, pQ180A

(B) The DNA sequencing chromatogram of pQ180A, using N155A-f as a sequencing primer. Part of the sense strand sequence is shown. The bold letter represents the substituted amino acid residue.

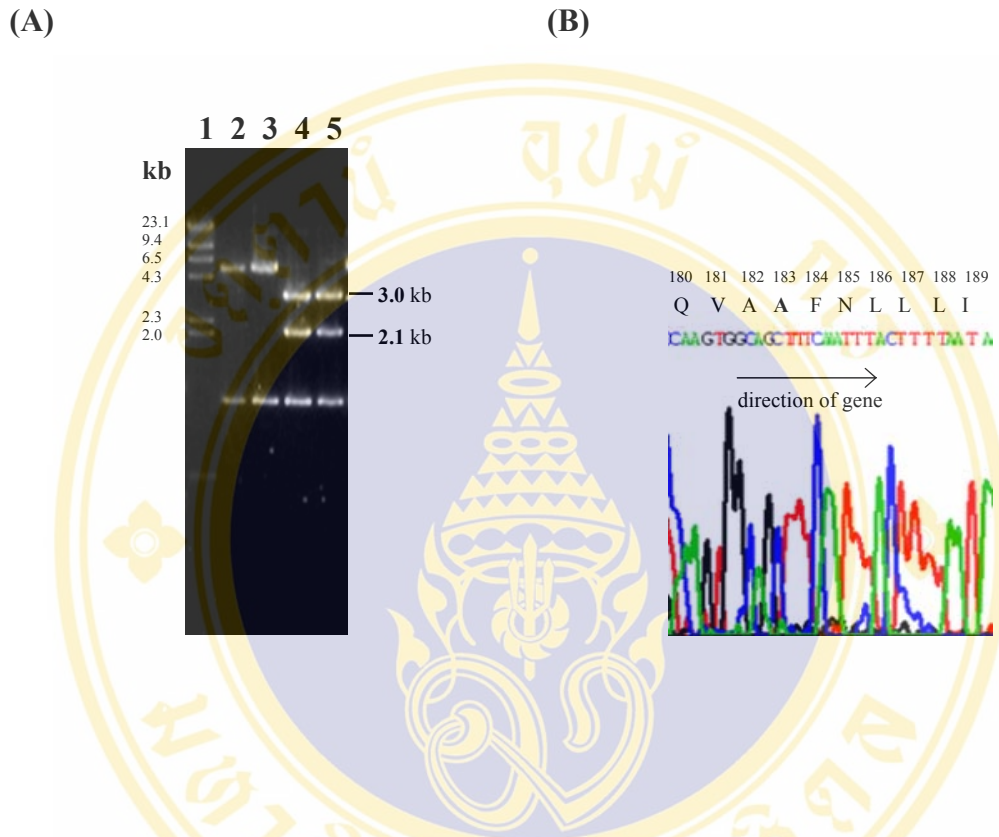


Figure 16: Restriction digestion and DNA sequence analysis of pN183A.

(A) 1% agarose gel electrophoresis (ethidium bromide-stained) of *Bgl*II digestion patterns of the wild-type and mutant plasmids. The 3.0- and 2.1-kb mutant specific bands are indicated.

- Lane 1: λ /*Hind*III digested DNA markers
- Lane 2: The *Bgl*II digested wild-type plasmid, pMU388
- Lane 3: The *Bgl*II digested mutant plasmid, pN183A clone no.1
- Lane 4: The *Bgl*II digested mutant plasmid, pN183A clone no.2
- Lane 5: The *Bgl*II digested mutant plasmid, pN183A clone no.3

(B) The DNA sequencing chromatogram of pN183A clone no.2, using N155A-f as a sequencing primer. Part of the sense strand sequence is shown. The bold letter represents the substituted amino acid residue.

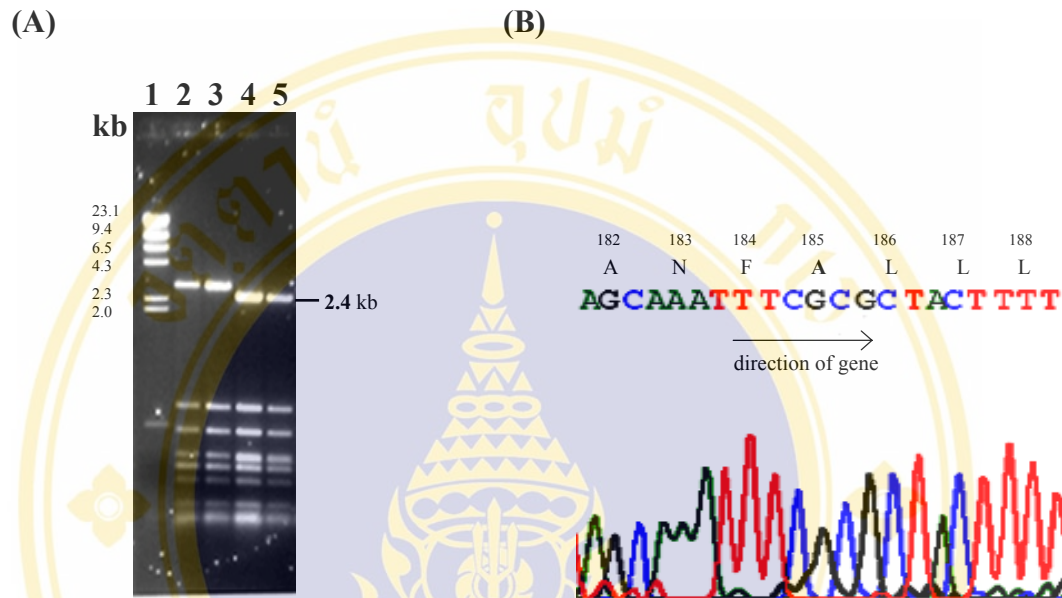


Figure 17: Restriction digestion and DNA sequence analysis of pN185A.

(A) 1% agarose gel electrophoresis (ethidium bromide-stained) of *Hha*I digestion patterns of the wild-type and mutant plasmids. The 2.4-kb mutant specific band is indicated.

- Lane 1: λ /*Hind*III digested DNA markers
- Lane 2: The *Hha*I digested wild-type plasmid, pMU388
- Lane 3: The *Hha*I digested mutant plasmid, pN185A clone no.1
- Lane 4: The *Hha*I digested mutant plasmid, pN185A clone no.2
- Lane 5: The *Hha*I digested mutant plasmid, pN185A clone no.3

(B) The DNA sequencing chromatogram of pN185A clone no.2, using N155A-f as a sequencing primer. Part of the sense strand sequence is shown. The bold letter represents the substituted amino acid residue.

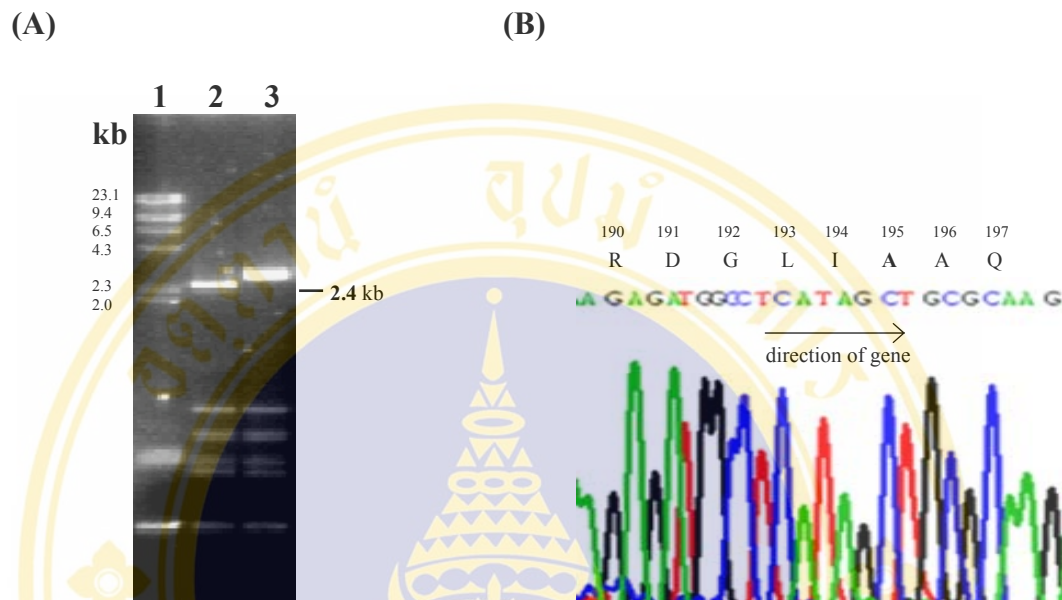


Figure 18: Restriction digestion and DNA sequence analysis of pN195A.

(A) 1% agarose gel electrophoresis (ethidium bromide-stained) of *HhaI* digestion patterns of the wild-type and mutant plasmids. The 2.4-kb mutant specific band is indicated.

- Lane 1: λ /*HindIII* digested DNA markers
- Lane 2: The *HhaI* digested mutant plasmid, pN195A
- Lane 3: The *HhaI* digested wild-type plasmid, pMU388

(B) The DNA sequencing chromatogram of pN195A, using N155A-f as a sequencing primer. Part of the sense strand sequence is shown. The bold letter represents the substituted amino acid residue.

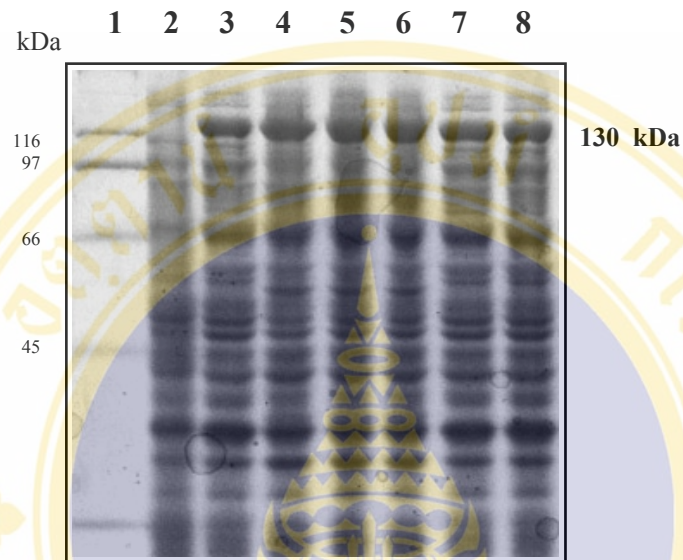


Figure 19: Expression of the Cry4Ba wild-type toxin and Y178A, Q180A, N183A, N185A, N195A mutant toxins.

The figure shows SDS-PAGE protein profiled (Coomassie blue-stained 10% gel) of crude extracts from IPTG induced *E. coli* recombinant cells containing different plasmids. The expected 130-kDa protoxin bands are indicated.

- Lane 1: Molecular mass protein standards
- Lane 2: Crude extracted proteins of *E. coli* containing pUC12
- Lane 3: Crude extracted proteins of *E. coli* containing pMU388
- Lane 4: Crude extracted proteins of *E. coli* containing pY178A
- Lane 5: Crude extracted proteins of *E. coli* containing pQ180A
- Lane 6: Crude extracted proteins of *E. coli* containing pN183A
- Lane 7: Crude extracted proteins of *E. coli* containing pN185A
- Lane 8: Crude extracted proteins of *E. coli* containing pN195A



Figure 20: Solubility of Cry4Ba wild-type and its mutant inclusions.

The figure shows Coomassie blue-stained SDS-PAGE (10% gel) comparing the solubility of the mutant inclusions in 50 mM carbonate buffer, pH 9.0. The expected 130-kDa protoxin bands are indicated.

- Lane 1: Molecular mass protein standards
- Lane 2: Total inclusion suspension of Cry4Ba wild-type
- Lane 3: Soluble fraction of Cry4Ba wild-type
- Lane 4: Total inclusion suspension of Y178A
- Lane 5: Soluble fraction of Y178A
- Lane 6: Total inclusion suspension of Q180A
- Lane 7: Soluble fraction of Q180A
- Lane 8: Total inclusion suspension of N183A
- Lane 9: Soluble fraction of N183A
- Lane 10: Total inclusion suspension of N185A
- Lane 11: Soluble fraction of N185A
- Lane 12: Total inclusion suspension of N195A
- Lane 13: Soluble fraction of N195A

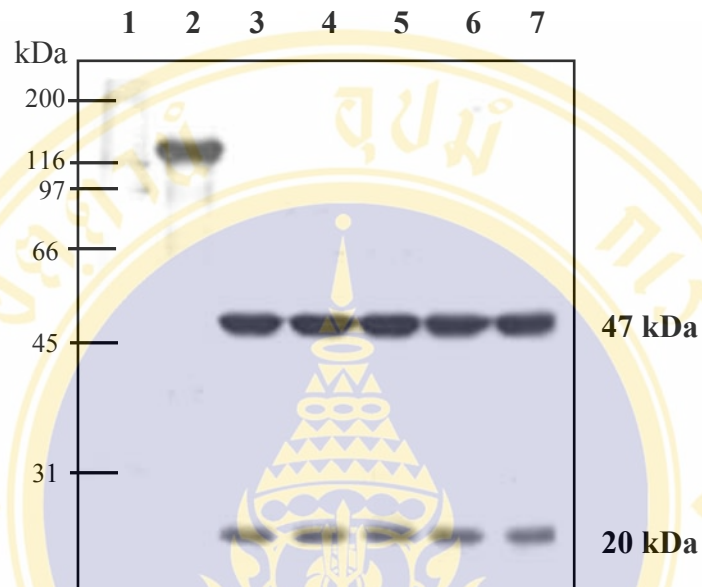


Figure 21: Trypsinised products of the Cry4Ba wild-type toxin and Y178A, Q180A, N185A, N195A mutant toxins.

The figure shows SDS-PAGE (Coomassie blue-stained 15% gel) of the trypsin treated products of Cry4Ba and its mutants. The expected bands of ca. 47 and ca. 20 kDa are indicated.

- Lane 1: Molecular mass protein standards
- Lane 2: Trypsin untreated products of Cry4Ba wild-type
- Lane 3: Trypsin treated products of Cry4Ba wild-type
- Lane 4: Trypsin treated products of Y178A
- Lane 5: Trypsin treated products of Q180A
- Lane 6: Trypsin treated products of N185A
- Lane 7: Trypsin treated products of N195A

Toxin	% Mortality using <i>E. coli</i> whole cells						
	pUC12	Cry4Ba	Y178A	Q180A	N183A	N185A	N195A
Mean	1.2	92.5	74.1	81.8	0.5	78.3	85.9
SEM	0.2	0.9	1.2	0.4	0.1	0.3	0.2

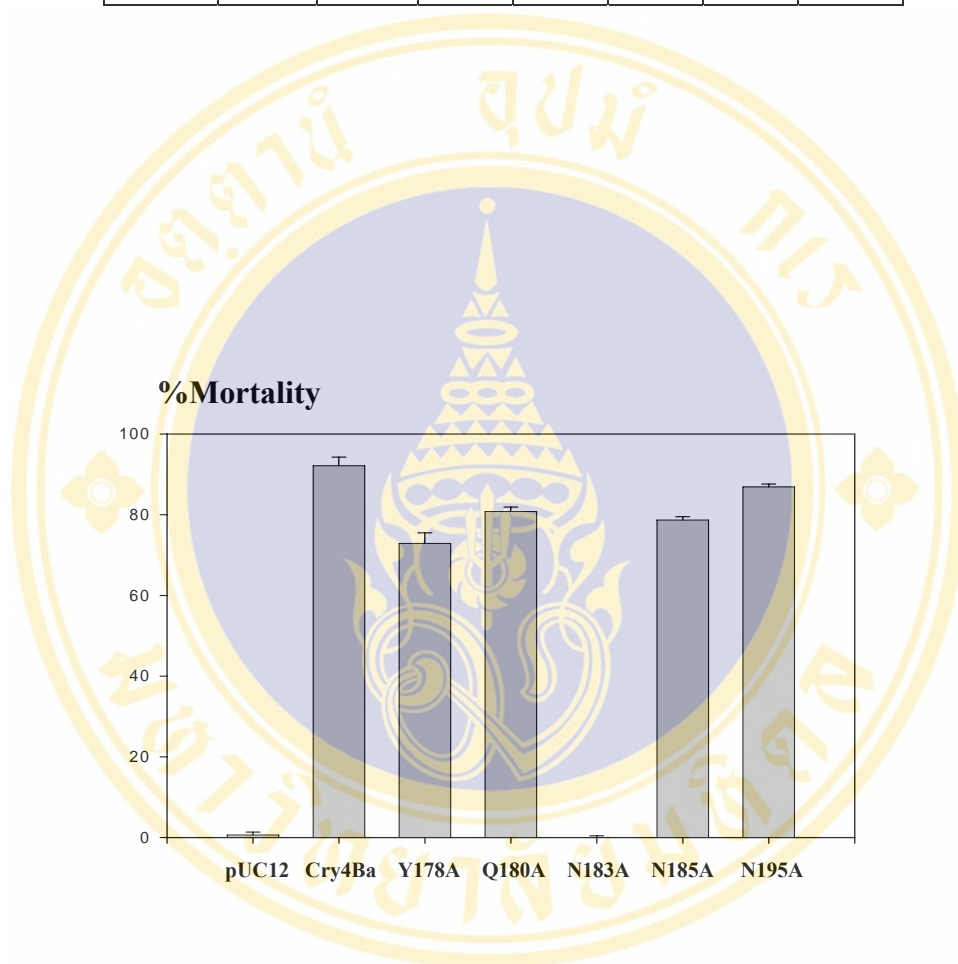


Figure 22: Larvicidal activity of the Cry4Ba and its alanine-substituted mutants.

The figure shows larvicidal activity of *E. coli* cells expressing the Cry4Ba or its mutant toxins (Y178A, Q180A, N183A, N185A and N195A) against *S. aegypti* larvae. The control sample was *E. coli* cells carrying pUC12 vector. Error bars represent standard errors of the mean (SEM) from three independent experiments. Inserted table shows each value in details.

4.5 Constructions of Cry4Ba mutant plasmids substituted at Asn¹⁸³

Previous studies suggested that polarity of only Asn¹⁸³ located in $\alpha 5$ is important for biological activity of the Cry4Ba toxin. The loss of biological activity of Cry4Ba-N183A may be caused by lack of an important functional group at position 183. Attempts were made to test this hypothesis by replacing asparagine with charged amino acid (lysine, arginine, aspartate), polar amino acid (glutamine, threonine, histidine), or nonpolar amino acid (phenylalanine). Structural analysis of the Cry4Ba crystal structure indicated this Asn¹⁸³ points toward $\alpha 7$ and forms hydrogen bond with Tyr²⁶⁷ (Fig. 54). To assume the importance of this interaction between Asn¹⁸³ and Tyr²⁶⁷, the alanine substitution at Tyr²⁶⁷ was also generated. The pMU388 plasmid containing the gene sequence encoding the 130-kDa Cry4Ba toxin was used as a template. Resulting plasmids of PCR amplifications were analysed on agarose gel electrophoresis as shown in Fig. 23. The results showed that the size of all the PCR products corresponds to the length of the pMU388 DNA template. The transformants from each mutation were screened for the presence of the mutant plasmids *via* restriction endonuclease analysis as shown in Fig. 24A-31A. The mutated region in each mutant plasmid was further confirmed by DNA sequencing (Fig. 24A-31A) which revealed that all mutant plasmids contain nucleotide changes at the desired positions.

4.6 Expression of Cry4Ba mutant toxins substituted at Asn¹⁸³

E. coli cells harboring each type of mutant plasmids were expressed upon IPTG induction and the crude extracts were subjected to SDS-PAGE. It was found that the expression levels of all Asn¹⁸³ and Tyr²⁶⁷ mutant protoxins were comparable to that of the wild-type Cry4Ba protoxin (Fig. 32) except for the Asn¹⁸³ mutant substituted with His and Asp (Fig. 33) which the expression levels were lower than that of the wild-type Cry4Ba and the other mutant toxins.

4.7 Solubilisation of the Cry4Ba mutant inclusions substituted at the position 183

After solubilising the protoxin inclusions of each mutant in carbonate buffer, pH 9.0, the amounts of the 130-kDa soluble proteins in the supernatant were compared with those of the proteins in the total fraction. Substitutions of Asn¹⁸³ with Gln or Lys did not affect the solubility of toxins while conversions to Arg, Thr or Phe adversely affected the solubilisation of toxin inclusions (**Fig. 34**). Due to an interaction between Asn¹⁸³ in $\alpha 5$ and Tyr²⁶⁷ in $\alpha 7$, an attempt was also made to assess the solubility of Tyr²⁶⁷ to Ala mutation. It was found that this mutant inclusion could not be solubilised in carbonate buffer. The solubilised mutant protoxins (N183Q and N183K) were also assessed for their proteolytic stability by digestion with TPCK-treated trypsin at 37°C for 16 hr and the proteolytic patterns were analysed on SDS-PAGE. Similar to the wild-type protoxin, the trypsin digestions of the solubilised mutant protoxins yielded proteolytic resistant products of ca. 47 kDa and ca. 20 kDa (**Fig. 35**).

Because of the insolubility in carbonate buffer, pH 9.0, the N183T was also assessed for its solubilisation in gut juices comparing to the wild-type Cry4Ba protoxin inclusion. Gut extracts were obtained from the fourth instar *S. aegypti* larvae. The result showed that both of wild-type and N183T mutant protoxin inclusions could be solubilised in gut juice extraction, however in a low amount, revealing bands of ca 130 kDa and 47 kDa (**Fig. 36**). The observation of ca 47-kDa band in wild-type implied that the gut juices contain some of trypsin-like enzyme which could digest inclusion of protoxins.

4.8 Larvicidal activity of Cry4Ba-N183 mutant toxins

Protoxin inclusions and *E. coli* whole cells expressing the mutant toxins or the wild-type Cry4Ba toxin were tested for their biological activity against *S. aegypti* larvae. As can be seen that both *E. coli* whole cells and protoxin inclusions gave similar results for the observed activity (**see Fig. 37 and 38**). The results also revealed that complete loss of larvicidal activity was observed for substitutions with arginine, lysine or phenylalanine. The substitutions with strong polar residue such as glutamine still retained high larvicidal activity compared to the wild-type Cry4Ba. Substitution

with weak polar residue such as threonine showed ~70% activity. However, the level of larvicidal activity of histidine and aspartate-substituted mutant was found to be ~20 and 30% compared to the wild-type toxin. It should be noted in here that the expression of these two mutants was lower than that of the wild-type and other mutants. Furthermore, the substitution at Tyr²⁶⁷ with Ala revealed a completely loss of larvicidal activity.



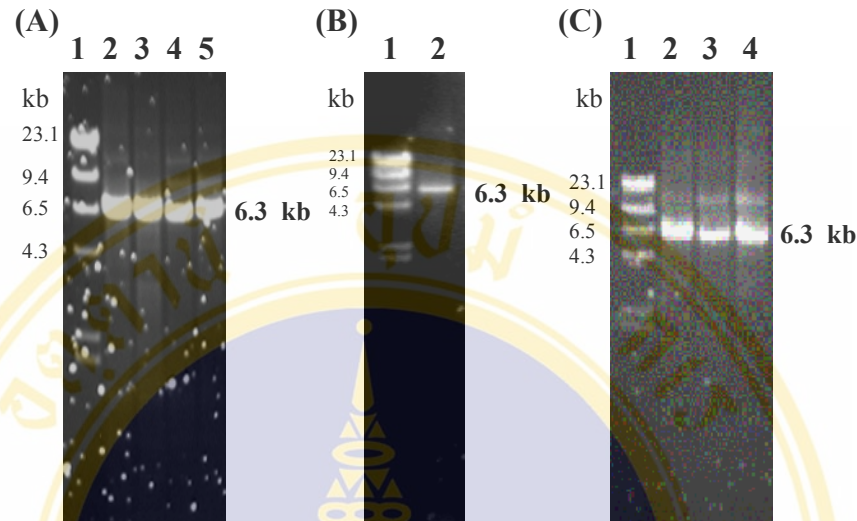


Figure 23: PCR amplification of Cry4Ba mutant plasmids: pN183Q, pN183R, pN183T, pN183H, pN183D, pN183K, pN183F and Y267A.

The figure shows 1.0% agarose gel electrophoresis (ethidium bromide-stained) of PCR products of Cry4Ba mutant plasmids, which amplified at 50°C. The expected 6.3-kb DNA band is indicated with the bold label.

- (A)** Lane 1: λ /*Hind*III digested DNA markers
 Lane 2: The PCR product of the pN183Q plasmid digested with *Dpn*I
 Lane 3: The PCR product of the pN183R plasmid digested with *Dpn*I
 Lane 4: The PCR product of the pN183T plasmid digested with *Dpn*I
 Lane 5: The PCR product of the pN183H plasmid digested with *Dpn*I
- (B)** Lane 1: λ /*Hind*III digested DNA markers
 Lane 2: The PCR product of the pN183D plasmid digested with *Dpn*I
- (C)** Lane 1: λ /*Hind*III digested DNA markers
 Lane 2: The PCR product of the pN183K plasmid digested with *Dpn*I
 Lane 3: The PCR product of the pN183F plasmid digested with *Dpn*I
 Lane 4: The PCR product of the pY267A plasmid digested with *Dpn*I

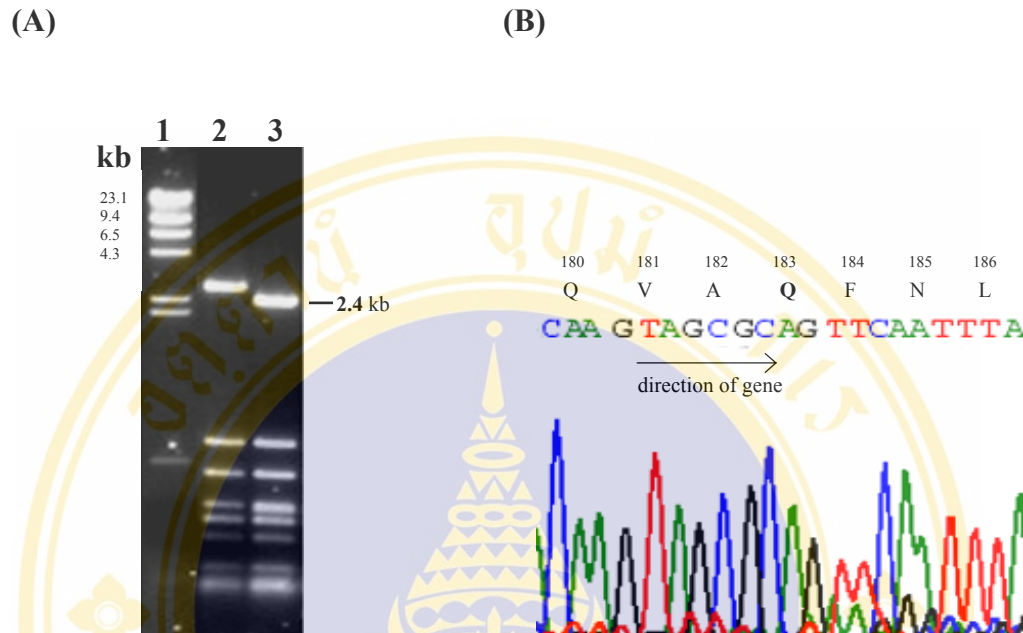


Figure 24: Restriction digestion and DNA sequence analysis of pN183Q.

(A) 1% agarose gel electrophoresis (ethidium bromide-stained) of *HhaI* digestion patterns of the wild-type and mutant plasmids. The 2.4-kb mutant specific band is indicated.

- Lane 1: λ /*HindIII* digested DNA markers
- Lane 2: The *HhaI* digested wild-type plasmid, pMU388
- Lane 3: The *HhaI* digested mutant plasmid, pN183Q

(B) The DNA sequencing chromatogram of pN183Q, using N151A-f as a sequencing primer. Part of the sense strand sequence is shown. The bold letter represents the substituted amino acid residue.

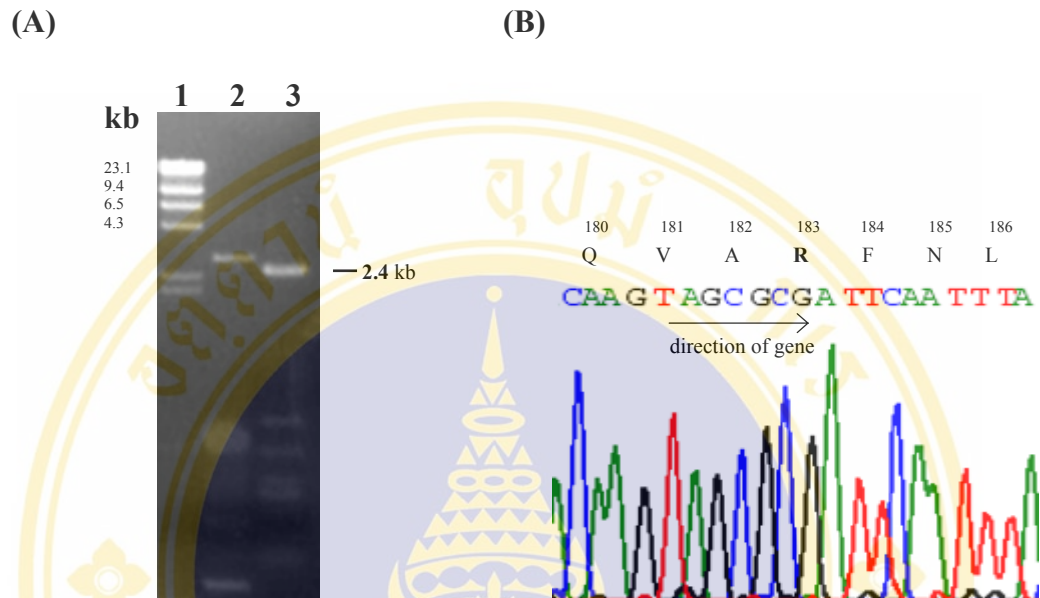


Figure 25: Restriction digestion and DNA sequence analysis of pN183R.

(A) 1% agarose gel electrophoresis (ethidium bromide-stained) of *HhaI* digestion patterns of the wild-type and mutant plasmids. The 2.4-kb mutant specific band is indicated.

- Lane 1: λ /*HindIII* digested DNA markers
- Lane 2: The *HhaI* digested wild-type plasmid, pMU388
- Lane 3: The *HhaI* digested mutant plasmid, pN183R

(B) The DNA sequencing chromatogram of pN183R, using N151A-f as a sequencing primer. Part of the sense strand sequence is shown. The bold letter represents the substituted amino acid residue.

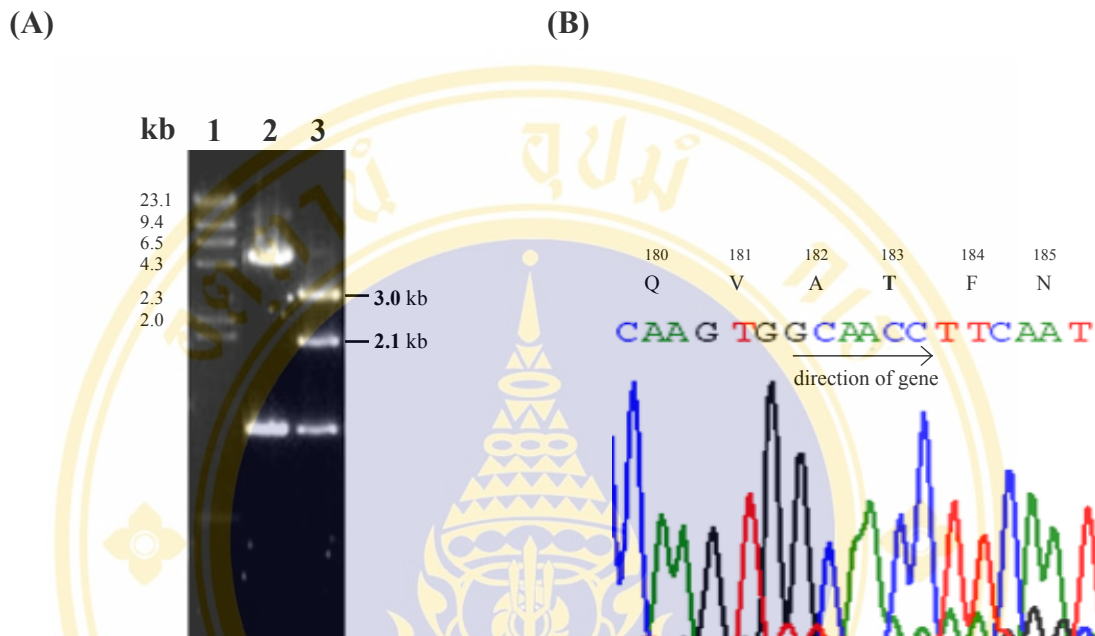


Figure 26: Restriction digestion and DNA sequence analysis of pN183T.

(A) 1% agarose gel electrophoresis (ethidium bromide-stained) of *Bgl*I digestion patterns of the wild-type and mutant plasmids. The 3.0- and 2.1-kb mutant specific bands are indicated.

Lane 1: λ /*Hind*III digested DNA markers

Lane 2: The *Bgl*I digested wild-type plasmid, pMU388

Lane 3: The *Bgl*I digested mutant plasmid, pN183T

(B) The DNA sequencing chromatogram of pN183T, using N151A-f as a sequencing primer. Part of the sense strand sequence is shown. The bold letter represents the substituted amino acid residue.

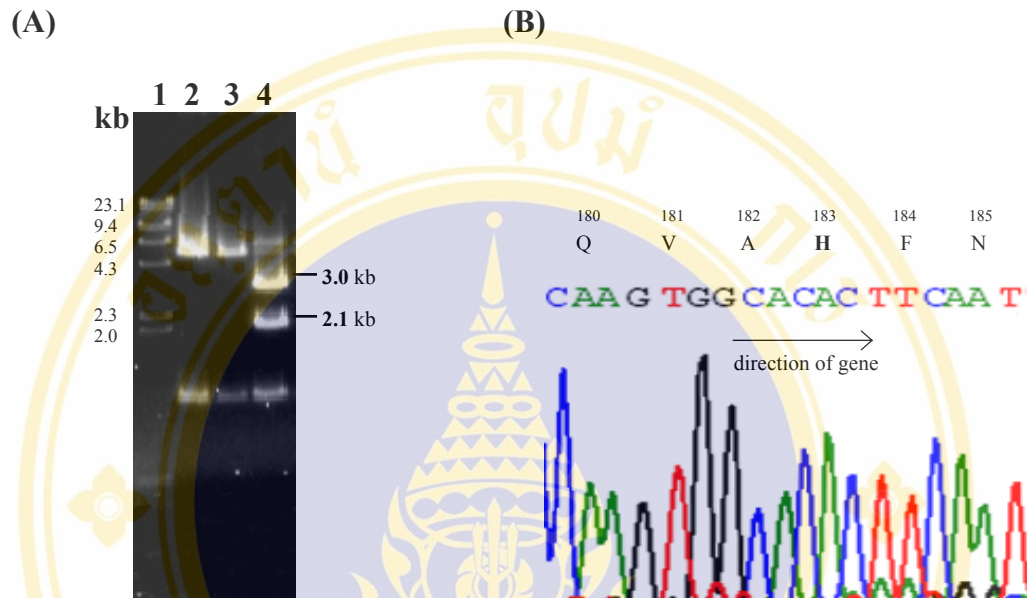


Figure 27: Restriction digestion and DNA sequence analysis of pN183H.

(A) 1% agarose gel electrophoresis (ethidium bromide-stained) of *Bgl*II digestion patterns of the wild-type and mutant plasmids. The 3.0- and 2.1-kb mutant specific bands are indicated.

Lane 1: λ /*Hind*III digested DNA markers

Lane 2: The *Bgl*II digested wild-type plasmid, pMU388

Lane 3: The *Bgl*II digested mutant plasmid, pN183H clone no.1 (negative screening)

Lane 4: The *Bgl*II digested mutant plasmid, pN183H clone no.2 (positive screening)

(B) The DNA sequencing chromatogram of pN183H clone no.2, using N151A-f as a sequencing primer. Part of the sense strand sequence is shown. The bold letter represents the substituted amino acid residue.

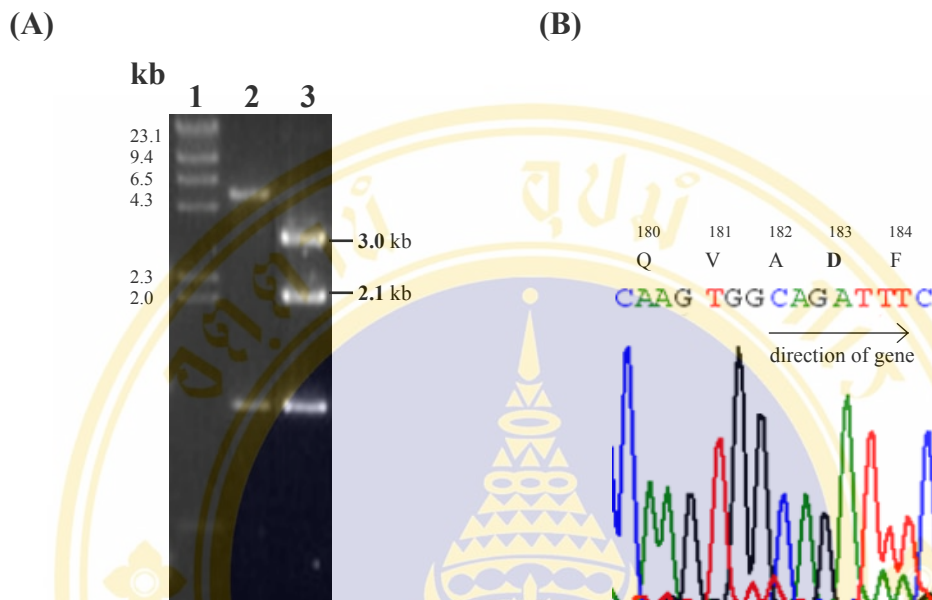


Figure 28: Restriction digestion and DNA sequence analysis of pN183D.

(A) 1% agarose gel electrophoresis (ethidium bromide-stained) of *Bgl*II digestion patterns of the wild-type and mutant plasmids. The 3.0- and 2.1-kb mutant specific bands are indicated.

- Lane 1: λ /*Hind*III digested DNA markers
- Lane 2: The *Bgl*II digested wild-type plasmid, pMU388
- Lane 3: The *Bgl*II digested mutant plasmid, pN183D

(B) The DNA sequencing chromatogram of pN183D, using N151A-f as a sequencing primer. Part of the sense strand sequence is shown. The bold letter represents the substituted amino acid residue.

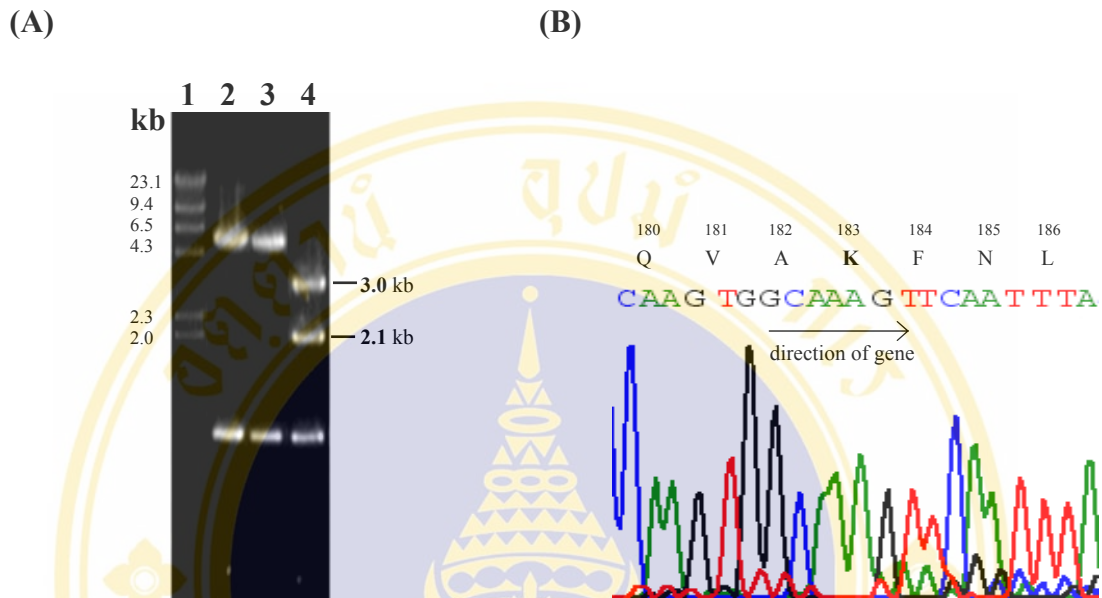


Figure 29: Restriction digestion and DNA sequence analysis of pN183K.

(A) 1% agarose gel electrophoresis (ethidium bromide-stained) of *Bgl*II digestion patterns of the wild-type and mutant plasmids. The 3.0- and 2.1-kb mutant specific bands are indicated.

Lane 1: λ /*Hind*III digested DNA markers

Lane 2: The *Bgl*II digested wild-type plasmid, pMU388

Lane 3: The *Bgl*II digested mutant plasmid, pN183K clone no.1 (negative screening)

Lane 4: The *Bgl*II digested mutant plasmid, pN183K clone no.2 (positive screening)

(B) The DNA sequencing chromatogram of pN183K clone no.2, using N151A-f as a sequencing primer. Part of the sense strand sequence is shown. The bold letter represents the substituted amino acid residue.

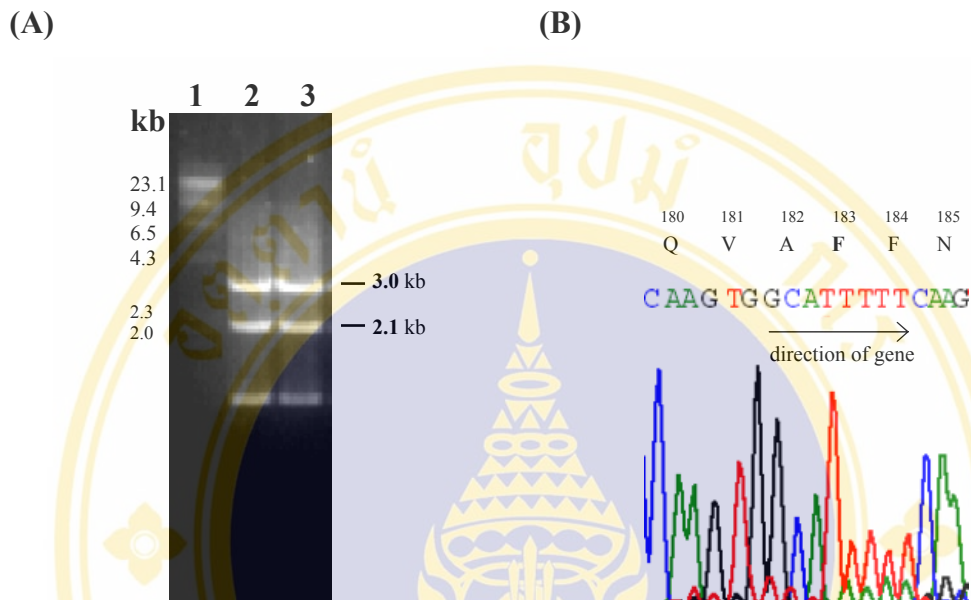


Figure 30: Restriction digestion and DNA sequence analysis of pN183F.

(A) 1% agarose gel electrophoresis (ethidium bromide-stained) of *Bgl*I digestion patterns of the wild-type and mutant plasmids. The 3.0- and 2.1-kb mutant specific bands are indicated.

Lane 1: λ /*Hind*III digested DNA markers

Lane 2: The *Bgl*I digested mutant plasmid, pN183F clone no.1 (positive screening)

Lane 3: The *Bgl*I digested mutant plasmid, pN183F clone no.2 (positive screening)

(B) The DNA sequencing chromatogram of pN183F clone no.1, using N151A-f as a sequencing primer. Part of the sense strand sequence is shown. The bold letter represents the substituted amino acid residue.

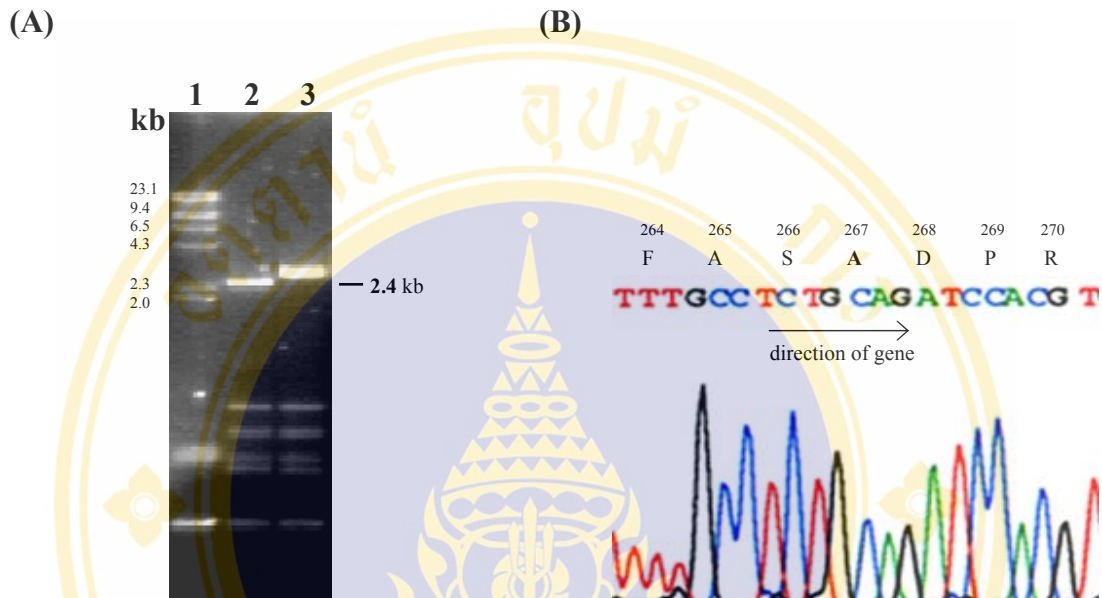


Figure 31: Restriction digestion and DNA sequence analysis of pY267A.

(A) 1% agarose gel electrophoresis (ethidium bromide-stained) of *Pst*I digestion patterns of the wild-type and mutant plasmids. The 2.4-kb mutant specific band is indicated.

- Lane 1: λ /*Hind*III digested DNA markers
- Lane 2: The *Pst*I digested mutant plasmid, pN183F
- Lane 3: The *Pst*I digested wild-type plasmid, pMU388

(B) The DNA sequencing chromatogram of pY267A, using N195A-f as a sequencing primer. Part of the sense strand sequence is shown. The bold letter represents the substituted amino acid residue.

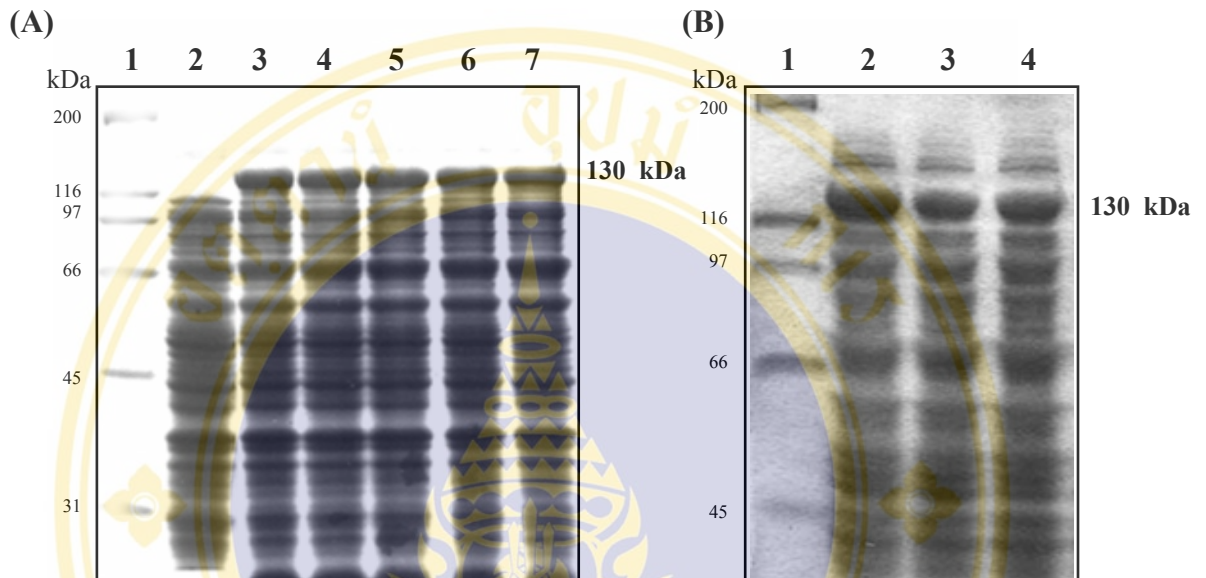


Figure 32: Expression of the Cry4Ba wild-type toxin and N183Q, N183R, N183T, N183F, N183K and Y267A mutant toxins.

The figure shows SDS-PAGE protein profiled (Coomassie blue-stained 10% gel) of crude extracts from IPTG induced *E. coli* recombinant cells containing different plasmids. The expected 130-kDa protoxin bands are indicated.

- (A) Lane 1: Molecular mass protein standards
 Lane 2: Crude extracted proteins of *E. coli* containing pUC12
 Lane 3: Crude extracted proteins of *E. coli* containing pMU388
 Lane 4: Crude extracted proteins of *E. coli* containing pN183Q
 Lane 5: Crude extracted proteins of *E. coli* containing pN183R
 Lane 6: Crude extracted proteins of *E. coli* containing pN183T
 Lane 7: Crude extracted proteins of *E. coli* containing pN185F
- (B) Lane 1: Molecular mass protein standards
 Lane 2: Crude extracted proteins of *E. coli* containing pMU388
 Lane 3: Crude extracted proteins of *E. coli* containing pN183K
 Lane 4: Crude extracted proteins of *E. coli* containing pY267A

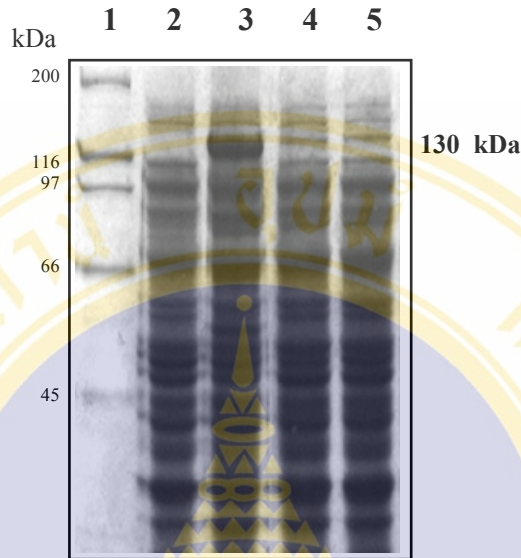


Figure 33: Expression of the Cry4Ba wild-type toxin and N183H, N183D mutant toxins.

The figure shows SDS-PAGE protein profiled (Coomassie blue-stained 10% gel) of crude extracts from IPTG induced *E. coli* recombinant cells containing different plasmids. The expected 130-kDa protoxin bands are indicated.

- Lane 1: Molecular mass protein standards
- Lane 2: Crude extracted proteins of *E. coli* containing pUC12
- Lane 3: Crude extracted proteins of *E. coli* containing pMU388
- Lane 4: Crude extracted proteins of *E. coli* containing pN183H
- Lane 5: Crude extracted proteins of *E. coli* containing pN183D

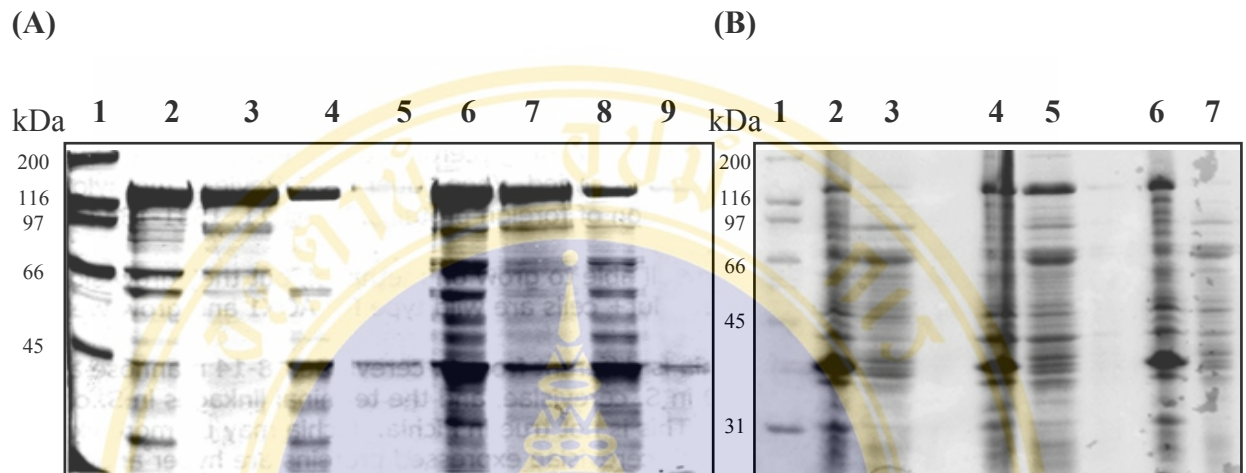


Figure 34: Solubility of Cry4Ba wild-type and its Asn¹⁸³ mutant inclusions *in vitro*.

The figure shows Coomassie blue-stained SDS-PAGE comparing the solubility of the mutant inclusions in 50 mM carbonate buffer, pH 9.0.

- (A) Lane 1: Molecular mass protein standards
 Lane 2: Total inclusion suspension of Cry4Ba wild-type
 Lane 3: Soluble fraction of Cry4Ba wild-type
 Lane 4: Total inclusion suspension of N183R
 Lane 5: Soluble fraction of N183R
 Lane 6: Total inclusion suspension of N183Q
 Lane 7: Soluble fraction of N183Q
 Lane 8: Total inclusion suspension of N183T
 Lane 9: Soluble fraction of N183T
- (B) Lane 1: Molecular mass protein standards
 Lane 2: Total inclusion suspension of N183F
 Lane 3: Soluble fraction of N183F
 Lane 4: Total inclusion suspension of N183K
 Lane 5: Soluble fraction of N183K
 Lane 6: Total inclusion suspension of Y267A
 Lane 7: Soluble fraction of Y267A

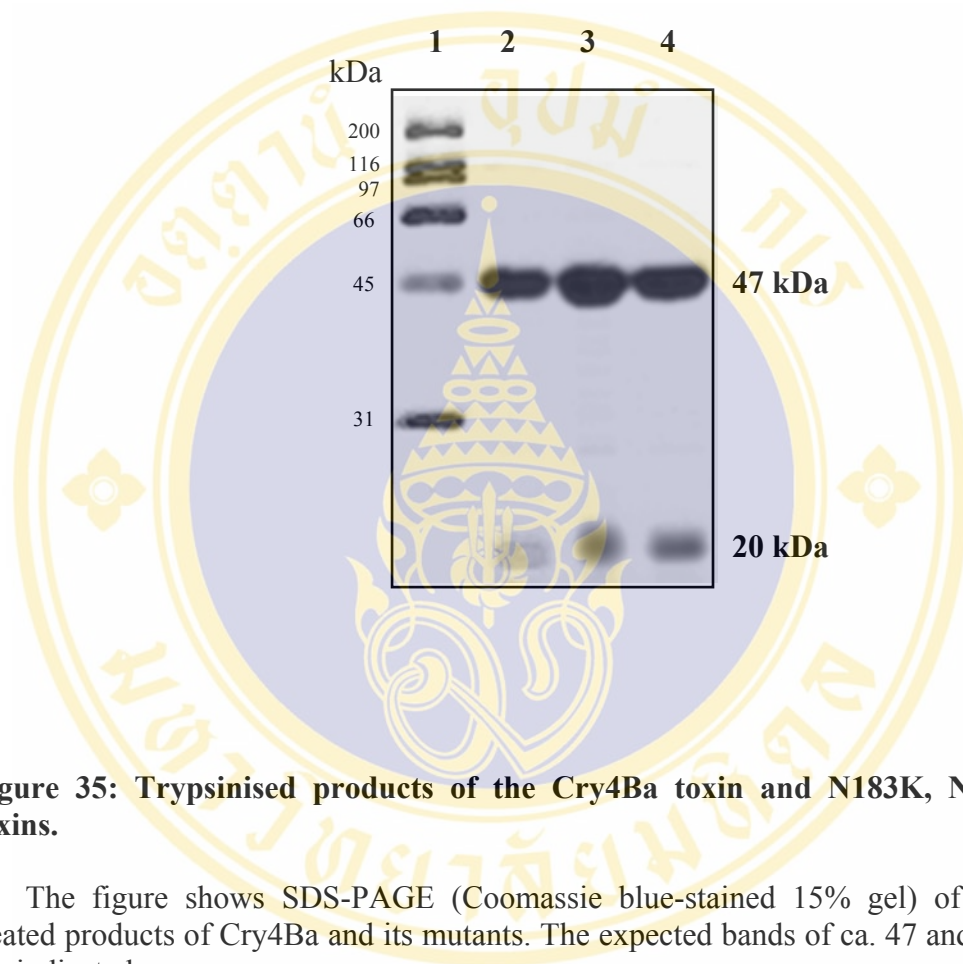


Figure 35: Trypsinised products of the Cry4Ba toxin and N183K, N183Q mutant toxins.

The figure shows SDS-PAGE (Coomassie blue-stained 15% gel) of the trypsin treated products of Cry4Ba and its mutants. The expected bands of ca. 47 and ca. 20-kDa are indicated.

- Lane 1: Molecular mass protein standards
- Lane 2: Trypsin treated products of active mutant N183K
- Lane 3: Trypsin treated products of Cry4Ba wild-type
- Lane 4: Trypsin treated products of inactive mutant N183Q

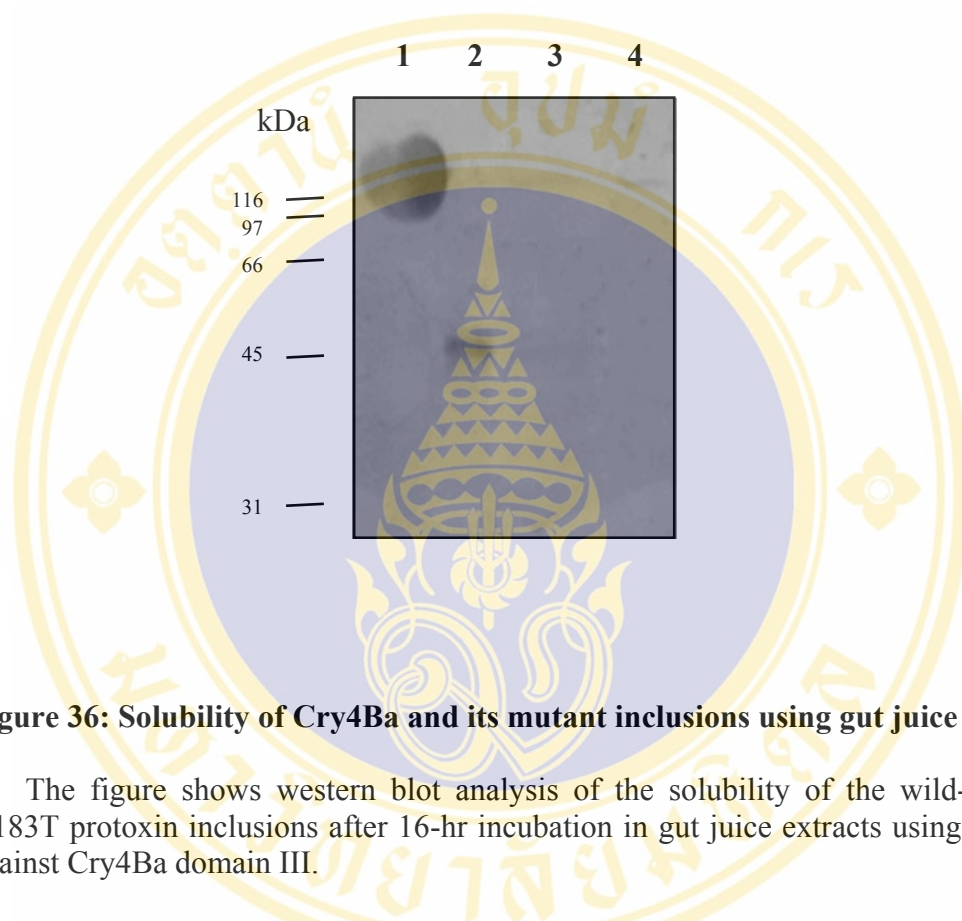


Figure 36: Solubility of Cry4Ba and its mutant inclusions using gut juice extracts.

The figure shows western blot analysis of the solubility of the wild-type and N183T protoxin inclusions after 16-hr incubation in gut juice extracts using antibody against Cry4Ba domain III.

Lane 1: Soluble fraction of Cry4Ba in 50 mM Na₂CO₃, pH 9.0

Lane 2: Trypsin treated products of Cry4Ba in 50 mM Na₂CO₃, pH 9.0

Lane 3: Soluble fraction of Cry4Ba in gut juice extracts

Lane 4: Soluble fraction of N183T in gut juice extracts

Toxin	% Mortality using <i>E. coli</i> whole cells									
	pUC12	Cry4Ba	N183Q	N183R	N183T	N183F	N183K	Y267A	N183H	N183D
Mean	2.3	93.7	90.1	0.7	63.5	0.3	0.6	1.0	20.7	31.1
SEM	0.4	1.5	0.2	0.2	1.2	0.1	0.2	0.3	1.9	4.1

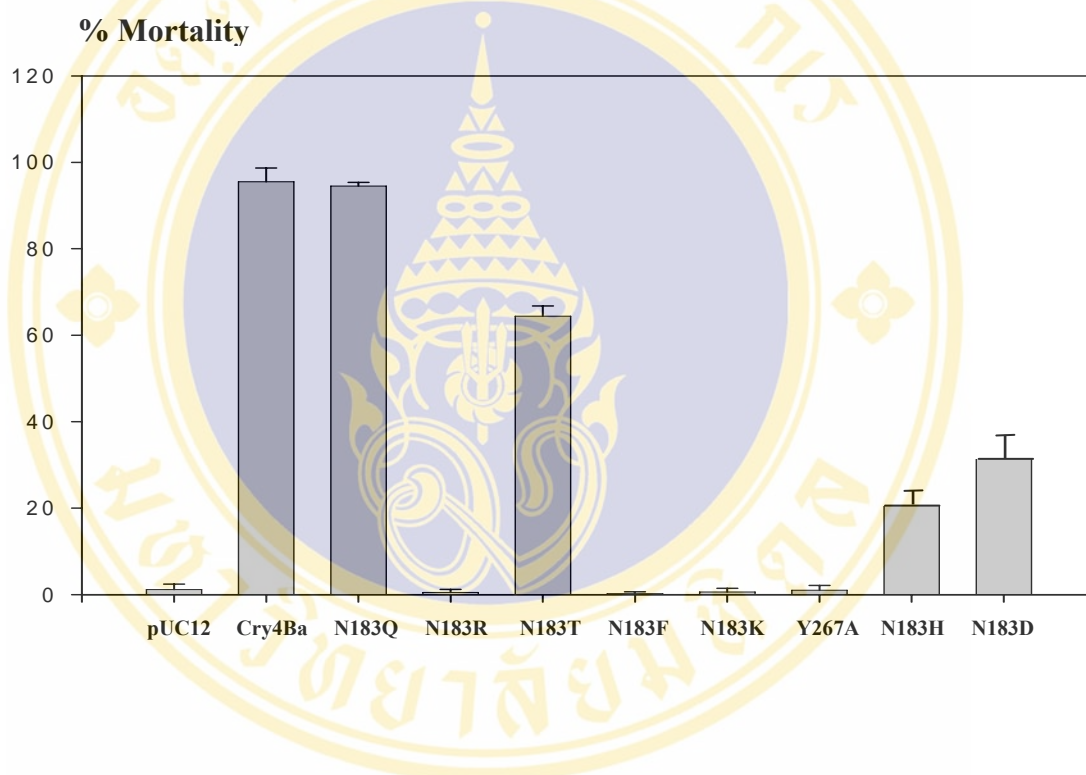


Figure 37: Larvicidal activity of the wild-type Cry4Ba and its mutants substituted at the position 183.

The figure shows comparison of larvicidal activity of *E. coli* cells expressing the wild-type Cry4Ba and its mutants substituted at the position 183 against *S. aegypti* larvae. The control sample was *E. coli* cells carrying pUC12 vector. Error bars represent standard errors of the mean (SEM) from four independent experiments. Inserted table shows each value in details.

Toxin	% Mortality using toxin inclusions			
	Cry4Ba	N183Q	N183T	N183K
Mean	90.1	88.9	61.5	0
SEM	0.6	3.3	0.7	0

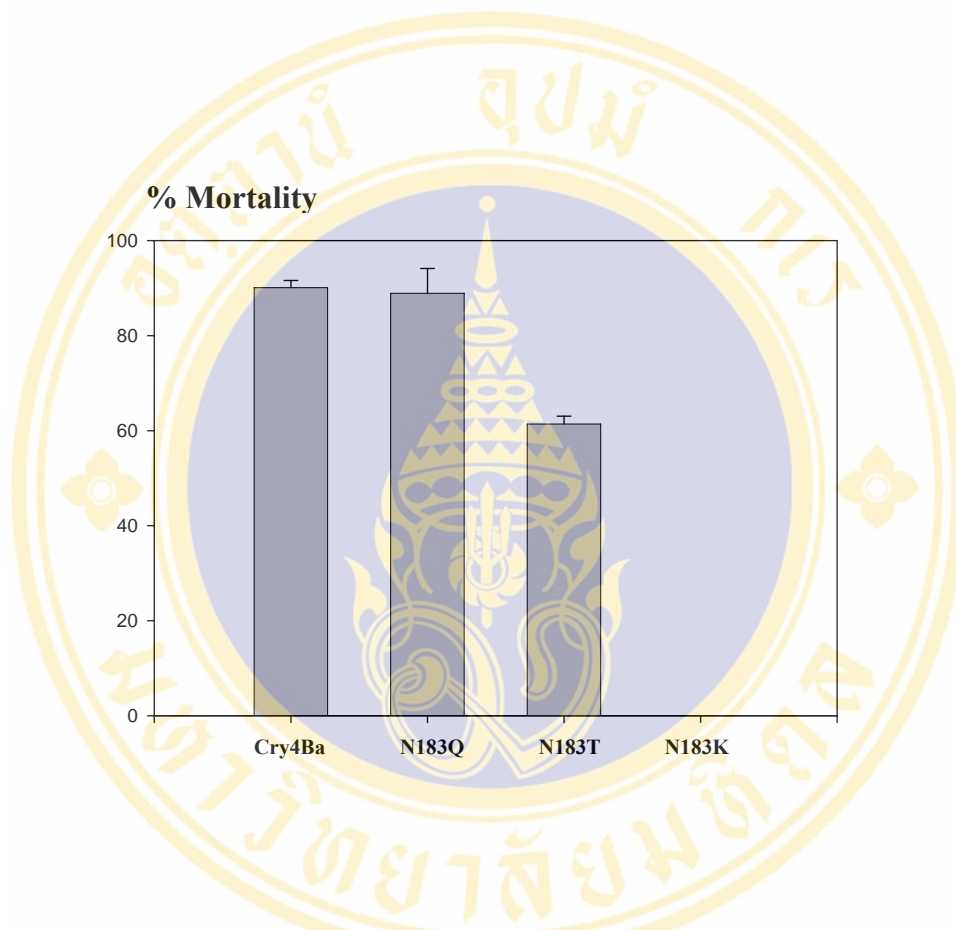


Figure 38: Larvicidal activity using toxin inclusions of Asn¹⁸³ mutants.

The figure shows comparison of larvicidal activity between the wild-type Cry4Ba and its mutant toxins against *S. aegypti* larvae using 6 μg protoxin inclusions. Error bars represent standard errors of the mean (SEM) from three independent experiments. Inserted table shows each value in details.

4.9 Mutagenesis of hydrophobic residues in $\alpha 5$ of the Cry4Ba toxin

Substitutions with serine of selected hydrophobic amino acids (Val¹⁸¹ and Ala¹⁸²) in $\alpha 5$ were performed *via* PCR-based directed mutagenesis. Results of PCR amplification, DNA sequencing and toxin expression are shown in **Fig. 39-42**. The expression level of both toxins was similar to that of the wild-type Cry4Ba toxin. In addition, larvicidal assays revealed that the substitutions of both Val¹⁸¹ and Ala¹⁸² with alanine as single or double mutations had a small effect on toxicity. All three mutants (V181S, A182S and V181S/A182S) still retained about 70% mortality (**Fig. 43**) compared to the wild-type toxin.

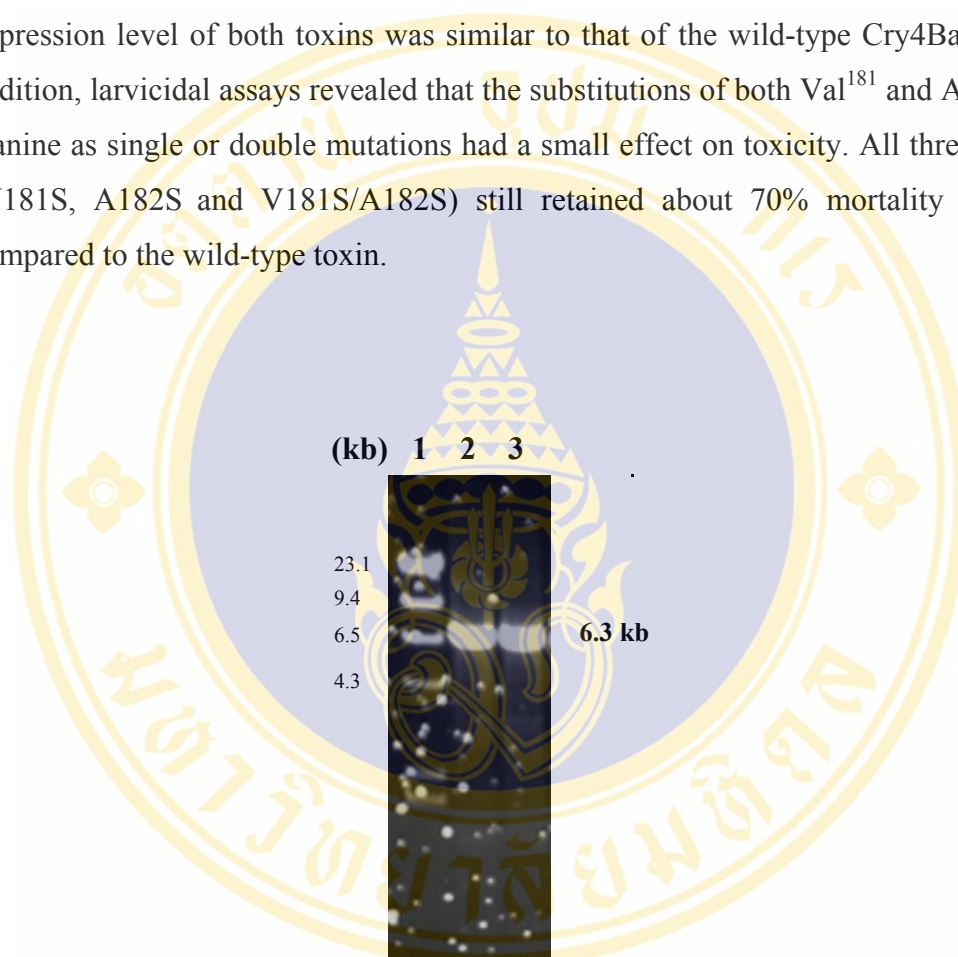


Figure 39: PCR amplification of Cry4Ba mutant plasmids: pV181S and pA182S.

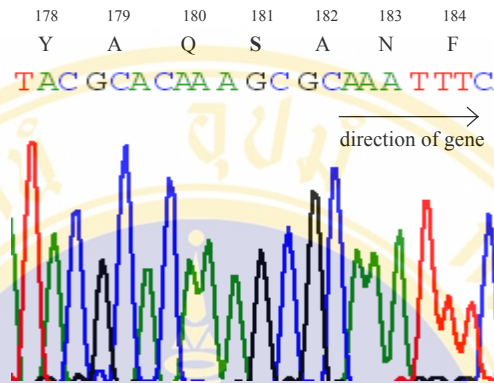
The figure shows 1.0 % agarose gel electrophoresis (ethidium bromide-stained) of PCR products of Cry4Ba mutant plasmids, which amplified at 48°C. The expected 6.3-kb DNA band is indicated with the bold label.

Lane 1: λ /HindIII digested DNA markers

Lane 2: The PCR product of the pV181S plasmid digested with *DpnI*

Lane 3: The PCR product of the pA182S plasmid digested with *DpnI*

(A)



(B)

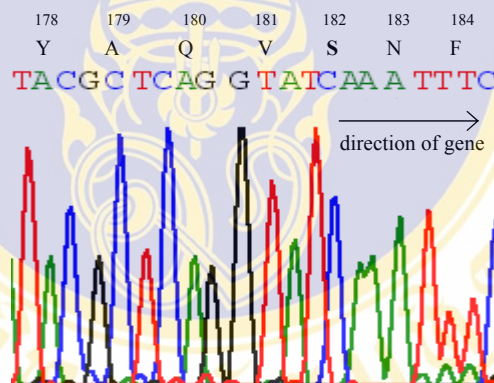


Figure 40: DNA sequence analysis of pV181S and pA182S.

The DNA sequencing chromatogram of pV181S (A) and pA182S (B), using N151A-f as a sequencing primer. Parts of these sense strand sequence are shown. The bold letter represents the substituted amino acid residue.

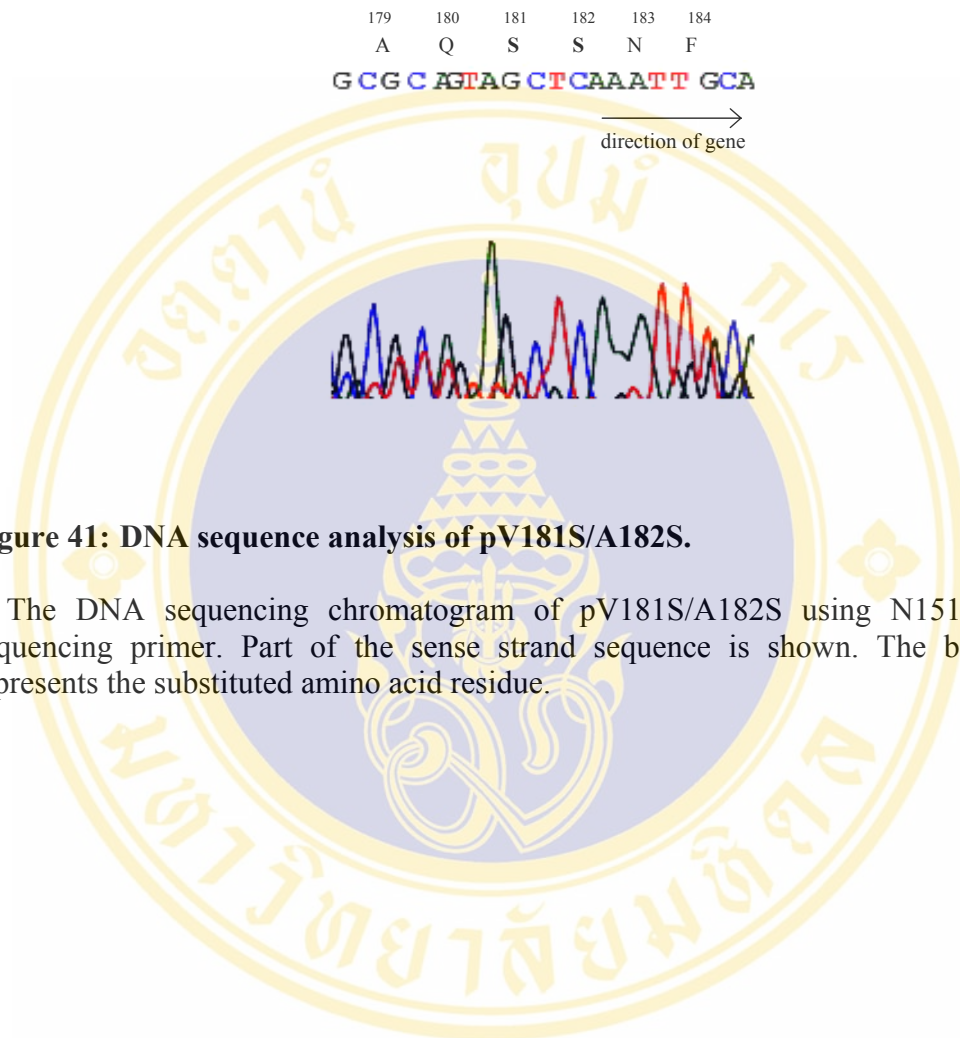


Figure 41: DNA sequence analysis of pV181S/A182S.

The DNA sequencing chromatogram of pV181S/A182S using N151R-f as a sequencing primer. Part of the sense strand sequence is shown. The bold letter represents the substituted amino acid residue.

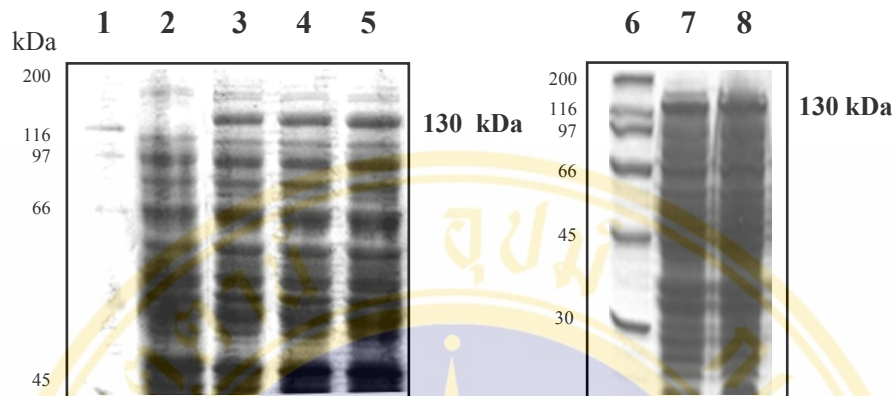


Figure 42: Expression of the Cry4Ba toxin and V181S, A182S and V181S/A182S mutant toxins.

The figure shows SDS-PAGE protein profiled (Coomassie blue-stained 10% gel) of crude extracts from IPTG induced *E. coli* recombinant cells containing different plasmids. The expected 130-kDa protoxin bands are indicated.

- Lanes 1 and 6: Molecular mass protein standards
- Lane 2: Crude extracted proteins of *E. coli* containing pUC12
- Lane 3: Crude extracted proteins of *E. coli* containing pMU388
- Lane 4: Crude extracted proteins of *E. coli* containing pV181S
- Lane 5: Crude extracted proteins of *E. coli* containing pA182S
- Lane 7: Crude extracted proteins of *E. coli* containing pV181S/A182S clone no.1
- Lane 8: Crude extracted proteins of *E. coli* containing pV181S/A182S clone no.2

Toxin	% Mortality using <i>E. coli</i> whole cells				
	pUC12	Cry4Ba	V181S	A182S	V181S/A182S
Mean	1.5	88.3	67.4	62.1	73.6
SEM	0.4	1.4	3.1	0.6	4.8

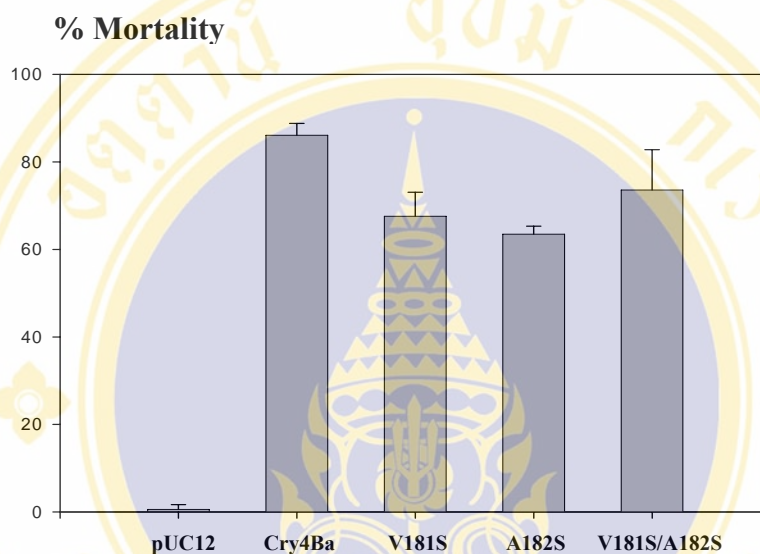


Figure 43: Larvicidal activity of the wild-type Cry4Ba and its mutants substituted at the position 181 and 182.

The figure shows comparison of larvicidal activity of *E. coli* cells expressing the wild-type Cry4Ba and its mutants substituted at the positions 181 and 182 against *S. aegypti* larvae. The control sample was *E. coli* cells carrying pUC12 vector. Error bars represent standard errors of the mean (SEM) from three independent experiments. Inserted table shows each value in details.

CHAPTER 5

RESULT II:

CHARACTERISATION OF Cry4Ba-N183 MUTANT TOXINS

5.1 Purification of Cry4Ba and Asn¹⁸³ mutant toxins

After solubilisation and trypsin activation in 50 mM Na₂CO₃, pH 9.0, the 65-kDa activated Cry4Ba wild-type and the N183K mutant toxin were subjected to size-exclusion FPLC (Superose-12 column), which was equilibrated with carbonate buffer, pH 9.0. It was found that purified toxin fractions (as indicated by arrow in chromatogram in **Fig. 44A-44B**) were eluted as a peak corresponding to 65-kDa bovine serum albumin. These peak fractions were then analysed on SDS-PAGE (**Fig. 44A-44B**) and used for further characterisation.

5.2 Structural determination of Cry4Ba and N183K mutant toxins

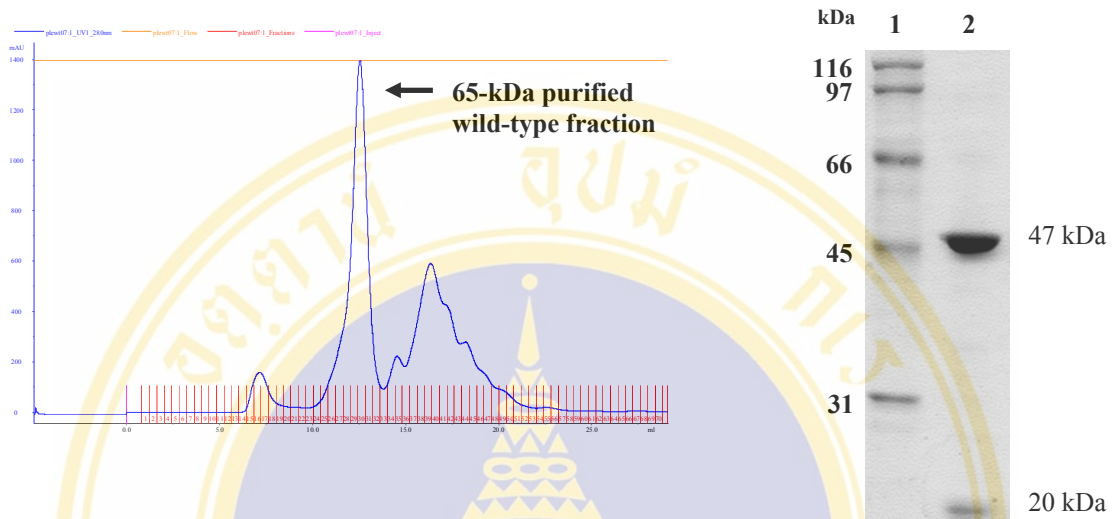
5.2.1 Secondary structure of Cry4Ba and N183K mutant toxins

CD spectroscopy was employed to compare secondary structure contents of wild-type and its mutant toxins. **Fig. 45** shows the CD spectra of the 65-kDa FPLC-purified toxins of Cry4Ba and its mutant in the 190-260 nm far UV regions. The CD spectrum of the larvicidal inactive N183K mutant was similar to that of the wild-type Cry4Ba toxin, suggesting that their overall secondary structure contents are likely the same.

5.2.2 Tertiary structure of Cry4Ba and N183K mutant toxin

Intrinsic fluorescence of tryptophan residues of Cry4Ba and its mutant was measured by spectrofluorometer. **Fig. 46** shows the fluorescence spectra of the 65-kDa FPLC-purified Cry4Ba and its mutant toxin at 340 nm. The fluorescence spectrum of the inactive N183K mutant was also found to be similar to that of the wild-type Cry4Ba toxin, suggesting that their overall tertiary structures are likely the same.

(A)



(B)

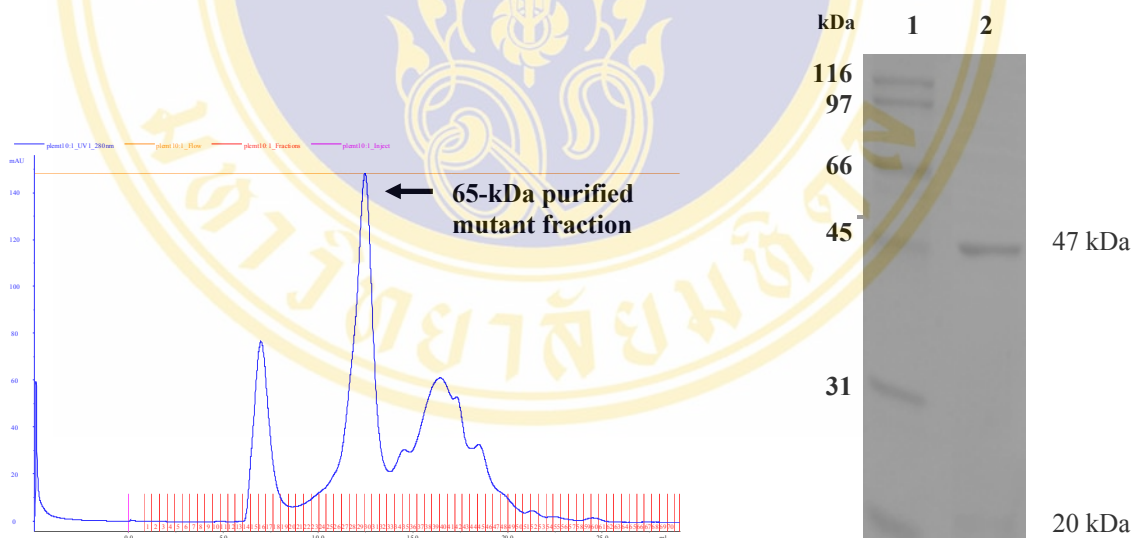


Figure 44: Chromatogram and SDS-PAGE analysis of purified Cry4Ba and N183K mutant toxins.

The figure shows FPLC-chromatogram from size-exclusion chromatography (Superose 12) and Coomassie blue-stained (15% gel) SDS-PAGE of purified fraction of; (A) the wild-type Cry4Ba toxin. (B) the N183K mutant toxin.

Lane 1: Molecular mass protein standards

Lane 2: The purified fraction of 65-kDa toxins after size exclusion chromatography

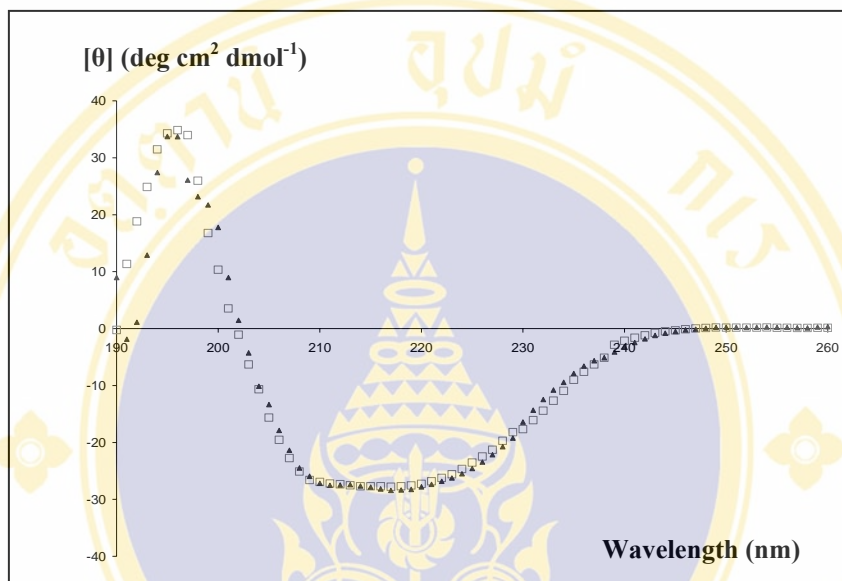


Figure 45: CD spectra of wild-type Cry4Ba and N183K mutant.

The figure shows CD spectra of the 65-kDa purified Cry4Ba toxin (□) in comparison with that of the N183K mutant (▲) in 50 mM Na₂CO₃, pH 9.0.

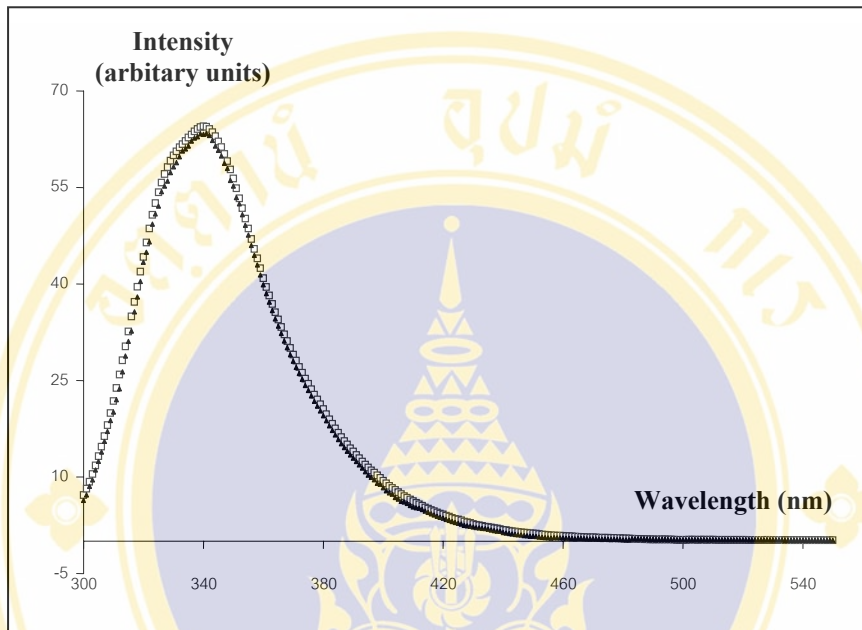


Figure 46: Intrinsic fluorescence spectra of the wild-type Cry4Ba toxin and the N183K mutant toxin.

The figure shows fluorescence spectra of the 65-kDa purified Cry4Ba toxin (□) in comparison with that of the N183K mutant (▲) in 50 mM Na_2CO_3 , pH 9.0.

5.3 Membrane perturbing activity of Cry4Ba and N183K mutant toxins

Membrane perturbation of the 65-kDa purified proteins of Cry4Ba wild-type and its mutant was investigated by using fluorescence spectroscopy as described in **Method: 3.2.20.2**. Calcein fluorescence dye was used as an internal marker to monitor liposome permeability changes after adding toxin. **Fig. 47-48** shows the fluorescence intensity after addition of the activated Cry4Ba and its mutant toxins into 2.5 μ M liposome vesicles. The ability of the N183K mutant (7.5 μ g/ml) to exert membrane perturbing activity towards lipid vesicles was much weaker than the wild-type toxin, indicating that Asn¹⁸³ is involved in membrane perturbation of the Cry4Ba toxin

5.4 Oligomerisation study of Cry4Ba and its mutant toxins

A gel electrophoresis system was employed to examine effects on toxin oligomerisation of the Cry4Ba toxin under various conditions. As shown in **Fig. 49A**, the 65-kDa activated wild-type toxin could form a mixture of monomers, dimers (ca. 110 kDa), and trimers (ca. 180 kDa) on liposome vesicles, with the predominant trimer species after 2-hr incubation. However, the 180-kDa trimeric band seemed to disappear after heating at 95°C and 70°C, but not at 60 °C for 10 min (**Fig. 49B**). In addition, the trimeric species could be detected on immunoblots probed with anti-Cry4Ba domain III monoclonal antibodies (**Fig. 50**), indicating that this 180-kDa trimeric band is an assembly of the monomeric Cry4Ba toxin. **Fig. 51** shows the Cry4Ba protein migrated as oligomeric bands on the gel regardless of whether it was cross-linked or not. However, the oligomerisation state of the Cry4Ba toxin seemed to be strengthened with the presence of liposome vesicles.

Unlike the Cry4Ba wild-type toxin, the N183K bio-inactive mutant toxin existed as monomeric species under the conditions used. In contrast, the Cry4Ba-R158A protein, the bioinactive mutant toxin with the alanine substitution at Arg¹⁵⁸ in α 4 (109), was still found to be able to form oligomers (**Fig. 52**). However, the N183K mutant toxin could migrate as oligomeric bands on the gel when it was cross-linked with glutaraldehyde agent (**Fig. 53**).

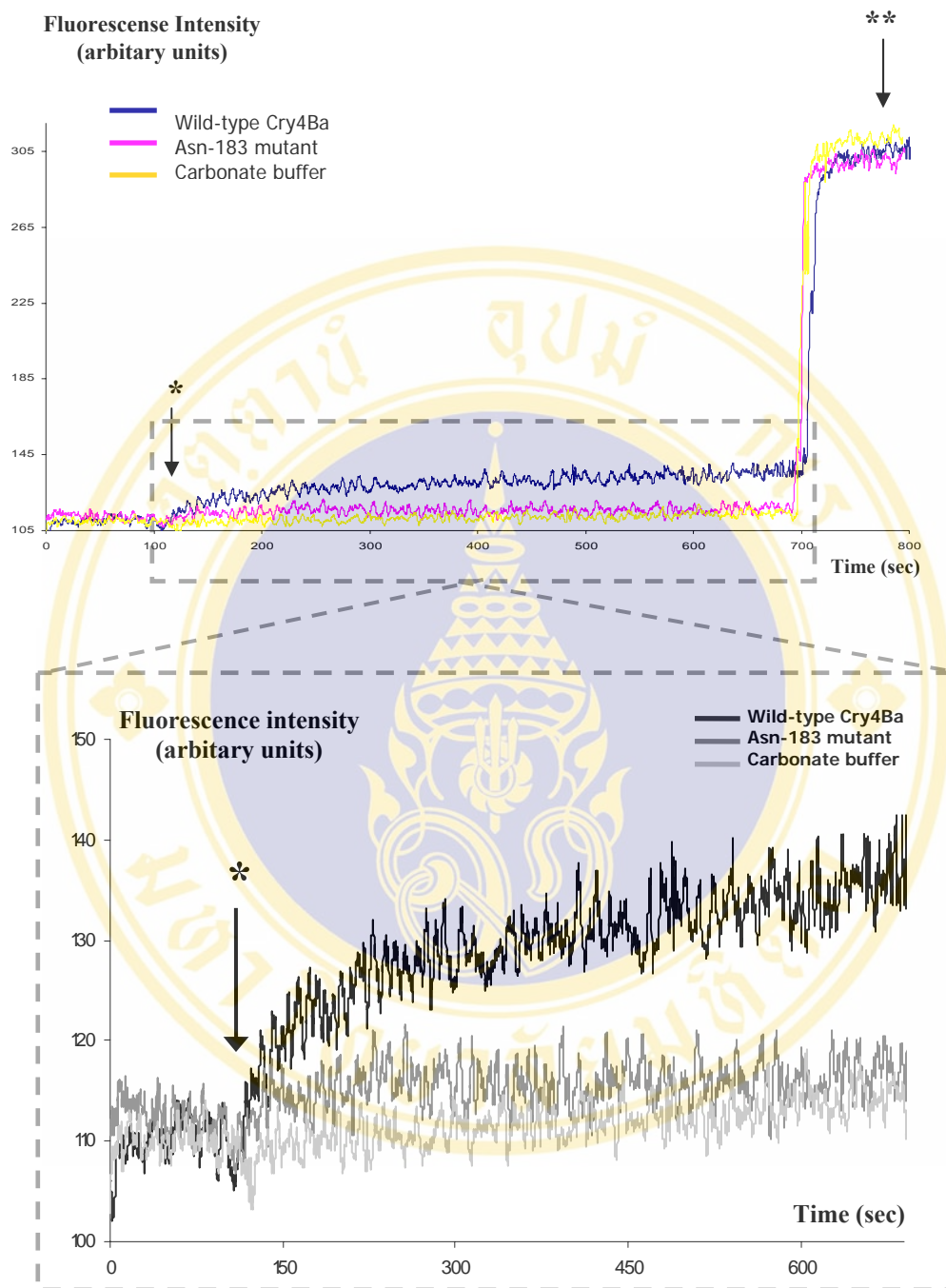


Figure 47: Effects of the Cry4Ba toxin on calcein release from liposomes.

The figure shows the overall of fluorescence intensity after addition of the activated Cry4Ba and its mutant toxin into 2.5 μ M liposome suspension in the liposome-entrapped calcein release assay, with excitation set at 485 nm and emission monitored at 520 nm. 100% calcein release was obtained by adding 0.1% Triton X-100 after a 10-min incubation with protein samples. Arrows indicate the time events when toxin (*) or Triton X-100 (**) was added into the suspension. The figure below is an expanded view.

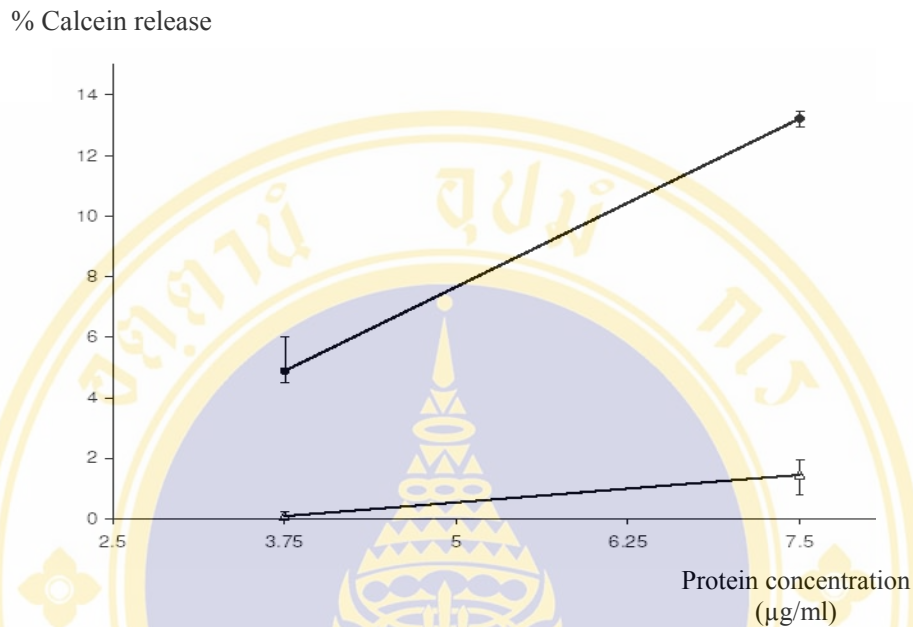


Figure 48: The relative release activities of the wild-type Cry4Ba and the N183K mutant, with varying concentrations.

The relative release activity of each protein sample, the wild-type (●) and the Asn¹⁸³ mutant (Δ) with different concentrations that are indicated as fraction of 100% release induced by Triton X-100. Error bars represent standard error of the mean from at least three independent experiments. The release in the control sample incubated with carbonate buffer rarely exceeded 1% and this value has been subtracted in the figure.

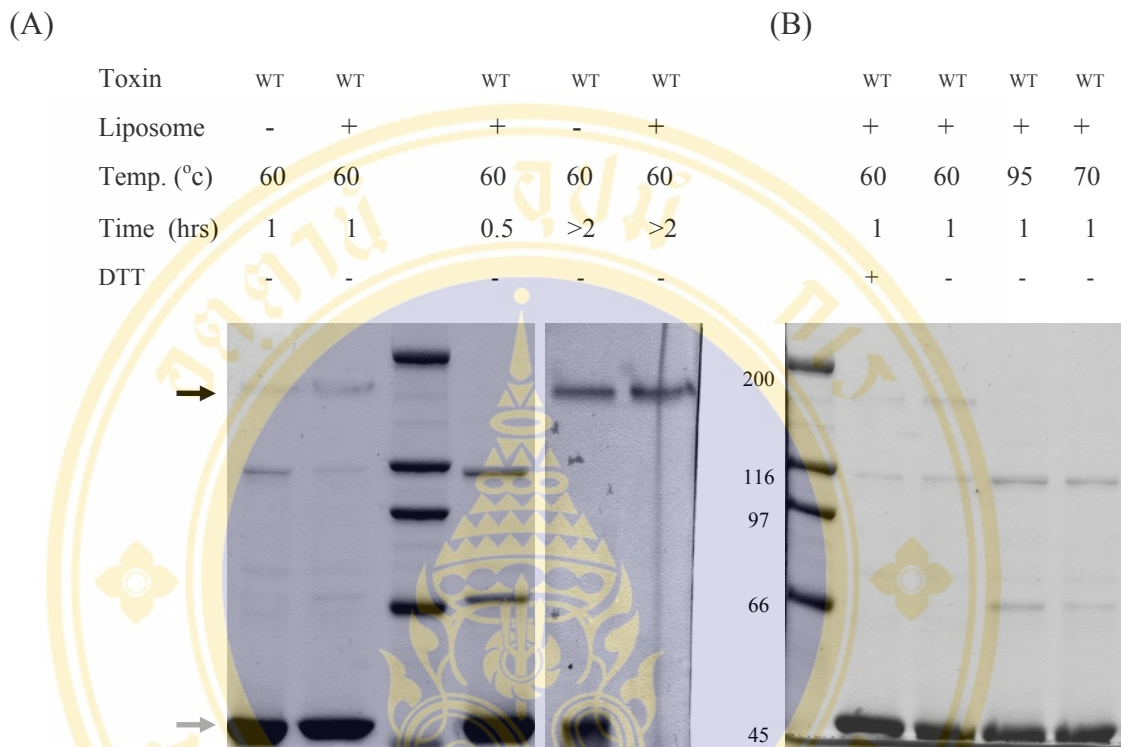


Figure 49: Oligomerisation state of the Cry4Ba wild-type in varying incubation time and temperature.

SDS-PAGE analysis of the oligomeric state of Cry4Ba wild-type in varying; (A) lengths of incubation time (a half hour to more than 2 hours). Black arrow shows the trimeric species of protein. Gray arrow shows the processed 47-kDa Cry4Ba fragment that remains non-covalently attached to the 20-kDa fragment under non-denaturing conditions. (B) temperature (60°C to 95°C) and in the presence of 25 mM DTT.

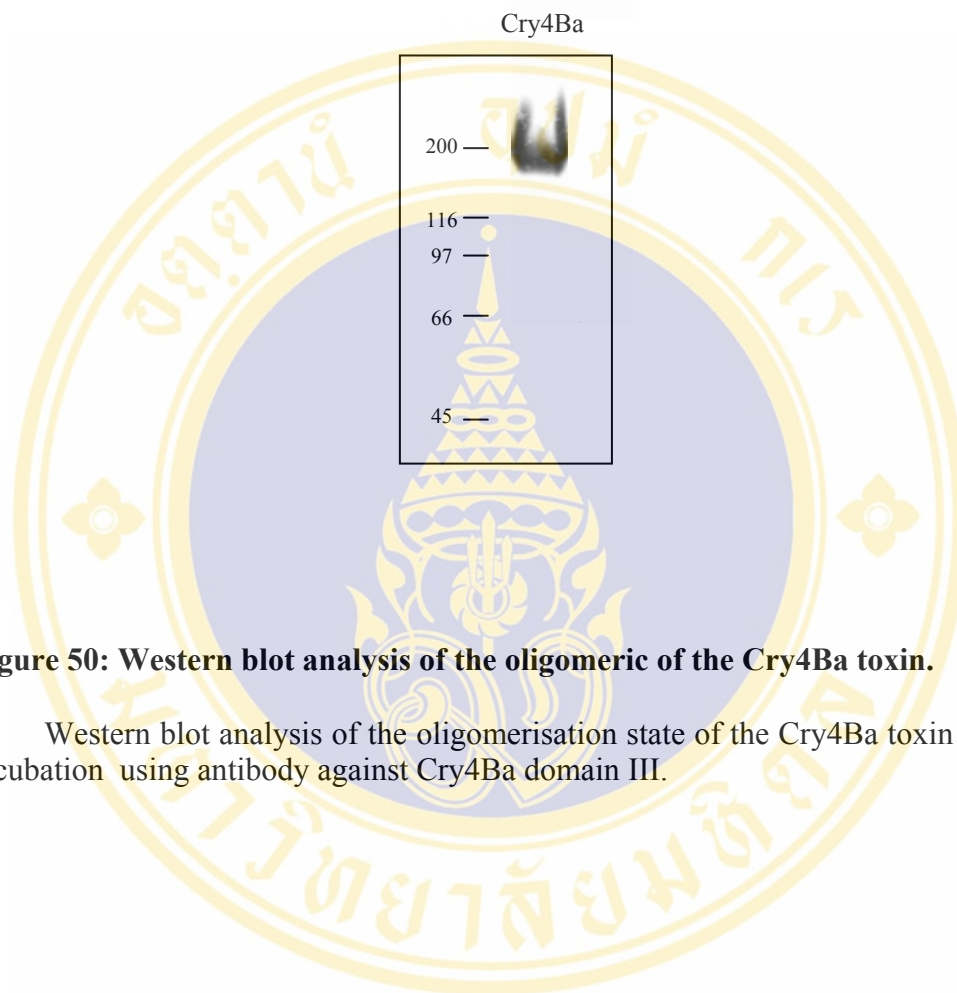


Figure 50: Western blot analysis of the oligomeric of the Cry4Ba toxin.

Western blot analysis of the oligomerisation state of the Cry4Ba toxin after 2-hr incubation using antibody against Cry4Ba domain III.

Toxin	-----All wild-type Cry4Ba-----							
Liposome	+	+	+	+	-	-	-	-
Temp. (°c)	60	60	60	60	60	60	60	60
GTA (µg)	0.003	-	0.005	-	0.005	0.01	0.01	0.02

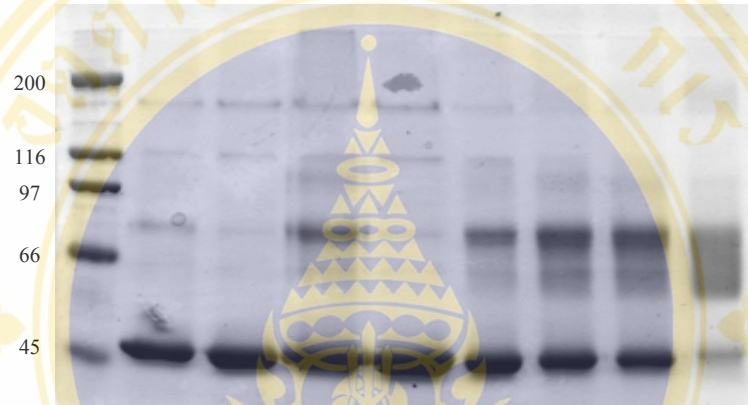


Figure 51: Oligomerisation state of the Cry4Ba wild-type in the presence of liposome and glutaraldehyde cross-linking agent.

SDS-PAGE analysis of the oligomeric state of Cry4Ba wild-type in the presence and in varying amounts of liposomes and glutaraldehyde cross-linking agent (GTA).

Toxin	WT	N183K	R158A	R158A
Liposome	+	+	+	+
Temp. (°c)	60	60	60	60
Time (hrs)	1	1	1	1

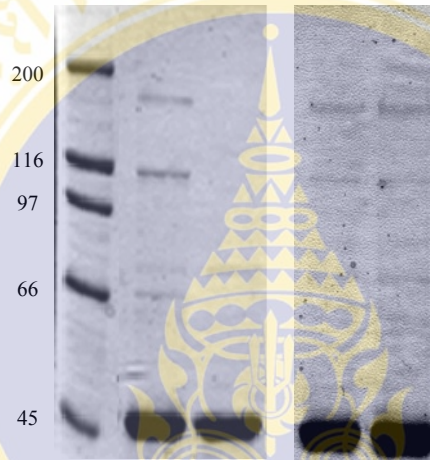


Figure 52: Oligomerisation state of the N183K and R158A mutant toxins.

SDS-PAGE analysis of the oligomeric state of Cry4Ba wild-type and its mutants at 1 hr of incubation time.

Toxin	-----All N183Kmutant-----								
Liposome	-	-	-	+	+	+	+	+	+
Temp. (°C)	60	60	60	60	60	60	60	70	60
GTA (µg)	0.2	0.2	0.6	0.2	0.2	0.6	0.2	0.2	-
DTT	-	+	-	-	+	-	-	-	-

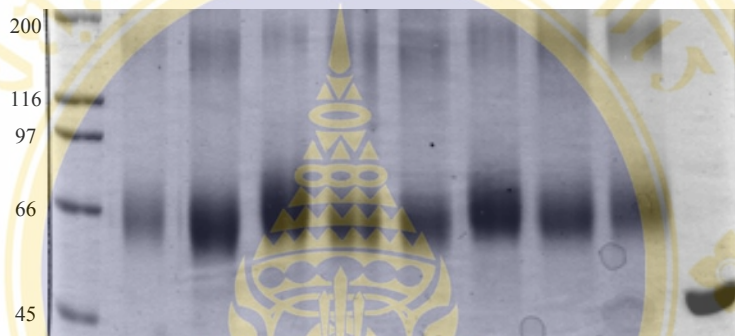


Figure 53: Oligomerisation state of the N183K mutant in the presence of liposome and DTT with varying glutaraldehyde concentrations.

SDS-polyacrylamide gel analysis of the oligomeric state of the N183K mutant in the presence of liposome and 25 mM DTT with varying glutaraldehyde concentrations.

CHAPTER 6

DISCUSSION

According to the umbrella model (4), part of the pore-forming domain of the activated Cry toxin is thought to insert into the membrane as a hairpin structure consisting of α -helices 4 and 5 with the remaining helices lying on the surface in an umbrella-like conformation. Mutation studies of specific residues within $\alpha 4$ indicated that this helix is oriented facing the lumen of the pore and is involved in ion-channel conduction as being evident by a dramatic loss in ion-channel activity for the specific mutation in $\alpha 4$ (7). Conversely, $\alpha 5$ is thought to be in contact with the lipid milieu of the membrane (81, 104). There are reports revealed for the Cry1A toxins that helix 5 may play a role in the oligomerisation of the $\alpha 4$ - $\alpha 5$ hairpin monomers (9, 10). However, the features required for the association of these inserted helices are less well understood nowadays.

A number of studies have indicated about the role of polar residues in driving and stabilising the association of the transmembrane helices within lipid bilayers (13-16). It has been suggested that the polar residues, which provide interhelical interactions (mainly hydrogen bonding), may be involved in the assembly process. Moreover, based on free energy estimation, the high cost of breaking these H-bonds inside lipid membrane implies that hydrogen bonding between α -helices could provide a strong stabilising force for helix association (13, 105). Hence, this thesis study was aimed to investigate the possible role for toxicity of polar amino acids in the transmembrane $\alpha 5$ of Cry4Ba in stabilising or driving helix association.

Alanine-scanning mutagenesis of polar residues (Tyr¹⁷⁸, Gln¹⁸⁰, Asn¹⁸³, Asn¹⁸⁵ and Asn¹⁹⁵) was initially performed. The expressed mutant toxins of Y178A, Q180A, N185A, and N195A were found to preserve the same biochemical characteristics as that of the wild type. However, a nearly complete loss of solubility was observed for the inclusions of the N183A mutants. When *E. coli* cells expressing each mutant toxin were bioassayed against *S. aegypti*, a completely loss of toxin activity was observed for N183A mutant whereas the other four mutant toxins exhibited only a negligible

reduction in larvicidal activity compared to the wild-type. These data suggested that Asn¹⁸³ is critically involved in biological activity of the Cry4Ba toxin.

More substitutions were generated at position 183 (N183R, N183T, N183Q, N183K, N183F, N183H and N183D) in order to elucidate and characterise the role of this critical residue. The resultant Cry4Ba mutant toxins were also found to be highly produced in *E. coli* as inclusion bodies upon IPTG induction. When equal amounts of cell lysates were analysed using SDS-PAGE, the N183R, N183T, N183Q, N183K and N183F mutants also yielded a 130-kDa protoxin band at the levels comparable to that of the wild-type toxin. However, the 130-kDa proteins were observed in a very low yield for the N183H and N183D mutants. Normally, the production yield of heterologous proteins in *E. coli* host may depend on many factors including the features of the gene sequence, compatibility of the codon usage, degradation of the protein by host cell proteases, and the nature of protein folding. Here, the case of the lower yields observed for the N183H and N183D mutants might be due to the introduction of mutations which could not permit the proper folding of the expressed proteins and consequently resulted in low yield productions.

The solubility of mutant protein inclusions (N183Q, N183T, N183R, N183K and N183F) in comparison with the wild-type inclusion was also assessed. It was found that all with exception of the N183Q and N183K mutants were insoluble in carbonate buffer, pH 9.0. Structural analysis of Cry4Ba revealed that Asn¹⁸³ of $\alpha 5$ points toward $\alpha 7$ and forms hydrogen bonding with Tyr²⁶⁷ at the end of $\alpha 7$ (**Fig. 53A**). This interaction is retained in the N183Q and N183K mutants as well as that of the wild-type. However, the four other mutants (N183A, N183T, N183R and N183F), which were found to be insoluble in carbonate buffer, provide no hydrogen bonding to Tyr²⁶⁷ (**Fig. 53B**). It seems that the dissolvability of the N183 mutant inclusions *in vitro* and hydrogen bond formation observed between Asn¹⁸³ in $\alpha 5$ and Tyr²⁶⁷ in $\alpha 7$ are correlated. At this stage, it may be that the loss of hydrogen bonding to $\alpha 7$ could disturb the structural characteristics that consequently affect toxin-inclusion solubilisation *in vitro*. This possibility was later confirmed when the replacement of Tyr²⁶⁷ with Ala also drastically perturbed dissolvability of the toxin inclusion.

When protoxin inclusions of Cry4Ba wild-type and N183T mutant were assessed for its solubilisation in gut juices. After 16-hr incubation, it was found that

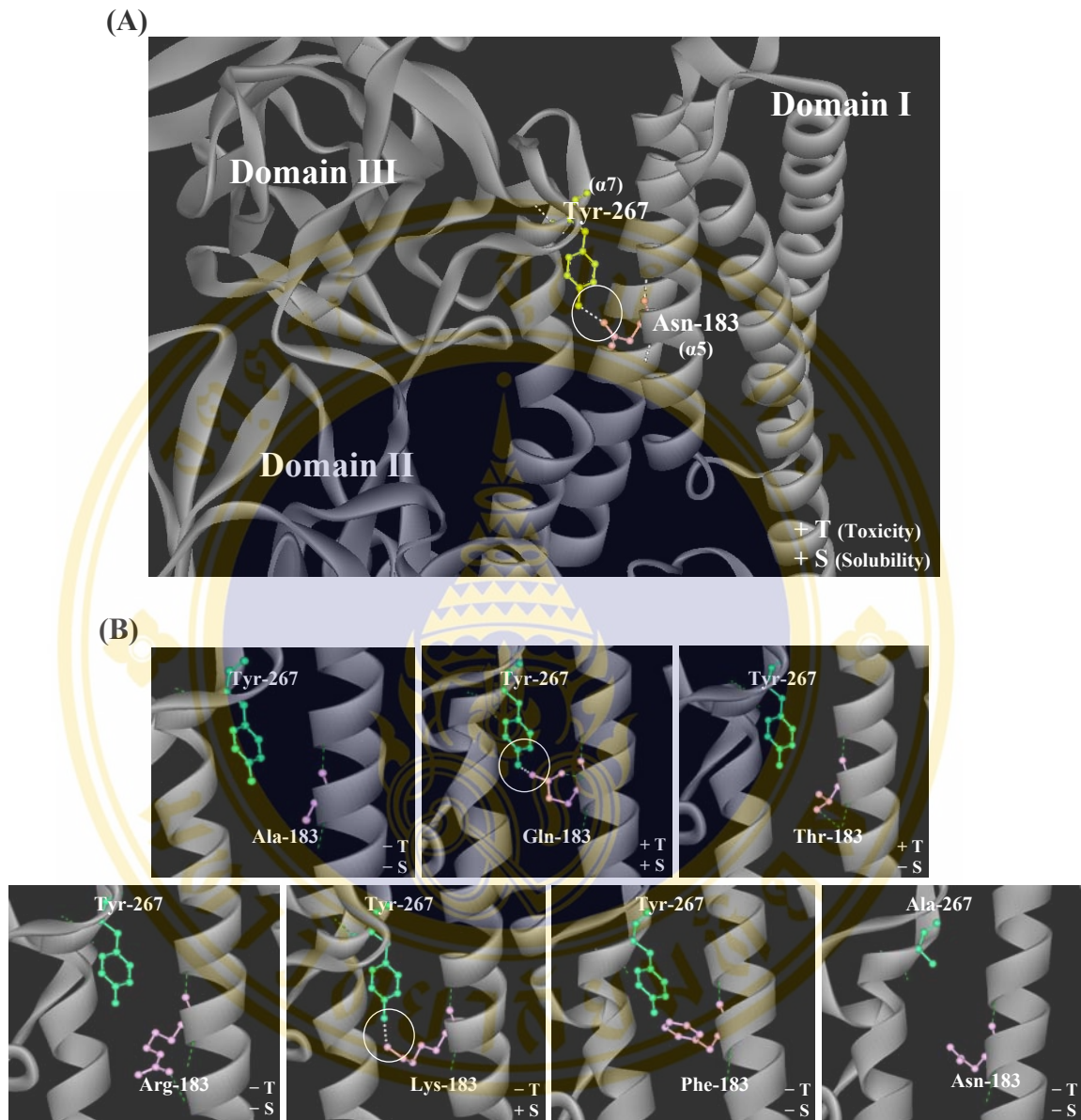


Figure 54: Hydrogen bonding between Asn¹⁸³ and Tyr²⁶⁷ in Cry4Ba.

- (A) Ribbon representations of part of the Cry4Ba crystal structure, illustrating the interaction *via* hydrogen bonding (encircled) between Asn¹⁸³ in $\alpha 5$ and Tyr²⁶⁷ at the C-terminus of $\alpha 7$ (shown in ball-and-stick form).
- (B) Between mutated residues at positions 183 and 267 could be observed only in the N183Q and N183K mutant toxins, but not in the five other mutant toxins. The structures were generated by WebLab ViewerPro (Accelrys Inc.)

both of inclusions could be solubilised in gut juice extracts, albeit very low amount, revealing a protoxin band of ca 130 kDa detected by western blot analysis against the Cry4Ba-domain III monoclonal antibody. The observation of a ca 47-kDa band of the wild-type implied that the gut juices might contain some kind of trypsin-like enzymes which could digest protoxin inclusion into a 47-kDa protease-resistant fragment.

Further mutagenic analysis at Asn¹⁸³ revealed that substitutions with residues, *i.e.* Gln, Thr, Asp and His still retained toxicity although a drastic reduction in toxicity was observed for N183D and N183H mutants as possibly to be due to the lower level of toxin expression. However, substitutions with residues, *i.e.* Arg, Lys and Phe were shown to completely abolish larvicidal activity. Further characterisation revealed that the total loss of larvicidal activity of the N183K mutant is unlikely due to misfolding or distortion of structure resulting from the single mutation at this position. Upon solubilisation and trypsin activation in the carbonate buffer, pH 9.0, the 130-kDa mutant protoxin was cleaved into 47-kDa and 20-kDa fragments, indicating that the N183K mutation had no apparent effect on proteolytic processing. Similar to the wild-type, these two trypsin-resistant fragments were also found associated to each other forming a 65-kDa protein complex under non-denaturing conditions *via* size-exclusion FPLC purification. Furthermore, secondary and tertiary structure determinations *via* circular dichroism and fluorescence spectroscopy revealed that both of wild-type Cry4Ba and N183K mutant exhibited similar spectra, suggesting the structure of the mutant toxin is not different from that of the wild-type toxin.

A gel electrophoresis system was used to directly examine both of Cry4Ba and its mutant for the distribution of the oligomeric forms. Here, preliminary conditions were tested in order to observe oligomer formation of the Cry4Ba wild-type toxin. Under conditions used, the 65-kDa activated Cry4Ba toxin was found to form a mixture of monomers, dimers, and trimers on liposome vesicles, with the trimer representing the predominant species after 2-hr incubation (*see* **Fig. 49A**). Of these, the results imply that the order of oligomeric forms could be extended with the longer time of incubation. The trimeric presenting here could also be detected on immunoblots probed with anti-Cry4Ba domain III monoclonal antibodies, indicating that this ca. 180-kDa trimeric band is an assembly of the 65-kDa monomeric Cry4Ba toxin. The presence of oligomers comprising dimer and trimer species was agree with results of Cry1Ac, Cry1Ab wild-

type toxins with no observation of species comprising four or more toxin molecules (9, 80). However, it has been suggested *via* atomic force microscopy that a toxin pore formed by the 65-kDa activated Cry4Ba toxin in a lipid environment consists of four subunits (76). Therefore, there is still an open question whether such higher-order oligomeric structures are present but they might not be stable under the conditions used in the experiments. In addition, it should be noted that the Cry4Ba protein migrated as oligomeric bands on the gel regardless of whether it was cross-linked or not, indicating the non-necessarity of glutaraldehyde cross-linked agent in the formation of oligomeric forms of the Cry4Ba protein. The ability to persist to SDS and heat of the Cry4Ba oligomers was also examined. Under these conditions, the highest order of oligomeric band was found to disappear somehow after heating at 95°C and 70°C, but not for 60°C for 10 min, indicating that the Cry4Ba oligomer is resistant to dissociation by SDS and partially resistant to dissociation by combination of SDS and heat. These characteristics are quite similar to those previously described for the small, heptameric oligomers of aerolysin (106) and the large, 40-50 oligomers of perfringolysin O (107), which display a resistance to SDS-dissociation and to relatively high temperature at 65°C. This could indicate that the forces facilitating the Cry4Ba monomer-monomer interactions may be similar to those that stabilise the oligomers of other pore-forming toxins. Furthermore, the data also showed that the subunit association is not mediated by disulfide bridges as they are also present in samples incubated with DTT (*see Fig. 49B*).

Upon the conditions used with the Cry4Ba wild-type toxin, the N183K mutant was existed only as monomeric species (*see Fig. 52-53*) although the longer time of incubation was used, indicating that the lack of toxicity may be caused by a deficiency in toxin oligomerisation within the target membrane. It should be noted that the N183K mutant toxin could migrate as oligomeric bands on the gel when it was cross-linked with glutaraldehyde. However, this cross-linking agent seemed to be unnecessary for oligomer formation of the wild-type toxin as mentioned earlier. Since glutaraldehyde could link protein molecules *via* lysine group creating structure more stable than that attained by the physical aggregation of protein molecules, the mutant protein that is replaced with lysine in the critical position 183 might possibly generate anomalous linking of protein subunits. Thus, by providing cross-linked molecules, oligomeric-forms of the N183K mutant could be observed on the SDS-gel. However, the bioinactive

Cry4Ba-R158A mutant with alanine-substitution at Arg¹⁵⁸ in α 4 [108], which was previously identified to be important for ion conduction [109], was still found to be able to form oligomers, suggesting that Arg¹⁵⁸ is not involved in toxin oligomerisation unlike Asn¹⁸³ in α 5.

For characterisation of the membrane-perturbation activity against large unilamellar vesicles whose compositions (PC/PE/Ch) are more relevant to the insect cell membranes (115), it was found that the ability of this mutant (at the equivalent protein concentration of 7.5 μ g/ml to wild-type toxin) to exert membrane perturbing activity towards lipid vesicles was much weaker than that of the wild-type toxin. This suggested that Asn¹⁸³ is likely to be involved in membrane perturbation of the Cry4Ba toxin. The release of calcein dye into the surrounding solution might be caused by the destabilisation of membrane vesicles rather than through the toxin-induced pore. The wild-type toxin could perhaps collide during lateral movement and form oligomers towards lipid vesicles that would destabilise and finally burst the lipid vesicles more effectively than the mutant. According to the analysis by SDS-PAGE, the mutant toxin that was not able to form oligomers within lipid vesicles would consequently provide weaker ability to perturb the lipid vesicles and cause a negligible leakage of calcein dye of liposome vesicles.

The distributions of hydrogen bonding between helices and the composition of amino acid residues that are involved in the interaction were widely studied in several transmembrane proteins including potassium channel protein (Fig. 55). It has been shown that almost all transmembrane helices in these proteins have interhelical hydrogen bonds and every helix in the data set is connected by at least one hydrogen bonding with its neighbors, and that the helical pairs with interhelical hydrogen bonding would have a tendency to pack tighter than their counterparts without interhelical hydrogen bonding (110). Thus, according to the crystal structure of the Cry4Ba toxin (35), if α 4 faces the pore lumen, the Asn¹⁸³ in α 5 may point to the side of closed helices 4 or 5 of nearby subunits in an oligomer. It should be noted that two types of hydrogen bonds are normally observed in the transmembrane regions of membrane proteins. One is the hydrogen bond that is formed between side chains of amino acids from neighboring helices. The other of hydrogen bond is formed between a side chain of an

amino acid of one helix and a carbonyl oxygen or an amide hydrogen of a polypeptide backbone from a neighboring helix (110). Perhaps, Asn¹⁸³ in $\alpha 5$ could provide an interhelical interaction with a residue or backbone of these closed helices and somehow stabilise the structure of the oligomeric toxin inside the lipid membrane (**Fig. 56**).

It has been shown that the interhelical interaction *via* polar residues *e.g.* Asn in a designed hydrophobic transmembrane helix could contribute to the structural stability of the oligomeric structure within lipid membranes by providing a strong driving force for dimer or trimer formation [15, 16]. Another study revealed that a buried Asn at the helical, trimeric interface of the hemagglutinin from the influenza A virus (residue 95) was found to engage in hydrogen bonding with Asn side chains from neighboring subunits (111). In addition, extension of the study indicated that two polar atoms of amino acids such as Asn, Gln, Asp and Glu formed a stable trimer, whereas residues with a single polar atom such as Thr, Ser or Lys showed a weaker tendency to associate to each other (112, 113). Thus, if the association of toxin monomers is important for toxicity, the substitution with Gln at Asn¹⁸³ in $\alpha 5$ of the Cry4Ba toxin would generate more stable oligomers than the Thr-substitution that would retain more larvicidal activity of the toxin (*see Fig. 37*). However the failure of the N183K mutant to form oligomers together with the loss of toxicity might be possibly due to the long side chain of substituted Lys. Due to side chains of amino acids could rotate freely, perhaps, specific hydrogen bonding that involve in a Lys side chain would require freezing five torsional angles resulting in an unfavorable entropy of interaction whereas only two and three torsional angles are required to specify the conformation of Asp and Glu, respectively. It has been shown that His residue was also found to play a role in stabilising the oligomeric complex of pore-forming protein of *Entamoeba histolytica* via its involvement of hydrogen bond formation (114). It should be noted that the strength of hydrogen bonding depends on many factors including angle, orientation and distance. Once the hydrogen bond moves beyond the range, it would lose its hydrogen bond character and become a weaker electrostatic interaction.

In addition, single or double mutagenic analysis at two highly conserved nonpolar residue (Val¹⁸¹ and Ala¹⁸²) in $\alpha 5$ revealed that substitutions with a polar residue *i.e.* Ser still retained high toxicity of the mutant toxins comparable to the wild-type. The result suggested that nonpolarity at these two positions may be unnecessary for larvicidal

activity of Cry4Ba unlike an identified polar residue at position 183. There was a report of Cry1Ac revealed that the mutation at Ala¹⁶⁴ at which situates in the same position in the helical wheel of nonpolar Val¹⁸¹ of the Cry4Ba toxin exhibited no toxicity (9). It has also been reported that the mutation of Asn¹³⁵ in $\alpha 4$ of the Cry1Ab toxin appeared to affect toxicity, possibly involved in toxin oligomerisation. It was also in contrast to the Cry4Ba toxin in which Asn¹⁵¹ that situates in the same position as Asn¹³⁵ of the Cry1Ab toxin exhibited no loss of larvicidal activity (80). This could be that differences in the location of the critical residues may conceivably reflect the diversity in the structure details for each group of insect-specific Cry toxins. However, because of $\alpha 5$ provides the most conserved residues along the helix, a number of distinct clusters of conserved residues were observed when plotting in different pitches of helix (Fig. 57). By and large, the apparent number of residues per turn in each helical wheel projection would be altered in the case of helices interacting with a right-handed or left-handed crossing-angle from 3.6 to 3.9 and 3.5 residues per turn, respectively (116, 117). Some of conserved residues in $\alpha 5$ lie up on the same faces of the 3.9 amino acids per turn helical wheel diagram (Fig. 56), implying clue that Cry4Ba might be a right-handed coiled-coil. Although the conserved residues are face into the same direction, some of these conserved residues (Y¹⁷⁸, Q¹⁸⁰, V¹⁸¹, A¹⁸²) were not crucial for their insecticidal activity. This could suggest that some conserved residues in $\alpha 5$ might not be necessary for determining toxicity of the Cry4Ba protein. Perhaps the clusters of these conserved residues might be important just in case of maintenance of topology of Cry toxin. However, it should be noted that mutations at conserved residues Arg¹⁹⁰ and Asp¹⁹¹ in $\alpha 5$ of the Cry4Ba toxin appear to affect toxicity. It was found that this Arg¹⁹⁰ could perform electrostatic interaction to adjacent Asp¹⁹¹ within the helix. Further characterisation revealed that these charged residues were critical for maintaining the structural folding of the Cry4Ba toxin (118, 119).

In conclusion, this study has identified a critical residue at position 183 within the transmembrane helix 5 of the 130-kDa Cry4Ba toxin. According to the results, the loss of toxicity of the Asn¹⁸³ mutant appears to affect monomer-monomer interaction, supporting its role of $\alpha 5$ to be pivotal in oligomerisation of Cry toxin. Nevertheless, further investigations of more detailed oligomeric behaviour and molecular organisation of the Cry4Ba toxin in the lipid membranes, particularly in the native midgut membranes

prepared from mosquito larvae, are of great interest. In addition, molecular dynamics simulations are needed to verify definitively on hydrogen bonding as well as the potential energy of Asn¹⁸³ on protein-protein interactions of the Cry4Ba toxin within the lipid membranes.



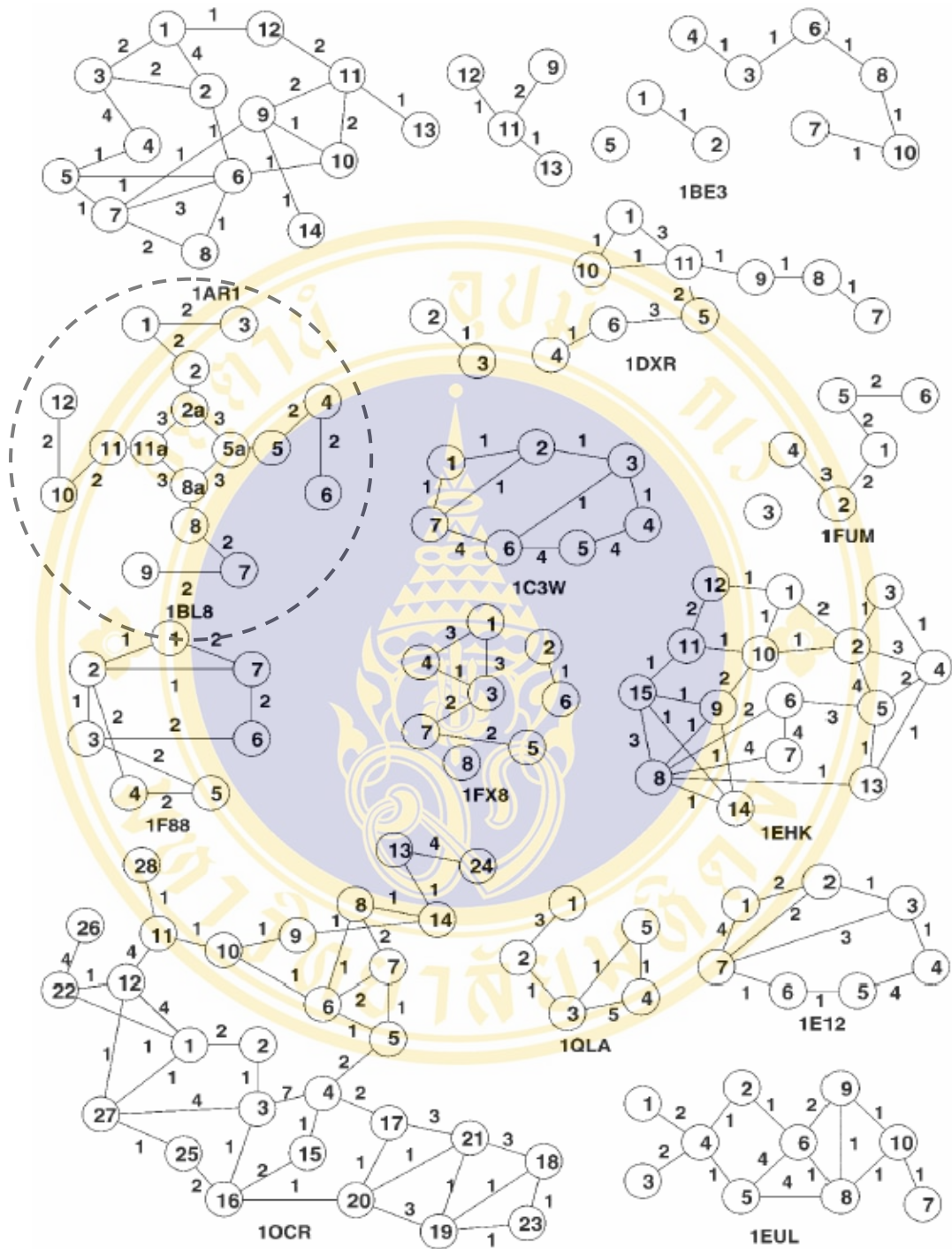


Figure 55: The topological maps of interhelical hydrogen bonding (top view) of the transmembrane region of several transmembrane proteins (111).

Two helices are connected by an edge if there is at least one hydrogen bonding between them. The number of observed interhelical hydrogen bonding is indicated next to the corresponding edge. The helices are numbered by the order in which they appear in the primary sequence. The large circle shows the interhelical interactions of potassium channel protein from *Streptomyces lividans*.

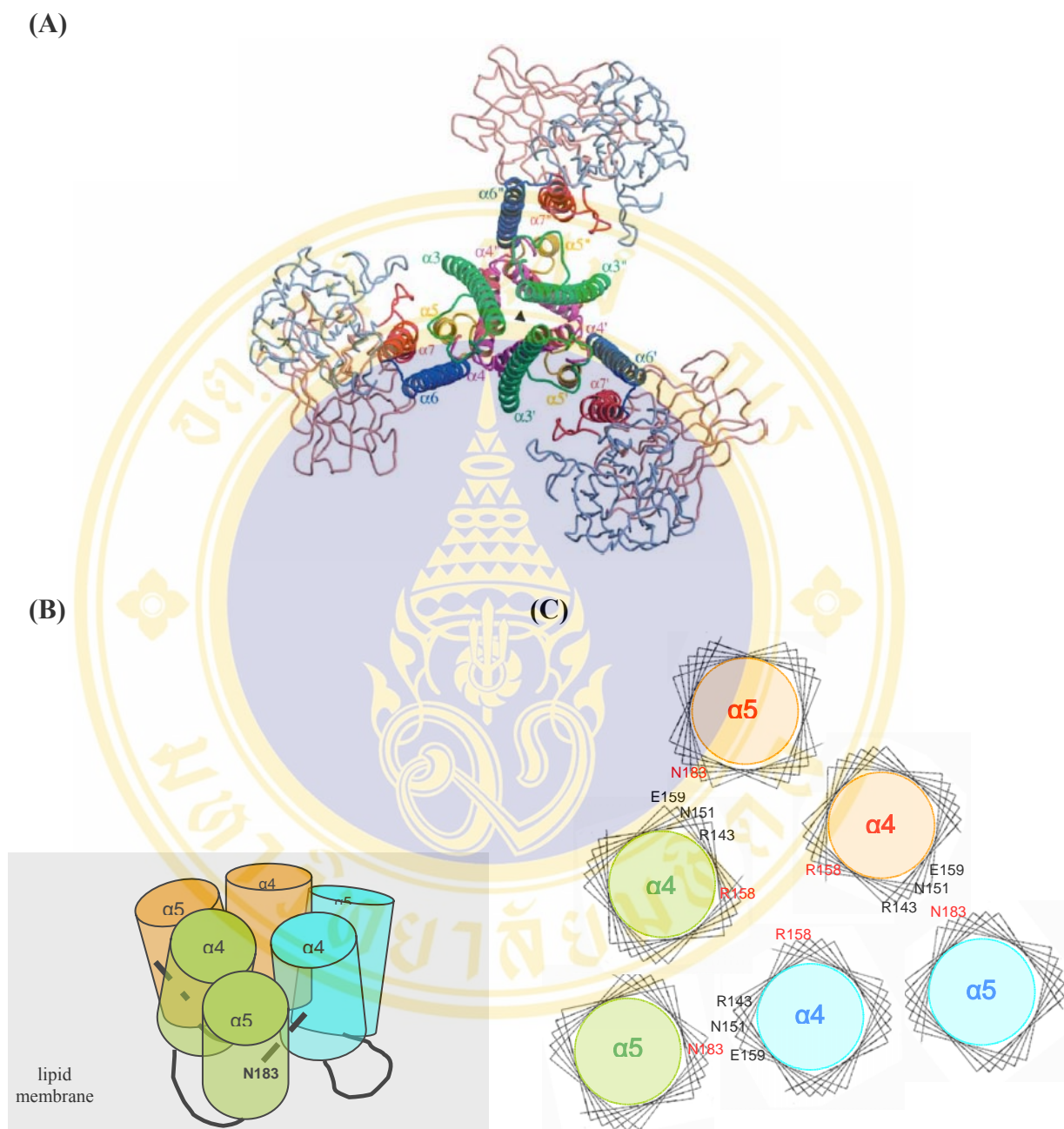


Figure 56: Schematic views of trimeric association of Cry4Ba.

(A) Crystal contacts of Cry4Ba around the 3-fold axis in the rhombohedral lattice $\alpha 5$ (yellow) is seen end-on with its N terminus pointing out of the page. $\alpha 3$ (green), $\alpha 4$ (magenta) and $\alpha 6$ (blue) are labeled ear their respective C terminus (35).

(B) A possible model of the trimeric association of $\alpha 4$ - $\alpha 5$ hairpin of Cry4Ba in the lipid membrane. Asn¹⁸³ is shown providing a possible interhelical interaction with a residue or backbone of closed helices. The nearby residues (R¹⁴³, N¹⁵¹, E¹⁵⁹) of $\alpha 4$ facing into Asn¹⁸³ are shown in (C).

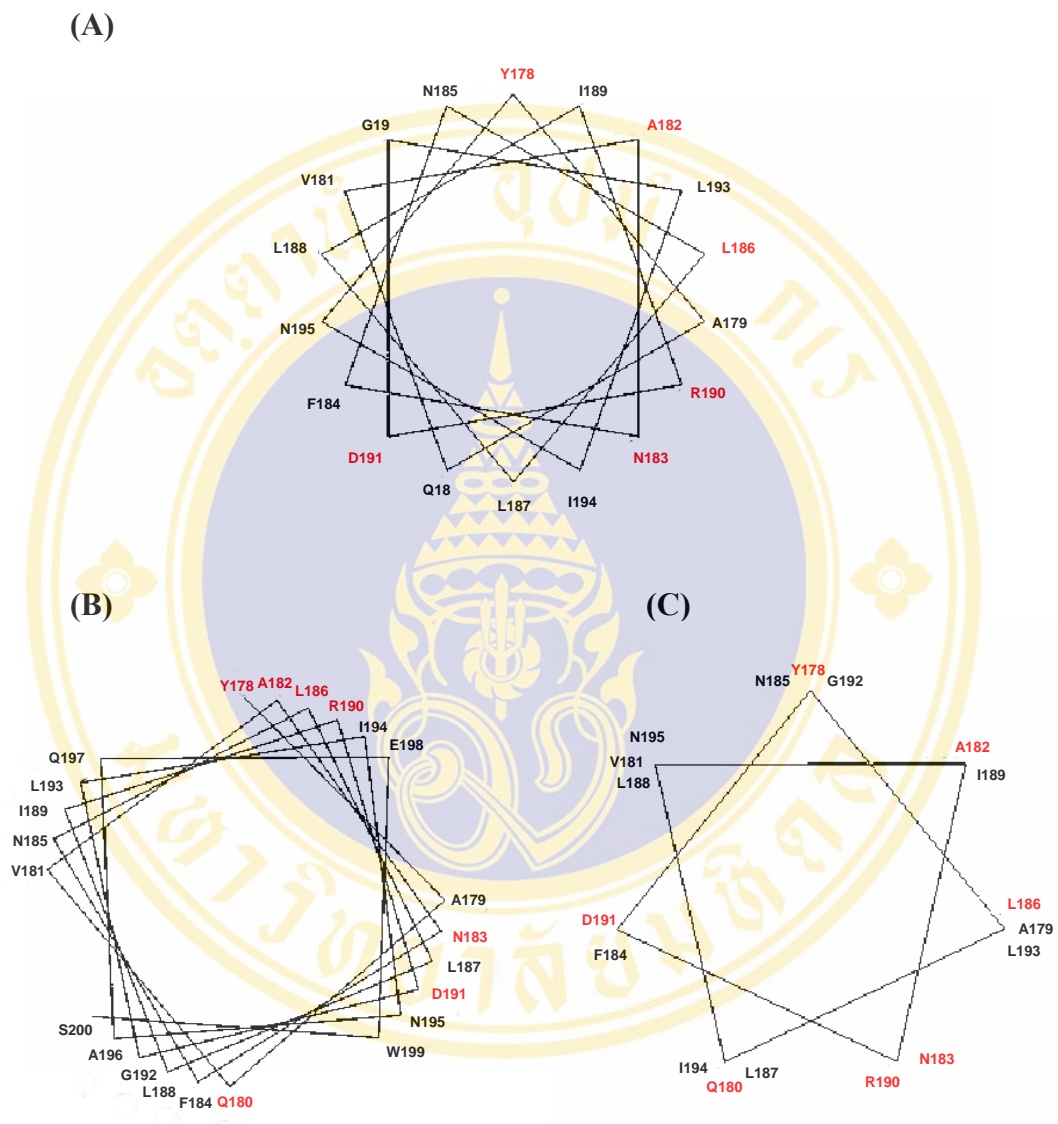


Figure 57: Helical wheel projections of helix 5 of Cry4Ba with three different pitches.

Clusters of conserved residues are shown in red color.

(A) 3.6 amino acids per turn (canonical helix).

(B) 3.9 amino acids per turn (right-handed coiled-coil).

(C) 3.5 amino acids per turn (left-handed coiled-coil).

CHAPTER 7

CONCLUSIONS

1. To investigate the possible role for toxicity of selected polar amino acids in transmembrane $\alpha 5$ of the *Bacillus thuringiensis* Cry4Ba mosquito-larvicidal protein, a PCR-based mutagenesis strategy was employed to obtain substitutions with polar and non-polar residues. Here, fifteen single mutants (Y178A, Q180A, N183A, N185A, N195A, N183Q, N183R, N183T, N183K, N183F, N183H, N183D, Y267A, V181S and A182S) and one double mutant (V181S/A182S) were successfully constructed. All the mutated sequences were verified by DNA sequencing.
2. Upon IPTG induction, all of the 130-kDa mutant protoxins were expressed in *E. coli* strain JM109 as cytoplasmic inclusions with the expression levels comparable to the wild-type Cry4Ba toxin. Nine mutant toxins (Y178A, Q180A, N185A, N195A, N183Q, N183K, V181S, A182S and V181S/A182S) were found to be structurally stable upon solubilisation and trypsin activation in carbonate buffer, pH 9.0.
3. Mosquito bioassays showed that N183A, N183R, N183K, N183F, Y267A mutant toxins exhibited completely loss of larvicidal activity against *S. aegypti* larvae while N183Q and N183T mutant toxin could retain about 90% and 60% of larvicidal activity, respectively, compared to the Cry4Ba wild-type. The result suggested that the polar residue at position 183 is essentially involved in larvicidal activity of Cry4Ba.
4. Mutagenic analysis at two selected nonpolar residues (Val¹⁸¹ and Ala¹⁸²) which are highly conserved among the Cry toxin family in $\alpha 5$ revealed that substitutions with a polar residue i.e. Ser, still retained high toxicity of the mutant toxins comparable to the wild-type, suggesting that nonpolar residue at these two positions may not be required for larvicidal activity of Cry4Ba.

5. Upon solubilisation and trypsin activation in carbonate buffer, pH 9.0, the bioinactive N183K protoxin was cleaved into 47-kDa and 20-kDa fragments. Similar to the wild-type, these two trypsin-resistant fragments were found associated to each other forming a 65-kDa protein complex under non-denaturing conditions *via* size-exclusion FPLC purification. In addition, CD and intrinsic fluorescence spectroscopy revealed that overall structural fold of the 65-kDa larvicidal inactive mutant (N183K) was similar to that of the Cry4Ba wild-type.
6. The 65-kDa purified bioinactive N183K toxin was characterised for its membrane-perturbation activity with large unilamellar vesicles consisting of PC/PE/Ch. Unlike the 65-kDa wild-type toxin, the inactive mutant (N183K) was found to be less active against liposome vesicles in releasing entrapped calcein-dye, suggesting that Asn¹⁸³ is involved in membrane perturbation of the Cry4Ba toxin.
7. A gel electrophoresis system was used to examine both of Cry4Ba and its mutant for the distribution of the oligomeric forms. Cry4Ba toxin was found to form a mixture of monomers, dimers, and trimers on liposome vesicles, with the trimer representing the predominant species after 2-hr incubation. Upon the conditions used with the wild-type toxin, the N183K mutant was existed only as monomeric species although the longer time of incubation was used, indicating the lack of toxicity may be caused by a deficiency in oligomerisation. Unlike N183K, the bioinactive R158A mutant in α 4, which was previously identified to be important for ion conduction, was still found to be able to form oligomers, suggesting that Arg¹⁵⁸ in 4 is not involved in toxin oligomerisation.
8. In conclusions, the loss of toxicity of the N183 mutant appeared to be caused by a decrease in monomer-monomer interactions *via* hydrogen bonding through this critical position, supporting its role of α 5 to be pivotal in Cry toxin oligomerisation in lipid membranes.

REFERENCES

1. Höfte H, Whiteley HR. Insecticidal crystal proteins of *Bacillus thuringiensis*. *Microbiol Rev* 1989; 53(2):242-255.
2. Tucker AD, Baty D, Parker MW, Pattus F, Lazdunski C, Tsernoglou D. Crystallographic phases through genetic engineering: experiences with colicin A. *Protein Eng.* 1989; 2(6): 399-405.
3. Li JD, Carroll J, Ellar DJ. Crystal structure of insecticidal delta-endotoxin from *Bacillus thuringiensis* at 2.5 Å resolution. *Nature* 1991; 353(6347): 815-821.
4. Gazit E, La Rocca P, Sansom MS, Shai Y. The structure and organization within the membrane of the helices composing the pore-forming domain of *Bacillus thuringiensis* delta-endotoxin are consistent with an "umbrella-like" structure of the pore. *Proc Natl Acad Sci USA* 1998; 95(21):12289-12294.
5. Uawithya P, Tuntitippawan T, Katzenmeier G, Panyim S, Angsuthanasombat C. Effects on larvicidal activity of single proline substitutions in alpha3 or alpha4 of the *Bacillus thuringiensis* Cry4B toxin. *Biochem Mol Biol Int* 1998; 44(4): 825-832.
6. Sramala I, Uawithya P, Chanama U, Leetachewa S, Krittanai C, Katzenmeier G et al. Single Proline Substitutions of Selected Helices of the *Bacillus thuringiensis* Cry4B Toxin Affect Inclusion Solubility and Larvicidal activity. *J Biochem Mol Biol & Biophys* 2000; 4: 187-193.
7. Masson L, Tabashnik BE, Liu YB, Brousseau R, Schwartz JL. Helix 4 of the *Bacillus thuringiensis* Cry1Aa toxin lines the lumen of the ion channel. *J Biol Chem* 1999; 274(45): 31996-32000.
8. Li J, Koni PA, Ellar DJ. Crystallization of a membrane pore-forming protein with mosquitocidal activity from *Bacillus thuringiensis* subspecies *kyushuensis*. *Proteins* 1995; 23(2): 290-293.

9. Aronson AI, Geng C, Wu L. Aggregation of *Bacillus thuringiensis* Cry1A toxins upon binding to target insect larval midgut vesicles. *Appl Environ Microbiol* 1999; 65(6): 2503-2507.
10. Nunez-Valdez M, Sanchez J, Lina L, Guereca L, Bravo A. Structural and functional studies of alpha-helix 5 region from *Bacillus thuringiensis* Cry1Ab delta-endotoxin. *Biochim Biophys Acta* 2001; 1546(1): 122-131.
11. Crickmore N, Zeigler DR, Feitelson J, Schnepf E, Van Rie J, Lereclus D et al. Revision of the nomenclature for the *Bacillus thuringiensis* pesticidal crystal proteins. *Microbiol Mol Biol Rev* 1998; 62(3): 807-813.
12. Angsuthanasombat C, Uawithya P, Leetachewa S, Pornwiroon W, Ounjai P, Kerdcharoen T, Katzenmeier G and Panyim S. *Bacillus thuringiensis* Cry4A and Cry4B mosquito-larvicidal proteins: homology-based 3D model and implications for toxin activity. *J. Biochem. Mol. Biol.* 2004; 37: 304-313.
13. White SH, Ladokhin AS, Jayasinghe S, Hristova K. How membranes shape protein structure. *J Biol. Chem.* 2001; 276: 32395-32398.
14. Stapley BJ, Doig AJ. Hydrogen Bonding Interactions between Glutamine and Asparagine in α -Helical Peptides. *J. Mol. Biol.* 1997; 272: 465-473.
15. Zhou FX, Cocco MJ, Russ WP, Brunger AT and Engelman DM. Interhelical hydrogen bonding drives strong interactions in membrane proteins. *Nat. Struct. Biol.* 2000; 7: 154-160.
16. Choma C, Gratkowski H, Lear JD and DeGrado WF. Asparagine-mediated self-association of model transmembrane helix. *Nat. Struct. Biol.* 2000; 7: 161-166.
17. Beegle CB, Yamamoto T. Invitation paper: History of *Bacillus thuringiensis* Berliner research and development. *The Canadian Entomol.* 1992; 124: 587-616.
18. Krieg A, Miltenburger HG. Bioinsecticides: I. *Bacillus thuringiensis*. *Adv Biotechnol Processes* 1984; 3: 273-290.
19. Carozzi HD, Hurst JA Ecology of *Bacillus thuringiensis* in storage moths. *J. Invert. Patho.* 1977; 30: 131-139.

20. Knowles BH, Francis PH, Ellar DJ. Structurally related *Bacillus thuringiensis* delta-endotoxins display major differences in insecticidal activity *in vivo* and *in vitro*. *J Cell Sci* 1986; 84: 221-236.
21. Zohdy NZ, Matter MM. Effect of *Bacillus thuringiensis* var. *israelensis* on some Egyptian mosquito larvae. *J Egypt Soc Parasitol* 1982; 12(2): 349-357.
22. Schnepf HE, Crickmore N, Van Rie J, Lereclus D, Baum J, Feitelson J, Zeigler DR, Dean DH. *Bacillus thuringiensis* and its pesticidal crystal proteins. *Microbiol Mol Biol Rev* 1998; 62: 775-806.
23. Yokoyama Y, Kohda K, Okamoto M. CytA protein, a delta-endotoxin of *Bacillus thuringiensis* subsp. *israelensis* is associated with DNA. *Biol Pharm Bull* 1998; 21(12): 1263-1266.
24. Prieto-Samsonov DL, Vazquez-Padron RI, Ayra-Pardo C, Gonzalez-Cabrera J, de la Riva GA. *Bacillus thuringiensis*: from biodiversity to Biotechnology. *J Microbiol Biotechnol* 1997; 19(3): 202-219.
25. Aronson AI, Shai Y. Why *Bacillus thuringiensis* insecticidal toxins are so effective: unique features of their mode of action. *FEMS Microbiol Lett* 2001; 195(1): 1-8.
26. Grochulski P, Masson L, Borisova S, Pusztai-Carey M, Schwartz JL, Brousseau R et al. *Bacillus thuringiensis* CryIA(a) insecticidal toxin: crystal structure and channel formation. *J Mol Biol* 1995; 254(3): 447-464.
27. Li J, Henderson R, Carroll J, Ellar D. X-ray analysis of the crystalline parasporal inclusion in *Bacillus thuringiensis* var. *tenebrionis*. *J Mol Biol* 1988; 199(3): 543-544.
28. Li J, Koni PA, Ellar DJ. Structure of the mosquitocidal delta-endotoxin CytB from *Bacillus thuringiensis* sp. *kyushuensis* and implications for membrane pore formation. *J Mol Biol* 1996; 257(1): 129-152.
29. Schnepf HE, Crickmore N, Van Rie J, Lereclus D, Baum J, Feitelson J, Zeigler DR, Dean DH. *Bacillus thuringiensis* toxins: regulation, activities and structural diversity. *Curr. Opin. Biotechnol.* 1995; 6: 305-312.
30. Gill SS, Cowles EA, Pietrantonio PV. The mode of action of *Bacillus thuringiensis* endotoxins. *Annu. Rev. Entomol.* 1992; 37: 615-636.

31. Angsuthanasombat C, Chungjatupornchai W, Kertbundit S, Luxananil P, Settasatian C, Wilairat P et al. Cloning and expression of 130-kd mosquito-larvicidal delta-endotoxin gene of *Bacillus thuringiensis* var. *Israelensis* in *Escherichia coli*. Mol Gen Genet 1987; 208(3): 384-389.
32. Chungjatupornchai W, Hofte H, Seurinck J, Angsuthanasombat C, Vaeck M. Common features of *Bacillus thuringiensis* toxins specific for Diptera and Lepidoptera. Eur J Biochem 1988; 173(1): 9-16.
33. Morse RJ, Yamamoto T, Stroud RM. Structure of Cry2Aa suggests an unexpected receptor binding epitope. Structure (Camb) 2001; 9(5): 409-417.
34. Galitsky N, Cody V, Wojtczak A, Ghosh D, Luft JR, Pangborn W et al. Structure of the insecticidal bacterial delta-endotoxin Cry3Bb1 of *Bacillus thuringiensis*. Acta Crystallogr D Biol Crystallogr 2001; 57(Pt 8): 101-1109.
35. Boonserm P, Davis P, Ellar DJ and Li J. Crystal structure of the mosquitolarvicidal toxin Cry4Ba and its biological implications. J. Mol. Biol. 2005; 348: 363-382.
36. De Maagd RA, Bravo A, and Crickmore N. How *Bacillus thuringiensis* has evolved specific toxins to colonize the insect world. Trends Genet. 2001; 17: 193-199.
37. De Maagd RA, Bravo A, Berry C, Crickmore N, Schnepf HE. Structure, diversity, and evolution of protein toxins from spore-forming entomopathogenic bacteria. Annu.Rev. Genet. 2003; 37: 409-433.
38. Vie V, Van Mau N, Pomarede P, Dance C, Schwartz JL, Laprade R, Frutos R, Rang C, Masson L, Heitz F, Le Grimellec C. Lipid-induced pore formation of the *Bacillus thuringiensis* Cry1Aa insecticidal toxin. J Membr Biol 2001; 180(3):195-203.
39. Rajamohan F, Lee MK, Dean DH. *Bacillus thuringiensis* insecticidal proteins: molecular mode of action. Prog Nucleic Acid Res Mol Biol 1998; 60: 1-27.
40. Schwartz JL, Garneau L, Savaria D, Masson L, Brousseau R, Rousseau E. Lepidopteran-specific crystal toxins from *Bacillus thuringiensis* form cation- and anion-selective channels in planar lipid bilayers. J Membr Biol 1993; 132(1):53-62.

41. Hill CA, Pinnock DE. Histopathological effects of *Bacillus thuringiensis* on the alimentary canal of the sheep louse, *Bovicola ovis*. *J Invertebr Pathol* 1998; 72(1): 9-20.
42. Whalon ME, Wingerd BA. Bt: mode of action and use. *Arch Insect Biochem Physiol* 2003; 54(4): 200-211.
43. Aronson AI, Shai Y. Why *Bacillus thuringiensis* insecticidal toxins are so effective: unique features of their mode of action. *FEMS Microbiol Lett*. 2001; 195(1): 1-8.
44. Aronson AI, Beckman W, Dunn P. *Bacillus thuringiensis* and related insect pathogens. *Microbiol Rev* 1986; 50(1): 1-24.
45. Nishimoto T, Yoshisue H, Ihara K, Sakai H, Komano T. Functional analysis of block 5, one of the highly conserved amino acid sequences in the 130-kDa CryIVA protein produced by *Bacillus thuringiensis* subsp. *israelensis*. *FEBS Lett* 1994; 348(3):249-254.
46. Choma CT, Surewicz WK, Carey PR, Pozsgay M, Raynor T, Kaplan H. Unusual proteolysis of the protoxin and toxin from *Bacillus thuringiensis*. Structural implications. *Eur J Biochem* 1990; 189(3): 523- 527.
47. Carroll J, Li J, Ellar DJ. Proteolytic processing of a coleopteran-specific delta endotoxin produced by *Bacillus thuringiensis* var. *tenebrionis*. *Biochem J* 1989; 261(1): 99-105.
48. Angsuthanasombat C, Crickmore N, Ellar DJ. Effects on toxicity of eliminating a cleavage site in a predicted interhelical loop in *Bacillus thuringiensis* CryIVB delta-endotoxin. *FEMS Microbiol Lett* 1993; 111(2-3): 255-261.
49. Nicholls CN, Ahmad W, Ellar DJ. Evidence for two different types of insecticidal P2 toxins with dual specificity in *Bacillus thuringiensis* subspecies. *J Bacteriol* 1989; 171(9): 5141-5147.
50. Bravo A, Sanchez J, Kouskoura T, Crickmore N. N-terminal activation is essential early step in the mechanism of action of the *Bacillus thuringiensis* Cry1Ac insecticidal toxin. *J Biol Chem* 2002; 277(27): 23985-23987.
51. Knowles BH Mechanism of action of *Bacillus thuringiensis* insecticidal δ -endotoxin. *Adv Insect Physiol* 1994; 24:276-307.

52. Knowles BH, Dow JAT. The crystal δ -endotoxins of *Bacillus thuringiensis*: models for their mechanism of action on the insect gut. *Bioassays* 1993; 15:469-476.
53. Rajamohan F, Lee MK, Dean DH. *Bacillus thuringiensis* insecticidal proteins: molecular mode of action. *Prog Nucleic Acid Res. Mol Biol.* 1998; 60:1-27.
54. Knowles BH, Ellar DJ. Colloid-osmotic lysis is a general feature of the mechanism of action of *Bacillus thuringiensis* delta-endotoxin with different insect specificity. *Biochem Biophys Acta* 1987; 924: 509-518.
55. Wright DJ, Iqbal M, Granero F, Ferre J. A change in a single midgut receptor in the diamondback moth is only in part responsible for field resistance to *Bacillus thuringiensis* subsp *kurstaki* and *B. thuringiensis* subsp *aizawai*. *Appl Environ Microbiol* 1997; 63: 1814-1819.
56. Tabashnik BE, Liu YB, Malvar T, Heckel DG, Masson L, Ballester V et al. Global variation in the genetic and biochemical basis of diamondback moth resistance to *Bacillus thuringiensis*. *Proc Natl Acad Sci USA* 1997; 94(24): 12780-12785.
57. Gahan LJ, Gould F, Heckel DG. Identification of a gene associated with Bt resistance in *Heliothis virescens*. *Science* 2001; 293(5531): 857-860.
58. Gomez I, Oltean D, Gill SS, Bravo A, Soberon M. Mapping the epitope in cadherin-like receptors involved in *Bacillus thuringiensis* Cry1A toxin interaction using phage display. *J Biol Chem.* 2001; 376: 28906-28912.
59. Gomez I, Miranda-Rios J, Rudino-Pinera E, Oltean D, Gill SS, Bravo A, Soberon M. Hydrophobic complementarity determines interaction of epitope ⁸⁶⁹HITDTNNK⁸⁷⁶ in *Manduca sexta* Bt-R1 receptor with loop 2 of domain II of *Bacillus thuringiensis* Cry1A toxins. *J Biol Chem.* 2002; 277: 30137-30143.
60. Belfiere CJ, Vadlamudi RK, Osman YA, Bulla LA. A specific binding protein from *Tenebrio molitor* for the insecticidal toxin of *Bacillus thuringiensis* subsp. *tenebrionis*. *Biochem. Biophys. Res. Commun.* 1994; 200: 359-364.

61. Vadlamudi RK, Weber EI, Ji T, Bulla LA. Cloning and Expression of a Receptor for an Insecticidal Toxin of *Bacillus thuringiensis*. *J Biol.Chem.* 1995; 270: 5490-5494.
62. Negamatsu Y, Toda S, Yagamuchi F, Ogo M, Nakamura M, Shibata Y, Katsumoto T. Identification of *Bombyx mori* midgut receptor for *Bacillus thuringiensis* insecticidal CryIA(a) toxin. *Biosci. Biotechnol. Biochem.* 1998; 62: 718-728.
63. Nagamatsu Y, Koika T, Sasaki K, Yoshimoto A, Furakawa Y. The cadherin-like protein is essential to specificity determination and cytotoxic action of the *Bacillus thuringiensis* insecticidal. *FEBS Lett.* 1999; 460: 385-390.
64. Yaoi K, Kadotani T, Kuwana IL, Shinkawa A, Takashashi T, Iwahana IL, Saio R. Aminopeptidase N from *Bombyx mori* as a candidate for the receptor of *Bacillus thuringiensis* Cry1Aa toxin. *Eur. J. Biochem.* 1997; 246: 652-657.
65. Gill SS, Cowles EA, Francis V. Identification, isolation, and cloning of a *Bacillus thuringiensis* CryIAC toxin-binding protein from the midgut of the lepidopteran insect *Heliothis virescens*. 1995; 270: 27277-27282.
66. Oltean DL, Pullikuth AK, Lee HK, Gill SS. Partial purification and characterization of *Bacillus thuringiensis* Cry1A toxin receptor A from *Heliothis virescens* and cloning of the corresponding cDNA.. *Appl. Environ. Microbiol.* 1999; 65: 4763-3768.
67. Luo MK, Tabashnik BE, Adang MJ. The *heliiothis virescens* 170 kDa aminopeptidase functions as "receptor A" by mediating specific *Bacillus thuringiensis* Cry1A delta-endotoxin binding and pore formation. *Insect Biochem Mol Biol.* 1997; 27(8-9): 735-43.
68. Lee MK, You TL, Young BA, Valailis AP, Dean DH. Aminopeptidase N purified from gypsy moth brush border membrane vesicles is a specific receptor for *Bacillus thuringiensis* CryIAC toxin.. *Appl. Environ. Microbiol.* 1996; 62: 2845-2849.

69. Bravo A, Gomez I, Conde J, Munoz-Garay C, Sanchez J, Miranda R, Zhuang M, Gill SS, Soberon M. Oligomerization triggers binding of a *Bacillus thuringiensis* Cry1Ab pore-forming toxin to aminopeptidase N receptor leading to insertion into membrane microdomains. *Biochim Biophys Acta*. 2004;1667(1): 38-46.
70. Pootanakit K, Angsuthanasombat C, Panyim S. Identification of two isoforms of Aminopeptidase N in *Aedes aegypti* larval midgut. *J Biochem. Mol. Biol*. 2003; 36:508-513.
71. Krieger IV, Revina LP, Kostina LI, Buzdin AA, Zalunin IA, Chestukhina GG, Stepanov VM. Membrane proteins of *Aedes aegypti* larvae bind toxins Cry4B and Cry11A of *Bacillus thuringiensis* ssp. *israelensis*. *Biochemistry (Mosc)* 1999; 64(10):1163-1168.
72. Lightwood DJ, Ellar DJ, Jarrett P. Role of proteolysis in determining potency of *Bacillus thuringiensis* Cry1Ac delta-endotoxin. *Appl Environ Microbiol*. 2000; 66(12): 5174-81.
73. Miranda R, Zamudio FZ, Bravo A. Processing of Cry1Ab delta-endotoxin from *Bacillus thuringiensis* by *Manduca sexta* and *Spodoptera frugiperda* midgut proteases: role in protoxin activation and toxin inactivation. *Insect Biochem Mol Biol*. 2001; 31(12): 1155-63.
74. Gomez I, Sanchez J, Miranda R, Bravo A, Soberon M. Cadherin-like receptor binding facilitates proteolytic cleavage of helix alpha-1 in domain I and oligomer pre-pore formation of *Bacillus thuringiensis* Cry1Ab toxin. *FEBS Lett*. 2002; 513(2-3): 242-6.
75. Rausell C, Munoz-Garay C, Miranda-CassoLuengo R, Gomez I, Rudino-Pinera E, Soberon M, Bravo A. Tryptophan spectroscopy studies and black lipid bilayer analysis indicate that the oligomeric structure of Cry1Ab toxin from *Bacillus thuringiensis* is the membrane-insertion intermediate. *Biochemistry*. 2004; 43(1): 166-74.
76. Puntheeranurak T, Stroh C, Zhu R, Angsuthanasombat C, Hinterdorfer P. Structure and distribution of the *Bacillus thuringiensis* Cry4Ba toxin in lipid membranes. *Ultramicroscopy* (in press)

77. Peyronnet O, Nieman B, Genereux F, Vachon V, Laprade R, Schwartz JL. Estimation of the radius of the pores formed by the *Bacillus thuringiensis* Cry1C delta-endotoxin in planar lipid bilayers. *Biochim Biophys Acta* 2002; 1567(1):113-122.
78. Rausell C, Pardo-Lopez L, Sanchez J, Munoz-Garay C, Morera C, Soberon M, Bravo A. Unfolding events in the water-soluble monomeric Cry1Ab toxin during transition to oligomeric pre-pore and membrane-inserted pore channel. *J Biol Chem*. 2004; 279(53): 55168-75.
79. Soberon M, Perez RV, Nunez-Valdez ME, Lorence A, Gomez I, Sanchez J et al. Evidence for intermolecular interaction as a necessary step for pore-formation activity and toxicity of *Bacillus thuringiensis* Cry1Ab toxin. *FEMS Microbiol Lett* 2000; 191(2): 221-225.
80. Tigue NJ, Jacoby J, Ellar DJ. The α -helix 4 residue, Asn135, is involved in the oligomerization of Cry1Ac1 and Cry1Ab5 *Bacillus thuringiensis* toxins. *Appl. Environ. Microbiol*. 2001; 67: 5715-5720.
81. Gazit E, Shai Y. Structural characterization, membrane interaction, and specific assembly within phospholipid membranes of hydrophobic segments from *Bacillus thuringiensis* var. *israelensis* cytolytic toxin. *Biochemistry* 1993; 32(46): 12363-12371.
82. Feng Q, Becktel WJ. pH-induced conformational transitions of Cry IA(a), CryIA(c), and Cry IIIA delta-endotoxins in *Bacillus thuringiensis*. *Biochemistry* 1994; 33(28): 8521-8526.
83. Guereca L, Bravo A. The oligomeric state of *Bacillus thuringiensis* Cry toxins in solution. *Biochim Biophys Acta* 1999; 1429(2): 342-350.
84. Gerber D, Shai Y. Insertion and organization within membranes of the delta-endotoxin pore-forming domain, helix 4-loop-helix 5, and inhibition of its activity by a mutant helix 4 peptide. *J Biol Chem* 2000; 275(31): 23602-23607.
85. Carrol J, Ellar DJ. An analysis of *Bacillus thurigiensis* delta-endotoxin action on insect midgut membrane permeability using a light-scattering assay. *Eur. J. Biochem*. 1993; 214: 771-778.

86. Lorence A, Darszon A, Diaz C, Lievano A, Quintero R, Bravo A. Deltaendotoxins induce cation channels in *Spodoptera frugiperda* brush border membranes in suspension and in planar lipid bilayers. FEBS Lett 1995; 360(3):217-222.
87. Slatin SL, Abrams CK, English L. Delta-endotoxins form cation-selective channels in planar lipid bilayers. Biochem Biophys Res Commun 1990; 169(2): 765-772.
88. Puntheeranurak, T., Uawithya, P., Potvin, L., Angsuthanasombat, C. and Schwartz, J.L. Ion channels formed in planar lipid bilayers by the dipteran-specific Cry4B *Bacillus thuringiensis* and its $\alpha 1$ - $\alpha 5$ fragment. Mol. Membr. Biol. 2004; 21: 67-74.
89. Schwartz JL, Garneau L, Savaria D, Masson L, Brousseau R, Rousseau E. Lepidopteran-specific crystal toxins from *Bacillus thuringiensis* form cation- and anion-selective channels in planar lipid bilayers. J Membr Biol 1993; 132(1): 53-62.
90. Tran LB, Vachon V, Schwartz JL, Laprade R. Differential effects of pH on the pore-forming properties of *Bacillus thuringiensis* insecticidal crystal toxins. Appl Environ Microbiol 2001; 67(10): 4488-4494.
91. Del Pilar Corena M, Fiedler MM, VanEkeris L, Tu C, Silverman DN, Linser PJ. Alkalinization of larval mosquito midgut and the role of carbonic anhydrase in different species of mosquitoes. Comp Biochem Physiol C Toxicol Pharmacol. 2004; 137(3): 207-25.
92. Clements, A. N. The Biology of Mosquitoes, vol. 1, Development Nutrition and Reproduction. New York: Chapman and Hall 1992.
93. Corena MP, Seron TJ, Lehman HK, Ochrietor JD, Kohn A, Tu C, Linser PJ. Carbonic anhydrase in the midgut of larval *Aedes aegypti*: cloning, localization and inhibition. J Exp Biol. 2002; 205(Pt 5): 591-602.
94. Borovsky D. Biosynthesis and control of mosquito gut proteases. IUBMB Life. 2003; 55(8): 435-41.

95. Siqueira HA, Nickerson KW, Moellenbeck D, Siegfried BD. Activity of gut proteinases from Cry1Ab-selected colonies of the European corn borer, *Ostrinia nubilalis* (Lepidoptera: Crambidae). *Pest Manag Sci.* 2004; 60(12): 1189-96.
96. Dai SM, Gill SS. In vitro and in vivo proteolysis of the *Bacillus thuringiensis* subsp. israelensis CryIVD protein by *Culex quinquefasciatus* larval midgut proteases. *Insect Biochem Mol Biol.* 1993; 23(2): 273-83.
97. Escobar E, Segura C, Vanegas M, Patarroyo ME, Orduz S. Proteolytic processing of the Cyt1Ab1 toxin produced by *Bacillus thuringiensis* subsp. medellin. *Mem Inst Oswaldo Cruz.* 2000; 95(5): 693-700.
98. Sambrook J, Maniatis T, Fritsch EF. *Molecular cloning a laboratory manual.* NY USA: Cold spring harbor laboratory press, 2001.
99. Angsuthanasombat C, Chungjatupornchai W, Kertbundit S, Luxananil P, Settasatian C, Wilairat P et al. Cloning and expression of 130-kd mosquito-larvicidal delta-endotoxin gene of *Bacillus thuringiensis* var. *Israelensis* in *Escherichia coli*. *Mol Gen Genet* 1987; 208(3): 384-389.
100. Bradford MM. A rapid and sensitive method for the quantitation of microgram quantities of protein utilizing the principle of protein dye binding. *Anal. Biochem.* 1976; 72: 248-254.
101. Uawithya P, Tuntitippawan T, Katzenmeier G, Panyim S, Angsuthanasombat C. Effects on larvicidal activity of single proline substitutions in alpha3 or alpha4 of the *Bacillus thuringiensis* Cry4B toxin. *Biochem Mol Biol Int* 1998; 44(4): 825-832.
102. Gerber D, Shai Y. Insertion and organization within membranes of the delta endotoxin pore-forming domain, helix 4-loop-helix 5, and inhibition of its activity by a mutant helix 4 peptide. *J Biol Chem* 2000; 275(31): 23602-23607.
103. Mesny, R.J., Volwerk, J.J. and Griffith, O.H. A simplified procedure for lipid phosphorus analysis shows that digestion rates vary with phospholipid structure. *Chem. Phys. Lipids.* 1986; 39: 185-191.

104. Wu D, Aronson AI. Localized mutagenesis defines regions of the *Bacillus thuringiensis* delta-endotoxin involved in toxicity and specificity. *J Biol Chem* 1992; 267(4): 2311-2317.
105. Smith WL, Garavito M, Ferguson-Miller S. Membrane protein structural biology minireview series. *J Biol. Chem.* 2001; 276: 32393-32394.
106. Garland, W.J., and Buckley, J.T. (1988) The cytolytic toxin aerolysin must aggregate to disrupt erythrocytes, and aggregation is stimulated by human glycophorin. *Infect. Immun.* 56, 1249-1253.
107. Hotze EM, Heuck AP, Czajkowsky DM, Johnson AE, Twenten R. Monomer-monomer interactions drive the prepore to pore conversion of a β -barrel-forming cholesterol-dependent cytolysin. *J. Biol. Chem.* 2002; 277: 11597-11605.
108. Sramala I, Leetachewa S, Krittanai C, Katzenmeier G, Panyim S, Angsuthanasombat C. Charged residue screening in helix 4 of the *Bacillus thuringiensis* Cry4B toxin reveals on critical residue for larvicidal activity. *J. Biochem. Mol. Biol. Biophys.* 2001; 5: 219-225.
109. Sramala I. Molecular biophysical studies of transmembrane helices in the pore-forming domain of the *Bacillus thuringiensis* Cry4B toxin. [Ph.D. thesis], Bangkok, Faculty of Graduate Studies, Mahidol University; 2002.
110. Adamian L, Liang J. Interhelical hydrogen bonds and spatial motifs in membrane proteins: polar clamps and serine zippers. *Proteins* 2002; 47: 209–218.
111. Weis WI, Brunger AT, Skehel JJ, Wiley DC. Refinement of the influenza virus A hemagglutinin by simulating annealing. *J. Mol. Biol.* 1990; 212: 737-761.
112. Gratkowski H, Lear JD, DeDrado WF. Polar side chains drive the association of model transmembrane peptides. *Proc. Natl. Acad. Sci. USA* 2001; 30: 880-885.
113. Dawson JP, Melnyk RA, Deber CM, Engelman DM. Sequence context strongly modulates association of polar residues in transmembrane helices. *J. Mol. Biol.* 2003; 331: 255-262.

114. Andra J, Leippe M. Pore-forming protein of *Entamoeba histolytica* significance of positively charged amino acid residue for its mode of action. FEBS Letters 1994; 354: 97-102.
115. Marheineke K, Grunewald S, Christie W, Reilander H. Lipid composition of *Spodoptera frugiperda* (Sf9) and *Trichoplusia ni* (Tn) insect cells used for baculovirus infection. FEBS Lett. 1998; 441: 49-52.
116. Yeh B, Kim YK, Jabbar W, Huang CL. Conformational changes of pore helix coupled to gating of TRPV5 by protons. EMBO J. 2005; 24: 3224-3234.
117. Arkin IT, Adams PD, Brunger AT, Smith SO, Engelman DM. Structural perspectives of phospholamban, a helical transmembrane pentamer. Annu. Rev. Biophys. Biomol. Struct. 1997; 26: 157-179.
118. Lemmon MA, Flanagan JM, Treutlein HR, Zhang J, Engelman DM. Sequence specificity in the dimerization of transmembrane α -helices. Biochemistry 1992; 31: 12719-12725.
119. Nishimoto T, Yoshisue H, Ihara K, Sakai H, Komano T. Functional analysis of block 5, one of the highly conserved amino acid sequences in the 130-kDa Cry4 protein produced by *Bacillus thuringiensis* subsp. *israelensis*. FEBS Letters 1994; 348: 249-254.



APPENDIX

Appendix 1: Complete nucleotide sequence of the *cry4Ba* gene

The nucleotide sequence of the *cry4Ba* gene in pMU388 is shown. The uppercase letters represent the deduced amino acid sequence. The alpha helices and beta strands in each domains are marked as box based on structural alignment and superpositions of individual domains of Cry1Aa, Cry3Aa and Cry2Aa (50).

```

atg aat tca ggc tat ccg tta gcg aat gac tta caa ggg tca atg 45
M N S G Y P L A N D L Q G S M

aaa aac acg aac tat aaa gat tgg cta gcc atg tgt gaa aat aac 90
K N T N Y K D W L A M C E N N

caa cag tat ggc gtt aat cca gct gcg att aat tct tct tca gtt 135
Q Q Y G V N P A A I N S S S V
α1
agt acc gct tta aaa gta gct gga gct atc ctt aaa ttt gta aac 180
S T A L K V A G A I L K F V N
α2a
cca cct gca ggt act gtc tta acc gta ctt agc gcg gtg ctt cct 225
P P A G T V L T V L S A V L P

att ctt tgg ccg act aat act cca acg cct gaa aga gtt tgg aat 270
I L W P T N T P T P E R V W N
α2b
gat ttc atg acc aat aca ggg aat ctt att gat caa act gta aca 315
D F M T N T G N L I D Q T V T
α3
gct tat gta cga aca gat gca aat gca aaa atg acg gtt gtg aaa 360
A Y V R T D A N A K M T V V K

gat tat tta gat caa tat aca act aaa ttt aac act tgg aaa aga 405
D Y L D Q Y T T K F N T W K R

gag cct aat aac cag tcc tat aga aca gca gta ata act caa ttt 450
E P N N Q S Y R T A V I T Q F
α4
aac tta acc agt gcc aaa ctt cga gag acc gca gtt tat ttt agc 495
N L T S A K L R E T A V Y F S
α5
aac tta gta ggt tat gaa tta ttg tta tta cca ata tac gca caa 540
N L V G Y E L L L L P I Y A Q

gta gca aat ttc aat tta ctt tta ata aga gat ggc ctc ata aat 585
V A N F N L L L I R D G L I N

gca caa gaa tgg tct tta gca cgt agt gct ggt gac caa cta tat 630
A Q E W S L A R S A G D Q L Y
α6
aac act atg gtg cag tac act aaa gaa tat att gca cat agc att 675
N T M V Q Y T K E Y I A H S I

aca tgg tat aat aaa ggt tta gat gta ctt aga aat aaa tct aat 720
T W Y N K G L D V L R N K S N
α7
gga caa tgg att acg ttt aat gat tat aaa aga gag atg act att 765
G Q W I T F N D Y K R E M T I

```

caa gta tta gat ata ctc gct ctt ttt gcc agt	tat gat cca cgt	810
Q V L D I L A L F A S	Y D P R	
cga tac cct gcg gac aaa ata gat aat acg aaa cta tca aaa aca		855
R Y P A D K I D N T K L S K T		
gaa ttt aca aga gag att tat aca gct tta gta gaa tct cct tct		900
E F T R E I Y T A L V E S P S		
agt aaa tct ata gca gca ctg gag gca gca ctt aca cga gat gtt		945
S K S I A A L E A A L T R D V		
cat tta ttc act tgg cta aag aga gta gat ttc tgg acc aat act		990
H L F T W L K R V D F W T N T		
ata tat caa gat tta aga ttt tta tct gcc aat aaa att ggg ttt		1035
I Y Q D L R F L S A N K I G F		
tca tat aca aat tct tct gca atg caa gaa agt gga att tat gga		1080
S Y T N S S A M Q E S G I Y G		
agt tct ggt ttt ggt tca aat ctt act cat caa att caa ctt aat		1125
S S G F G S N L T H Q I Q L N		
tct aat gtt tat aaa act tct atc aca gat act agc tcc ccc tct		1170
S N V Y K T S I T D T S S P S		
aat cga gtt aca aaa atg gat ttc tac aaa att gat ggt act ctt		1215
N R V T K M D F Y K I D G T L		
gcc tct tat aat tca aat ata aca cca act cct gaa ggt tta agg		1260
A S Y N S N I T P T P E G L R		
acc aca ttt ttt gga ttt tca aca aat gag aac aca cct aat caa		1305
T T F F G F S T N E N T P N Q		
cca act gta aat gat tat acg cat att tta agc tat ata aaa act		1350
P T V N D Y T H I L S Y I K T		
gat gtt ata gat tat aac agt aac agg gtt tca ttt gct tgg aca		1395
D V I D Y N S N R V S F A W T		
cat aag att gtt gac cct aat aat caa ata tac aca gat gct atc		1440
H K I V D P N N Q I Y T D A I		
aca caa gtt ccg gcc gta aaa tct aac ttc ttg aat gca aca gct		1485
T Q V P A V K S N F L N A T A		
aaa gta atc aag gga cct ggt cat aca ggg ggg gat cta gtt gct		1530
K V I K G P G H T G G D L V A		
ctt aca agc aat ggt act cta tca ggc aga atg gag att caa tgt		1575
L T S N G T L S G R M E I Q C		
aaa aca agt att ttt aat gat cct aca aga agt tac gga tta cgc		1620
K T S I F N D P T R S Y G L R		
ata cgt tat gct gca aat agt cca att gta ttg aat gta tca tat		1665
I R Y A A N S P I V L N V S Y		
gta tta caa gga gtt tct aga gga aca acg att agt aca gaa tct		1710
V L Q G V S R G T T I S T E S		

acg ttt tca aga cct aat aat ata ata cct aca gat tta aaa tat 1755
 T F S R P N N I I P T D L K Y

gaa gag ttt aga tac aaa gat cct ttt gat gca att gta ccg atg 1800
 E E F R Y K D P F D A I V P M

aga tta tct tct aat caa ctg ata act ata gct att caa cca tta 1845
 R L S S N Q L I T I A I Q P L

aac atg act tca aat aat caa gtg att att gac aga atc gaa att 1890
 N M T S N N Q V I I D R I E I

att cca atc act caa tct gta tta gat gag aca gag aac caa aat 1935
 I P I T Q S V L D E T E N Q N

tta gaa tca gaa cga gaa gtt gtg aat gca ctg ttt aca aat gac 1980
L E S E R E V V N A L F T N D

gcg aaa gat gca tta aac att gga acg aca gat tat gac ata gat 2025
 A K D A L N I G T T D Y D I D

caa gcc gca aat ctt gtg gaa tgt att tct gaa gaa tta tat cca 2070
 Q A A N L V E C I S E E L Y P

aaa gaa aaa atg ctg tta tta gat gaa gtt aaa aat gcg aaa caa 2115
K E K M L L L D E V K N A K Q

ctt agt caa tct cga aat gta ctt caa aac ggg gat ttt gaa tcg 2160
 L S Q S R N V L Q N G D F E S

gct acg ctt ggt tgg aca aca agt gat aat atc aca att caa gaa 2205
 A T L G W T T S D N I T I Q E

gat gat cct att ttt aaa ggg cat tac ctt cat atg tct ggg gcg 2250
 D D P I F K G H Y L H M S G A

aga gac att gat ggt acg ata ttt ccg acc tat ata ttc caa aaa 2295
 R D I D G T I F P T Y I F Q K

att gat gaa tca aaa tta aaa ccg tat aca cgt tac cta gta agg 2340
 I D E S K L K P Y T R Y L V R

gga ttt gta gga agt agt aaa gat gta gaa cta gtg gtt tca cgc 2385
 G F V G S S K D V E L V V S R

tat ggg gaa gaa att gat gcc atc atg aat gtt cca gct gat tta 2430
 Y G E E I D A I M N V P A D L

aac tat ctg tat cct tct acc ttt gat tgt gaa ggg tct aat cgt 2475
 N Y L Y P S T F D C E G S N R

tgt gag acg tcc gct gtg ccg gct aac att ggg aac act tct gat 2520
 C E T S A V P A N I G N T S D

atg ttg tat tca tgc caa tat gat aca ggg aaa aag cat gtc gta 2565
 M L Y S C Q Y D T G K K H V V

tgt cag gat tcc cat caa ttt agt ttc act att gat aca ggg gca 2610
 C Q D S H Q F S F T I D T G A

tta gat aca aat gaa aat ata ggg gtt tgg gtc atg ttt aaa ata 2655
 L D T N E N I G V W V M F K I

tct tct cca gat gga tac gca tca tta gat aat tta gaa gta att 2700

S S P D G Y A S L D N L E V I
 gaa gaa ggg cca ata gat ggg gaa gca ctg tca cgc gtg aaa cac 2745
 E E G P I D G E A L S R V K H

 atg gag aag aaa tgg aac gat caa atg gaa gca aaa cgt tcg gaa 2790
 M E K K W N D Q M E A K R S E

 aca caa caa gca tat gat gta gcg aaa caa gcc att gat gct tta 2835
 T Q Q A Y D V A K Q A I D A L

 ttc aca aat gta caa gat gag gct tta cag ttt gat acg aca ctc 2880
 F T N V Q D E A L Q F D T T L

 gct caa att cag tac gct gag tat ttg gta caa tcg att cca tat 2925
 A Q I Q Y A E Y L V Q S I P Y

 gtg tac aat gat tgg ttg tca gat gtt cca ggt atg aat tat gat 2970
 V Y N D W L S D V P G M N Y D

 atc tat gta gag ttg gat gca cga gtg gca caa gcg cgt tat ttg 3015
 I Y V E L D A R V A Q A R Y L

 tat gat aca aga aat att att aaa aat ggt gat ttt aca caa ggg 3060
 Y D T R N I I K N G D F T Q G

 gta atg ggg tgg cat gta act gga aat gca gac gta caa caa ata 3105
 V M G W H V T G N A D V Q Q I

 gat ggt gtt tct gta ttg gtt cta tct aat tgg agt gct ggc gta 3150
 D G V S V L V L S N W S A G V

 tct caa aat gtc cat ctc caa cat aat cat ggg tat gtc tta cgt 3195
 S Q N V H L Q H N H G Y V L R

 gtt att gcc aaa aaa gaa gga cct gga aat ggg tat gtc acg ctt 3240
 V I A K K E G P G N G Y V T L

 atg gat tgt gag gag aat caa gaa aaa ttg acg ttt acg tct tgt 3285
 M D C E E N Q E K L T F T S C

 gaa gaa gga tat att acg aag aca gta gat gta ttc cca gat aca 3330
 E E G Y I T K T V D V F P D T

 gat cgt gta cga att gag ata ggc gaa acc gaa ggt tcg ttt tat 3375
 D R V R I E I G E T E G S F Y

 atc gaa agc att gaa tta att tgc atg aac gag 3408
 I E S I E L I C M N E

BIOGRAPHY

NAME	Miss Supaporn Likitvivanavong
DATE OF BIRTH	22 February 1980
PLACE OF BIRTH	Bangkok, Thailand
INSTITUTIONS ATTENDED	Kasetsart University, 1995-1998 Bachelor of Science (Microbiology) Mahidol University, 1999-2002 Master of Science (Microbiology) Mahidol University, 2003-2006 Doctor of Philosophy (Molecular Genetics and Genetic Engineering)
SCHOLARSHIP	The Development & Promotion of Science & Technology Talents (DPST), Institute for Promotion of Science & Technology, Thailand
HOME ADDRESS	1011/7 Phetkasem 106 Rd. Nongkhaem Bangkok, Thailand 10160